NOVEL POLYMER ELECTROLYTE MEMBRANES FOR FUEL CELL APPLICATIONS

Zhilian Zhou

A dissertation submitted to the faculty of the University of North Carolina at Chapel Hill in partial fulfillment of the requirements for the degree of Doctor of Philosophy in the Department of Chemistry

Chapel Hill
2006

Approved by

Advisor: Professor Joseph M. DeSimone

Reader: Professor Valerie S. Ashby

Reader: Professor Maurice S. Brookhart

Reader: Professor Jeffery S. Johnson

Reader: Professor Muhammad N. Yousaf

Reader: Professor Yue Wu

ABSTRACT

ZHILIAN ZHOU: Novel Polymer Electrolyte Membranes for Fuel Cell Applications
(Under the direction of Dr. Joseph M. DeSimone)

Polymer electrolyte membranes (PEMs) for fuel cells have been synthesized from easily processable, 100% curable, low molecular weight reactive liquid precursors that are photo-chemically cured into highly proton conductive solid membranes. The liquid precursors were directly cured into membranes of desired dimensions without the need for further processing steps such as melt extrusion or solvent casting. By employing chemical cross-linking, high proton conductivities can be achieved through the incorporation of significant levels of acidic groups without rendering the material water soluble, which plagues commonly used uncross-linked polymers. Fabrication of membrane electrode assemblies (MEAs) from these PEMs resulted in fuel cells that outperformed those based on commercial materials. Moreover, these liquid precursors enabled the formation of 3-dimensional, patterned PEMs with high fidelity, micron scale features by using soft lithographic/micro-molding techniques. The patterned membranes provided larger interfacial area between the membrane and catalyst layer than standard flat PEMs. MEAs composed of the patterned membranes demonstrated higher power densities over that of flat ones without an increase in the geometric volume of the fuel cells. This can potentially miniaturize fuel cells and promote their application in portable devices.

DEDICATION

To my parents, Shuqin Dong and Wenxiang Zhou, for inspiration

and

To my husband, Yongchao, for love and support

ACKNOWLEDGEMENTS

I would like to express my gratitude to the many people who have helped me during my graduate study. First of all, I would like to thank my advisor, Prof. Joseph M. DeSimone for his constant guidance and encouragement. I have learned immensely from him in the past three years in many different areas. I have enjoyed being a part of DeSimone Group, and would like to thank the group members for their friendship and help. I also would like to thank my advisors at University of Minnesota, Prof. Tim P. Lodge and Prof. Marc A. Hillmyer for their directions and support. My experience at Minnesota is a very precious part of my life.

I would like to thank Dr. Lei Zhang for performing the SEM measurements. I am grateful to Sherryl Yu and Frank Sun for their help in AFM measurements. I would also like to thank Dr. Ginger Denison, Liz Enlow, Dr. Jason Rolland, Dr. Junhoe Cha, Dr. Ben Maynor, Dr. Colin Wood and Dr. Ashish Pandya for helping me with various aspects of experiments. I appreciate the help and friendship of Ji Guo, Jennifer Kelly, Zhaokang Hu, Matthew Cottle, Ben Pierce, the rest of DeSimone group and all my friends at Chapel Hill.

I would like to thank my family for a life time love: my mom and dad and my twin brothers, who have been a constant source of support. Finally, I want to thank my husband, Yongchao, for sharing the journey of life and always being there for support and love.

TABLE OF CONTENTS

Page

LIST OF TABLES

LIST OF FIGURES

LIST OF ABBREVIATIONS AND SYMBOLS

AFC	alkaline fuel cell
AFM	atomic force microscopy
CMA	cyano methyl acrylate
DMFC	direct methanol fuel cell
DMS	dynamic mechanical spectroscopy
DMTA	dynamic mechanical and thermal analysis
DSC	differential scanning calorimetry
DVPH	divinyl perfluoriated hexane
EW	equivalent weight
ETFE	poly(ethylene-tetrafluoroethylene)
FEP	poly(fluoroethylene-*co*-hexafluoropropylene)
FVB	fluorovinyl benzene
g	gram
IEC	ion exchange capacity
MCFC	molten carbonate fuel cell
MEA	membrane electrode assembly
nm	nanometer
NMR	nuclear magnetic resonance
p-AAO	porous anodic aluminum oxide
PAFC	phosphoric acid fuel cells
PBI	polybenzimidazole
PCMA	poly(cyano methyl acrylate)

PEEK	poly(ether ether ketone)
PEM	polymer electrolyte membrane or proton exchange membrane
PFPE	perfluoropolyether
PFPE-DMA	α, ω-methacryloxy functionalized PFPE
PS	polystyrene
PSSNa	poly(sodium styrenesulfonate)
PSEPVE	perfluoro(4-methyl-3,6-dioxa-7-octene-1-sulfonyl fluoride)
PTFE	poly(tetrafluoroethylene)
PVDF	poly(vinylidene fluoride)
RH	relative humidity
SOFC	solid oxide fuel cells
SAXS	small angle x-ray scattering
SANS	small angle neutron scattering
SPEEK	sulfonated poly(ether ether ketone)
SPI	sulfonated copolyimide
sPFPE	styrenically functionalized perfluoropolyether
SS	sulfonated styrenic monomer
SSA	styrene sulfonic acid
SSE	styrene sulfonate ester
TBA	tetrabutylammonium hydroxide
TFE	tetrafluoroethylene
TEM	transmission electron microscopy
Tg	glass transition temperature

TGA	thermogravimetric analyzer
V	volt
μm	micrometer (micron)

Chapter 1

LITERATURE REVIEW AND INTRODUCTION

1.1 Introduction to fuel cells

Due to the limited availability of nonrenewable energy resources and the associated environmental issues, there is growing demand to develop alternative power sources. As a potential candidate for environmentally benign and highly efficient power generation technologies, fuel cells are attracting enormous interest.[1-3] Fuel cells are electrochemical devices that directly convert chemical energy from a fuel oxidation reaction into electrical energy. Compared with other power sources, fuel cells have much higher energy efficiency, less CO_2 emissions and other negative environmental impacts.[2] Unlike internal combustion engines, where the heat of combustion of the fuel is first converted into mechanical energy which is then converted into electricity, the efficiency of fuel cells is not limited by the Carnot cycle. For a low temperature fuel cell, where the product is liquid water, the maximum efficiency is approximately 83%.[4] In practical fuel cells, the theoretical efficiency is not achieved due to irreversible voltage losses associated with the flow of the current and the actual construction of the cell. The voltage losses are produced from electrode polarization, internal cell and external resistances, mass transport limitations and limitations in cell materials.[4] Considering these factors, the efficiency of practical fuel cells is typically in the range of 40 to 60% at present. When hydrogen is used as the fuel, the only by-products of fuel cells are heat and water, therefore they do not impose any negative environmental impact. As long as the fuel and the oxidant are supplied, fuel cells can continuously generate electricity. Due to these advantages, there are extensive research efforts, both academically and industrially, to develop fuel cells as power sources for portable electronic devices, transportation vehicles, and distributed power generation.

Based on the temperature of operation and the type of electrolyte used, fuel cells can be classified into five categories: polymer electrolyte membrane or proton exchange membrane (PEM) fuel cells; phosphoric acid fuel cells (PAFC), alkaline fuel cells (AFC), solid oxide fuel cells (SOFC); and molten carbonate fuel cells (MCFC).[5,6] All these fuel cells have a similar basic working mechanism, but differ in many other aspects such as operating temperature, electrolyte, catalyst and system structure and therefore have different applications. Figure 1.1 shows the types of fuel cells and compares their advantages and disadvantages.[6]

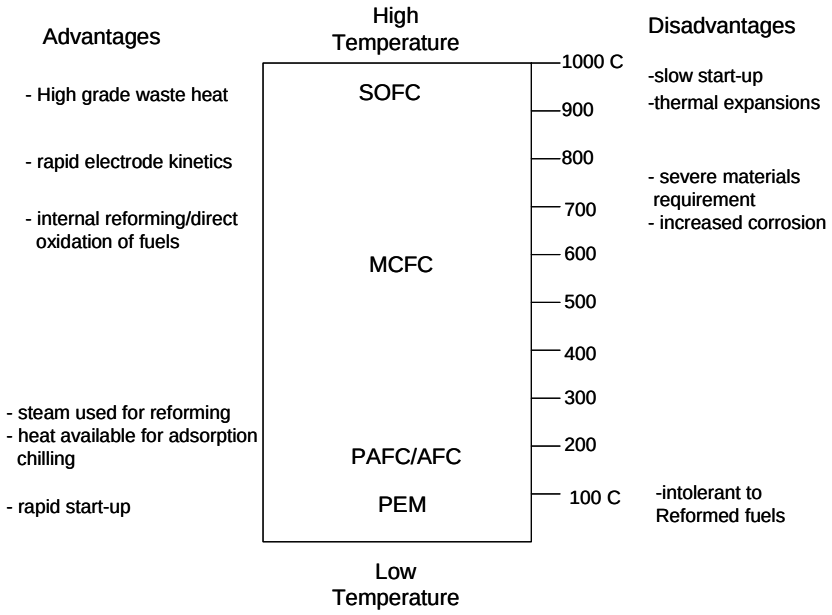

Figure 1.1 Comparison of different types of fuel cells.[6]

Alkaline fuel cells (AFC) have impressive specific power and energy density values even at low operation temperature since the oxygen reduction kinetics is more facile in alkaline electrolytes. However, a critical disadvantage of alkaline electrolytes is that they do

not reject CO_2 and applications are restricted to operation on fuel and oxidants that do not contain CO_2. With high tolerance to CO_2, fast start-up and simplicity in design, PEM fuel cells are considered the technology of choice for low temperature operations. Phosphoric acid fuel cells (PAFC) are the only type of fuel cells used in commercial products. Their higher operating temperatures (150-200 ^oC) reduce the complexity of power plants and make the waste heat more valuable, but they also introduce materials challenges that are not so difficult to meet in low temperature technologies. Molten carbonate fuel cells (MCFC) usually operate around 650 ^oC. Such a high temperature provides several key advantages: the opportunity to achieve very high efficiency with co-generation cycles; the possibility to use non-noble metal catalysts; and better tolerance to different fuels. However, the higher temperature also limits the materials that can be used. In solid oxide fuel cells (SOFC), the electrolyte management problems that are common to other fuel cell types are not a concern. Due to their high operation temperature, typically about 1000 ^oC, SOFC are more tolerant of reformed fuels and have the potential to achieve very high efficiency in a co-generation system. However, much like the MCFC, the high operating temperature also creates a host of durability issues. The focus of our efforts is on polymer electrolyte membrane (PEM) fuel cells, therefore a more thorough discussion of PEM fuel cells and previous reported efforts on PEMs is given below.

1.2 Polymer electrolyte membrane fuel cells

Of the various fuel cell systems considered, polymer electrolyte membrane fuel cells seem to be the most suitable power source for passenger vehicles and portable devices. This is due to their simplicity in design, low operation temperature, CO_2 tolerance, high power

density and high energy conversion efficiency.[7] PEM fuel cells were first deployed in the Gemini space program in the early 1960s. According to the fuel used, PEM fuel cells can be categorized as hydrogen fuel cells and direct organic fuel cells. With methanol as the fuel, the most typical direct organic fuel cells are direct methanol fuel cells.

The electrochemical processes in the fuel cell take place at the catalyst layers. In hydrogen fuel cells, the processes at the anode and cathode, respectively, are:

$$\text{Anode:} \quad 2H_2 \rightarrow 4H^+ + 4e$$

$$\text{Cathode:} \quad O_2 + 4e + 4H^+ \rightarrow 2H_2O$$

At the anode, hydrogen is oxidized to form protons and electrons in the presence of catalyst. The protons migrate through the polymer membrane from the anode to the cathode, while the electrons move through the external circuit to generate electricity. At the cathode, oxygen reacts with the coming protons to form water. The only by-product of this electrochemical process is heat and water.

In direct organic fuel cells, small organic molecules like methanol are used, and the reaction at the anode is more complicated than for hydrogen fuel cells. In addition to protons and electrons, carbon dioxide is produced. The methanol oxidation reaction is more difficult than the hydrogen oxidation reaction since it involves the transfer of six electrons and the efficiency of catalyst is poor. Despite the sluggish methanol oxidation process, direct methanol fuel cells do have some advantages over hydrogen fuel cells. Hydrogen is typically obtained by reforming hydrocarbon fuels such as natural gas, gasoline or alcohol, and a series of clean-up processes have to be applied to obtain high purity hydrogen. These reforming and purification processes increase the total cost and complicate the design of fuel cell stacks.

Methanol, however, can be directly fed into the fuel cell and therefore simplify the system design. This makes direct methanol fuel cells particularly attractive for portable power applications.

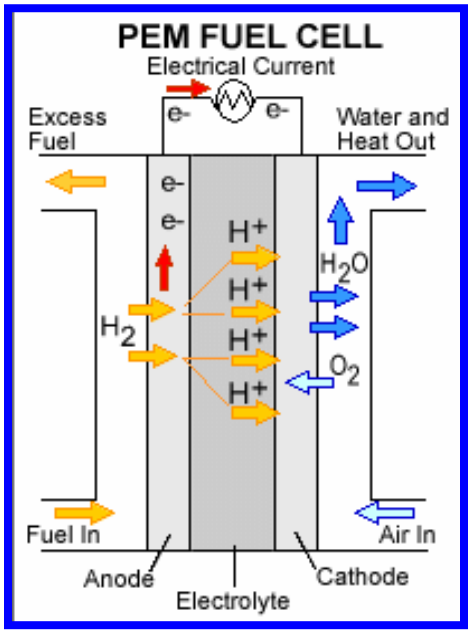

Figure 1.2 Schematic representation of a single fuel cell[8]

Figure 1.2 is a schematic representation of a single PEM fuel cell.[8] The heart of the cell is a solid polymer membrane, which serves as a proton conductor as well as a fuel barrier and a mechanical separator between the anode and the cathode. Catalyst layers, typically 5-50 μm thick, containing platinum or platinum deposited on carbon, are bonded onto both sides of the polymer electrolyte membrane. The so-called membrane electrode assembly (MEA) consists of the PEM and the bonded catalyst layers. Electro-catalyst with small particle size and high surface area is desired, which helps to maximize the reaction rate and minimize the electrode polarisation.[4] The gas diffusion layers in immediate contact with the

catalyzed membrane are made of carbon cloth or porous carbon paper. These layers provide effective reactive gas supply to the catalyst layer and effective water supply and removal in either liquid or vapor form. In other modes of PEM fuel cell fabrication, the catalyst layer is applied to the porous carbon backing layer and this catalyzed carbon paper (or cloth) is subsequently assembled with the polymeric membrane. In this case, the term "electrode" refers to the carbon paper with the catalyst layer on one of its surface. And the MEA includes the PEM and the electrodes. The electrodes are required to be porous so that there is adequate space for the diffusion of gas to the active zones of the electro-catalyst. It is also important, particularly for the cathode (where water is formed), that the gas diffusion electrode is hydrophobic so that the electrode does not become flooded with water resulting in mass transport limitations. For effective fuel cell operation, a three phase boundary is required, where the electro-catalysts are in contact with ionic conductors whilst access to reactant gas is provided.[4] A complete cell includes current collector plates that usually contain machined flow channels, as required for effective distribution of reactant gases along the surface of the electrodes. These plates become bipolar plates in the fuel cell stack, in which case they would have gas flow fields on both sides.

1.3 Polymer electrolyte membranes

As indicated by the name of PEM fuel cells, the center piece of this device is a solid, polymeric membrane which separates the anode from the cathode, prevents the fuel and the oxidant from mixing, and serves as a proton conductor. The requirements for high performance polymer electrolyte membranes (PEMs) include: high proton conductivity, low electronic conductivity, low permeability to the fuel and the oxidant, oxidative and hydrolytic

stability under fuel cell operation conditions, good mechanical properties in both the dry and hydrated states, capability for fabrication into MEAs, physical strength and ductility to survive the stress of electrode attachment, and reasonable cost.[9] The properties of PEM materials strongly depend on the concentration of ion conducting sites (typically sulfonic acid) in the membrane. Equivalent weight (EW) and ion exchange capacity (IEC) are used interchangeably (IEC = 1000/EW) to characterize the ion content of the membranes. EW, with a unit of g/mol, measures the weight of dry polymer having one molar equivalent of ion conducting sites; while IEC is a measure of the number of proton conducting sites per unit mass of the membrane expressed in units of milliequivalents per gram (meq/g).

1.3.1 Nafion® and other polyperfluorosulfonic acid membranes

The current bench mark polymer electrolyte membrane is Nafion®, a product of DuPont that satisfies an array of requirements for good performance in fuel cells. Nafion® is a copolymer of tetrafluoroethylene (TFE) and perfluoro(4-methyl-3,6-dioxa-7-octene-1-sulfonyl fluoride) (PSEPVE), whose chemical structure is shown in Figure 1.3. To prepare such a perfluorinated membrane, unsaturated monomers of TFE and PSEPVE are copolymerized by a free radical initiated reaction. The copolymer is then extruded in the melt processable sulfonyl fluoride form to form a membrane with certain thickness, which is later converted to the acid form by base hydrolysis and acid treatment. Extrusion of the sulfonyl fluoride precursor can cause micro-structural orientation in the machine direction, which can affect the swelling and other properties of the ionomer form of the membrane.[10] Since this polymer does not form true solutions, the common method of light scattering and gel permeation chromatography can not be used to determine the molecular weight of the

polymer. A rough estimation gives the molecular weight in the range of 10^5 to 10^6 Da.[11] Dispersions of Nafion® can be obtained by heating the polymer in mixtures of water and alcohol at 240 ^oC in an autoclave under pressure.[12] Nafion® dispersions are important for fabrication of traditional catalyst inks and used to coat the electrode structure in MEA preparation. Such dispersions can be dried to form the so called "recast" Nafion® membrane, whose morphology and physical properties are different from the extruded membranes.

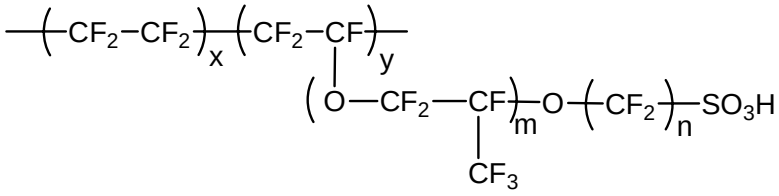

Nafion: m = 1, n = 2

Flemion: m = 0, 1; n = 1-5

Aciplex: m = 0, 3; n = 2-5

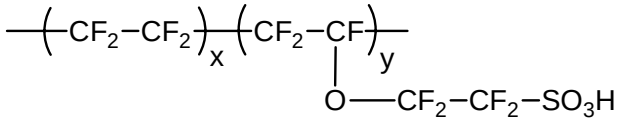

Dow membrane

Figure 1.3 Chemical structures of Nafion® and other perfluorosulfonate proton exchange membranes.

Due to its Teflon like molecular backbone and perfluorinated nature, Nafion® has very good thermal and chemical stability in both oxidative and reductive atmospheres. The

presence of semi-crystalline domains in extruded Nafion® membranes is responsible for is good mechanical strength, which is important for demanding fuel cell applications. The perfluorosulfonic acid groups impart Nafion® many of its desirable properties as a proton exchange membrane.

In theory, the ion concentration of Nafion® can be controlled by changing the ratio of the TFE and PSEPVE monomers. Nafion® has been commercially available in equivalent weights (EW) of 900, 1100 and 1200 g/mol. However, Nafion® 1100 EW with thickness of 2, 5, 7, and 10 mil (1 mil equals 25 μm) (Nafion 112, 115, 117 and 1110) are the only grades of Nafion® that are widely used and studied. This equivalent weight provides high proton conductivity under conditions of high water availability and good mechanical properties that are important for fuel cell applications. However, Nafion® with higher ion concentration is not readily available since the competing β-scission processes during polymerization result in such lower molecular weight materials that they are unusable for PEMs. The low equivalent weight (EW<900) polymers are soluble in many polar solvents.[11]

As the bench mark gold standard PEM material, the properties of Nafion® have been extensively studied and provide a baseline for comparison with other alternative PEM materials. Water uptake is important in determining the performance of PEM materials. Some principal factors that affect the water absorption of Nafion® include the concentration of ion conducting sites, *i.e.* EW or IEC; the type of counter-ion present in the membrane;[13] and thermal history of the membrane.[14,15] Without any thermal treatment, Nafion® 117 absorbs 34 wt% water from liquid water, corresponding to 21.5 water molecules per acid group.[14] Water sorption of Nafion® from vapor phase is also studied at different temperatures.[14-18] There is significant difference in water uptake by Nafion® from liquid and

saturated water vapor. For Nafion® 1100 EW, 14 water molecules per sulfonate group are absorbed from vapor phase at 100% relative humidity,[16,17] while 22 water molecules are taken per acid group from liquid water.[14] For applications in direct methanol fuel cells, the methanol uptake in Nafion® membranes is also reported.[19]

Proton conductivity is the most important property for polymer electrolyte membranes to have good performance in fuel cells. The magnitude of the specific conductivity is determined by the product of charge carrier density and charge carrier mobility. Therefore, the proton conductivity of PEMs strongly depends on IEC (or EW) and the water content of the membrane, which affects the mobility of protons. In proton conductivity measurement, it is important to ensure that the measurement is free of electrode polarization effects. This can be done by either a four-electrode[20] or a two-electrode[21] AC impedance method. Similar to water uptake, proton conductivity of Nafion® depends on factors such as concentration of the ion conducting sites, water availability, temperature, type of counter-ion, etc. The proton conductivity of Nafion® 1100 EW is about 0.1 S/cm at room temperature under fully hydrated (immersed in water) conditions.[21] The influence of water availability on the proton conductivity of Nafion® has been clearly demonstrated.[14,15,20,22] For partially hydrated membranes in contact with water vapor, the proton conductivity decreases with decreasing water content in almost a linear fashion until a threshold is reached, at which point the conductivity drops substantially.[14,15] Effects of the cation type[23] and solvent[23,24] on the proton conductivity of Nafion® are also studied.

The structural aspects of Nafion® have been studied by small angle X-ray and neutron scattering (SAXS, SANS),[25-28] transmission electron microscopy (TEM)[29-31] and atomic force microscopy (AFM).[32-34] Microscopic studies can provide direct visualization of

size, shape, and geometrical distribution of separated domains, but usually give "local pictures" of the sample and need expertise in sample preparation. The scattering techniques, on the other hand, are indirect methods and usually need to assume a particular model in data analysis, but display a "global picture" of the sample. Structural models of Nafion® have been developed on the basis of scattering and microscopic data, the most notable one is a cluster-network model proposed by Gierki and co-workers.[25,35] In this model, the polymeric ions and the absorbed electrolyte phase separate from the fluorocarbon backbone into ionic clusters, which are approximately spherical in shape with an inverted micellar structure and are connected by short narrow channels. Another well adapted model for Nafion® morphology is a three-phase model proposed by Yeager and Steck.[36] In this model, region A contains fluorocarbon backbone materials, some of which is in a microcrystalline form. The ion cluster region C incorporates sulfonate exchange sites, the majority of sorbed water, and some counter-ions. The interfacial region B is viewed as one of the relatively large fractional void volume, containing pendant side chain materials, a small amount of sorbed water, some sulfonate exchange sites which have not been incorporated into clusters, and a fraction of the counter-ions.

On the basis of the available data, proton transport has been interpreted by assuming that three transport mechanisms or domains exist: Grotthus transport; classical transport of hydronium ion in aqueous solution; and a "surface' transport mechanism in which it is assumed that protons experience additional energy barriers for transport along the aqueous /polymer interface in the membrane network at low water content, when protons are, on average, located close to the pore surface.[22] The transport of protons is strongly dependent upon the structure and physicochemical nature of the polymer with the level of hydration. At

high hydration levels, the proton conductivity of Nafion® is high because there is enough water for the ion clusters to swell and connect to each other over a percolation threshold.[37] Moreover, the Grotthuss mechanism is the major transport mechanism at high levels of hydration,[21] in which the transport of protons is determined by the rate at which the hydrogen bond between a hydronium ion and a water molecule forms rather than the slower rate at which hydronium ions migrate *en masse*. As the level of hydration is reduced, the proton conductivity of Nafion® will plummet due to corresponding morphology and proton transport mechanism changes.

Other perfluorosulfonate proton exchange membranes with structures similar to Nafion® have been developed by other companies,[38] whose chemical structures are shown in Figure 1.3. The Asahi Glass Company developed the Flemion membranes, which have equivalent weight of 1000 g/mol and dry state thickness of 50, 80, and 120 μm. The Asahi Chemical Industry manufactured a series of Aciplex® membranes, which have equivalent weights of 1000-1200 g/mol and thicknesses of 25-100 μm. The Dow Chemical Company also developed a material with a shorter side chain than that of Nafion® as shown in Figure 1.3. The Dow membranes have an equivalent weight of 800 g/mol and a thickness in the wet state of 125 μm.[38]

Despite their advantages, Nafion® and other polyperfluorosulfonic acid membranes suffer from several shortcomings which limit their utility and performance such as high synthesis and processing costs,[39] diminished proton conductivity under conditions of low water availability,[40-42] and high fuel crossover when used in direct methanol fuel cells.[43]

1.3.2 Alternative proton exchange membranes

Due to the shortcomings of Nafion® and other polyperfluorosulfonic acid membranes, there have been extensive research efforts, both academically and industrially, to develop alternative materials as proton exchange membranes and understand the complex relationships between chemical structure, morphology, physicochemical properties and fuel cell performance of these membranes. This section will review several categories of PEMs that have been widely studied. Discussion will be focused on PEMs made of homopolymer and copolymer materials. Blends of polymers, high molecular weight-low molecular weight composite membranes and organic-inorganic composite membranes will not be covered.

1.3.2.1 PEMs based on poly(ether sulfones)

Poly(arylene ether sulfone)s are thermoplastic materials that have good thermal and mechanical properties. This family of polymers is attractive for use in PEMs because of their well-known oxidative and hydrolytic stability under harsh conditions. The basic repeat units in this family of polymers consists of phenyl rings separated by alternate ether and sulfone linkages. Some poly(arylene ether sulfone)s contain additional spacers such as 2-propylidene and hexafluorinated 2-propylidene. Figure 1.4 shows the chemical structure of some sulfonated poly(arylene ether sulfone)s. The aromatic ether part of the molecules confers flexibility while the sulfone group is stable with respect to oxidation and reduction.

Active proton conducting sites can be introduced to poly(arylene ether sulfone)s by a polymer post-modification approach[44-47] or by direct co-polymerization of sulfonated monomers.[48] Post-modification reactions are usually restricted due to their lack of precise control over the degree and location of functionalization, the possibility of side reactions, or

degradation of the polymer backbone.[9] Direct polymerization of sulfonated monomers provides the possibility of control over the position, number, and distribution of proton conducting groups along the polymer backbone, allowing tuning of the microstructure and concomitant properties of the membrane materials.

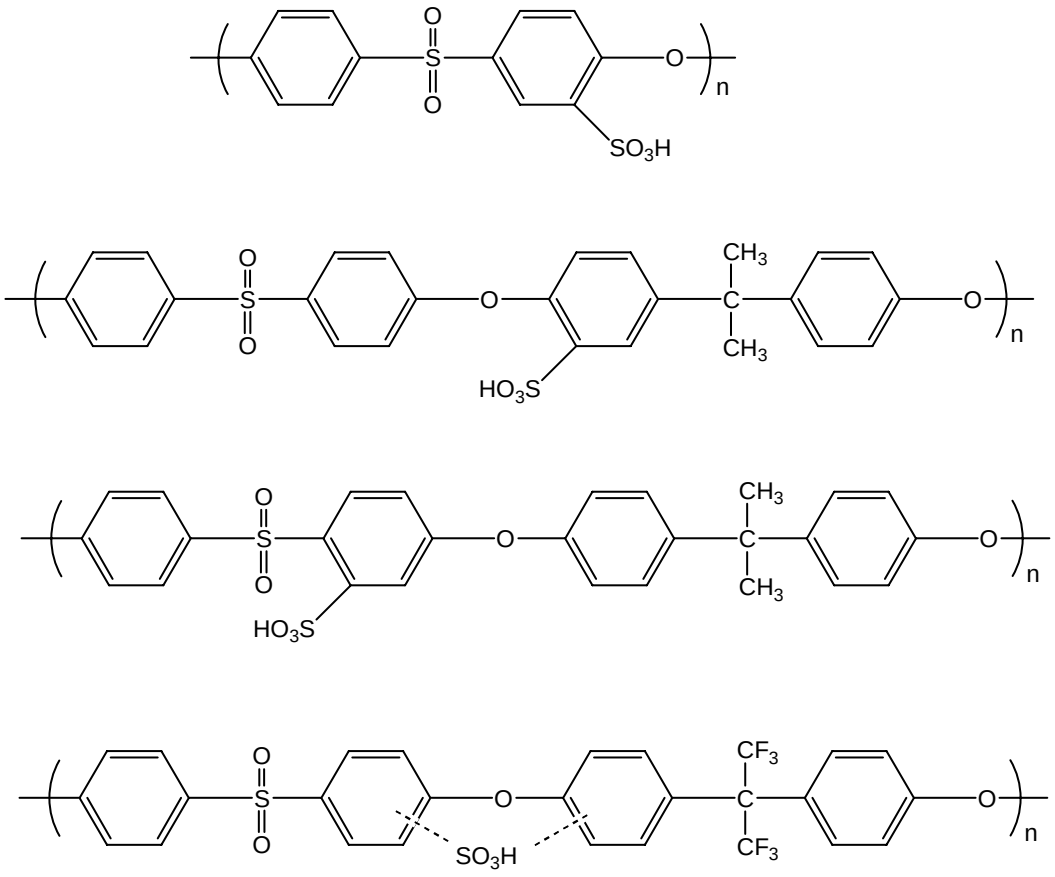

Figure 1.4 Chemical structure of sulfonated poly(ethersulfone)s

Sulfonated poly(ether sulfone)s PSU Udel with an IEC value up to 1.85 meq/g was prepared by a polymer post-modification method. Its proton conductivity was lower than Nafion® despite the higher concentration of proton conducting sites.[44] This was explained by

the stronger clustering of SO_3H groups and the more flexible backbone and side groups in Nafion® compared to the relatively rigid backbones of aryl polymers. Random sulfonated poly(arylene ether sulfone)s with IEC values between 0.4 and 2.2 meq/g were prepared by direct copolymerization method.[48] This polymer displayed proton conductivity of 0.01-0.16 S/cm at 30 ^oC under fully hydrated conditions, but the PEMs were accompanied by excessive swelling at high sulfonation level.

The great tendency of sulfonated poly(arylene ether sulfone)s to swell in water has led to studies on the cross-linking of these materials in order to improve their mechanical stability. Sulfonated poly(ether sulfone)s have been partially cross-linked by activation of the ion-exchange groups with subsequent reaction with di- or oligo-functional cross-linkers.[49,50] One example of this is the activation of sulfonic acid groups via conversion to the sulfonic acid chloride/bromide or to the sulfonic acid imidazolide with subsequent reaction with aromatic/aliphatic diamines.[49] However, the sulfonamide cross-linking bridges are not sufficiently stable to hydrolysis, which limits the applicability of such cross-linked membranes in electro-chemical processes. In an effort to generate stable cross-links, blends of sulfinated and sulfonated polysulfone Udel^{TM} were partially cross-linked by disproportionation reaction of sulfinic acid groups, ending up with a $–S(O)_2$-S- cross-linking bridge.[51] Another method was developed to cross-link sulfonated poly(ether sulfone)s by activation of sulfonic acid groups via conversion to sulfinate and subsequent alkylation of the sulfinate groups with dihalgenoalkanes.[50] Figure 1.5 shows the reaction schemes of these cross-linking approaches. For all these methods, cross-linking takes place between sulfonic acid groups, resulting in a decrease in the concentration of ion-conducting sites and therefore lower proton conductivity of the membrane.

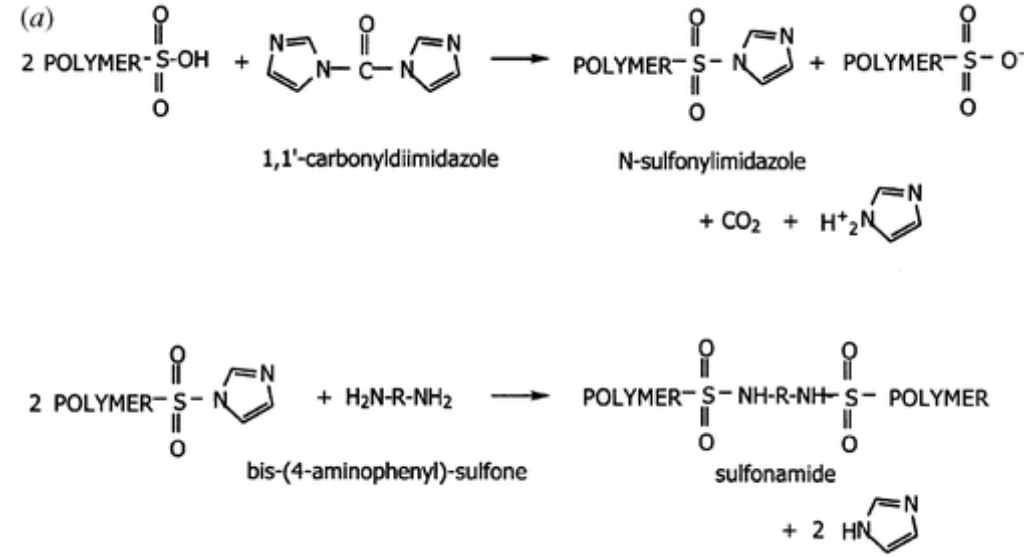

(b)

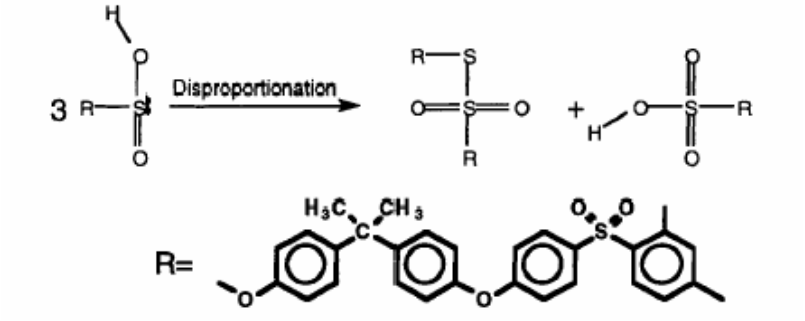

(c)

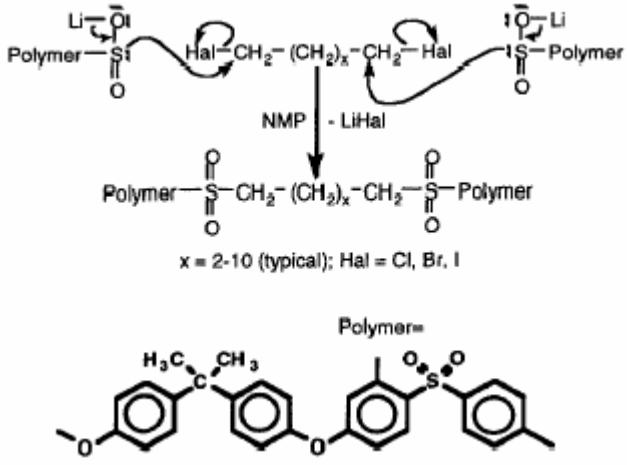

Figure 1.5 Cross-linking of sulfonated polyethersulfones. (a) Cross-linking via reaction of sulfonic acid imidazolide with diamines.[49] (b) Cross-linking via disproportionation of sulfinic acid.[51] (c) Cross-linking via reaction of PSU sulfinate with dihalogenoalkanes.[50]

In order to improve the properties of sulfonated poly(arylene ether sulfone)s, inorganic compounds was added to form nano-composite proton exchange membranes.[52] Acidification treatment was also applied with an aim to improve their proton conductivity at high temperature.[53]

1.3.2.2 PEMs based on poly(ether ketone)s

The poly(ether ketone)s are a family of polyarylenes linked through various sequence of ether (E) and ketone (K) units with good oxidative and hydrolytic stability. Some poly(ether ketone)s contain additional spacers such as hexafluorinated 2-propylidene. Poly(ether ether ketone) (PEEK) (commercially available as Victrex®) is a high performance, semicrystalline polymer with good thermal stability, chemical resistance, and mechanical properties. Figure 1.6 shows the chemical structure of unsulfonated and sulfonated PEEK.

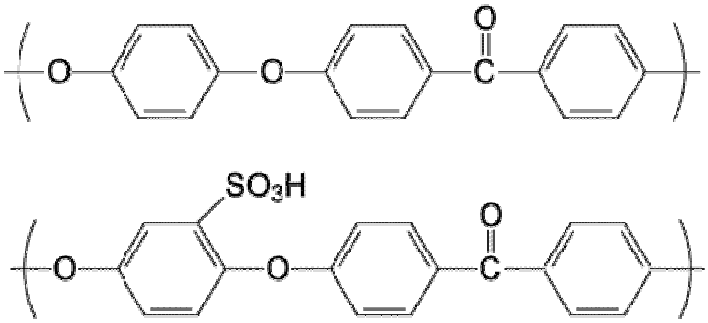

Figure 1.6 Chemical structures of unsulfonated and sulfonated PEEK[9]

Similar to poly(ether sulfone)s, sulfonic acid groups can be introduced to poly(ether ketone)s by a polymer post-modification approach[54] or by direct polymerization of sulfonated monomers.[39,55] Advantages and disadvantages of these two approaches have been discussed in the previous section. Properties of the sulfonated poly(ether ketone)s are strongly dependent on the sulfonation level, *i.e.*, IEC of the membranes. For example, sulfonated PEEK becomes water soluble as the IEC value increases above 1.8 meq/g unless the polymer is cross-linked, blended, or otherwise modified.[56] By thermal gravimetric analysis, sulfonated PEEKs display a decomposition temperature of 240-350 ^{o}C,[39,54,55] depending on the degree of sulfonation and heating rate during measurement. Water uptake, swelling ratio and proton conductivity of the sulfonated PEEK membranes depend on the level of sulfonation, relative humidity and temperature.[39,54,55] The specific synthesis route and membrane preparation method also have been seen to influence the properties of the resulting PEMs. A sulfonated poly(ether ketone) synthesized by direct polymerization with an IEC of 1.52 meq/g had a conductivity of 0.07 S/cm at 25 ^{o}C under fully hydrated conditions and a water uptake of 54% by weight.[39] A sulfonated PEEK prepared by a polymer post-modification approach with an IEC of 1.9 meq/g displayed a conductivity of 0.01 S/cm at 20^{o}C under fully hydrated conditions and each acid group absorbed 49 water molecules.[57]

In order to improve the mechanical strength and decrease the degree of swelling, sulfonated PEEK can be chemically cross-linked through bridging links between the reactive sulfonic acid functions. Cross-linking can be carried out by using suitable aromatic or aliphatic amines[58] or by intra/inter chain reaction of the sulfonic acid groups induced by thermal treatment in the presence of cross-linkers such as polyols.[59] While the cross-linked

membranes have smaller swelling ratios, consumption of proton conducting sites during the cross-linking reaction results in decreased proton conductivity.[59]

Due to the flexibility of incorporating various chemical moieties, sulfonated poly(ether ketone)s can serve as hosts for inorganic compounds to form composite proton exchange membranes.[60] Blend membranes based on poly(ether sulfone)s and poly(ether ketone)s are also studied.[61,62]

1.3.2.3 PEMs based on poly(imide)s

Sulfonated polyimides have been developed and studied as proton exchange membranes.[63-71] Five-membered ring (phthalic) polyimides are high performance materials. But when the sulfonated phthalic polyimides are used as proton exchange membranes in fuel cells, they are hydrolytically unstable due to chain scissions. Because of their lower ring strain, six-membered ring (naphthalenic) polyimides have superior chemical and thermal stability compared to the five-membered ring structure. The sulfonated naphthalenic polyimides are more stable to hydrolysis, and better suited for PEM fuel cell applications but their stability is still questionable.[9]

Genies et al. have developed a synthetic route to make random and sequenced sulfonated copolyimide (SPIs), as shown in Figure 1.7 (a).[63] The incorporation of diamine comonomers can adjust the membrane properties such as flexibility and water uptake by pushing apart the rigid rod backbone of the polymer and creating free volume for water. By comparing SPIs prepared from different diamines with IEC values ranging from 0.56 to 1.86 meq/g, it is found that for a given polymer structure, water uptake increases as the IEC value increases but the number of water molecules per acid group (λ) remains constant, indicating

that water is mainly located in the hydrophilic domains. This is different from most ionomeric membranes such as Nafion®, in which the λ value increases significantly with IEC. For SPIs with higher IEC values, the conductivity is rather low compared to typical proton exchange membranes with similar IEC. For example, the conductivity of a SPI membrane with an IEC of 1.86 meq/g was only 0.0086 S/cm at room temperature under fully hydrated conditions. Sequence length also has influence on the properties of SPI membranes. As the ionic block length is varied between 1 to 9 for SPIs with an IEC of 0.86 meq/g, the proton conductivity exhibits a maximum value for an ionic block average length equal to 3 monomer units, which has the lowest water uptake. This observation seems in contrast with the general idea that conductivity increases with the membrane water content and suggests that the conductivity also depends on micro-structural changes accompanying different sequence length. Compared to random copolyimides, both λ and conductivity are higher for sequenced SPIs.[63]

Okamoto and coworkers compared a series of main-chain-type SPIs where the sulfonic acid groups were directly bonded to the polymer backbone with side-chain-type SPIs where sulfonic acid groups were attached to the side chain.[66] Figure 1.7 (b) shows the chemical structures of these SPIs. By transmission electron micrographic (TEM) studies, it was found that the side-chain-type SPI membranes had a clear microphase-separated structure that was not observed for the main-chain-type membranes. Under similar conditions, the main-chain-type SPIs tended to have larger water uptake while the side-chain-type membranes displayed more significant anisotropic membrane swelling. Compared to Nafion®, the proton conductivity of the reported SPIs showed stronger dependence on water availability. Under fully hydrated conditions, main-chain-type SPI membrane with high IEC

had a reasonably high proton conductivity while that of the side-chain-type SPI was about half of that of Nafion®. This might be related to difference in the membrane morphology and the connectivity between ionic domains.

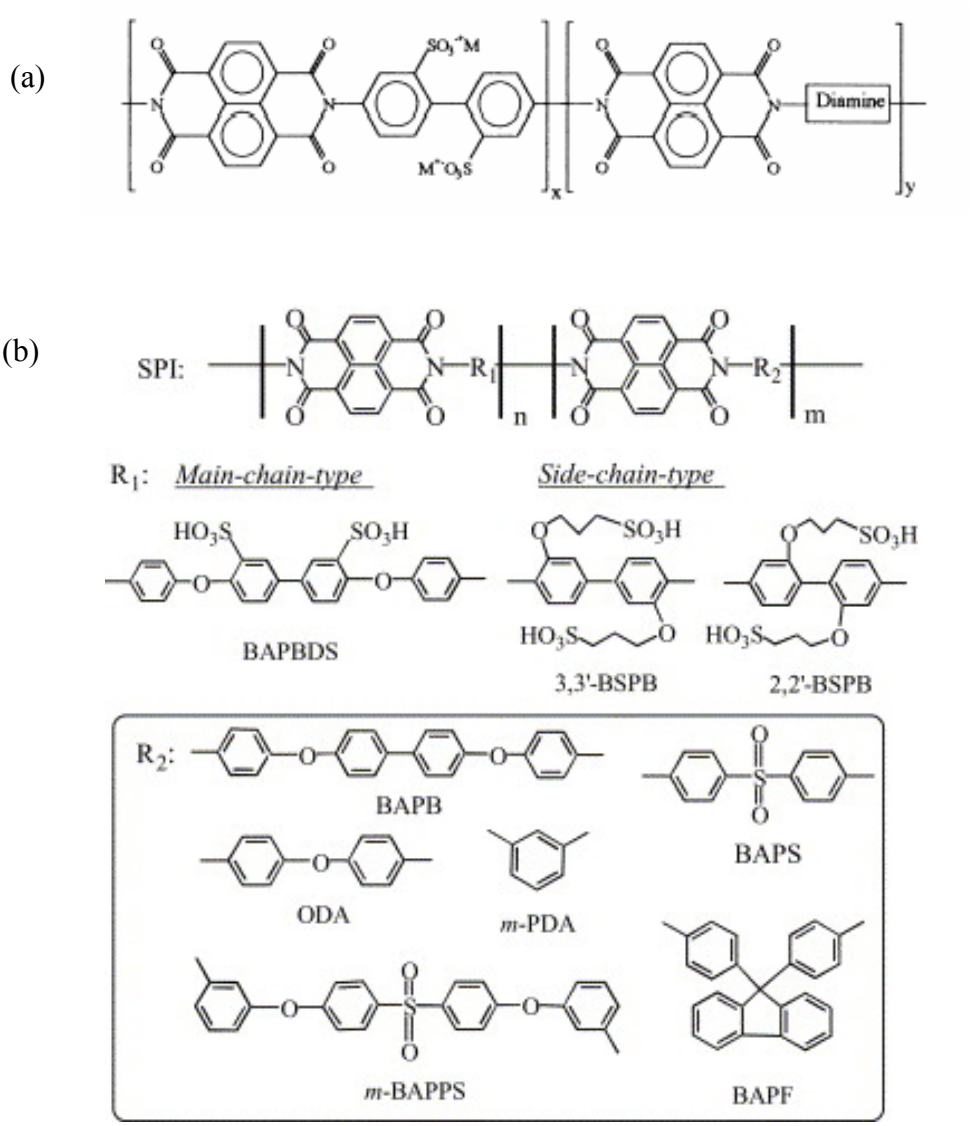

Figure 1.7 Sulfonated six-membered ring polyimide. (a) Random and sequenced sulfonated copolyimides (x=1-9).[63] (b) Main-chain-type and side-chain-type sulfonated copolyimides.[66]

1.3.2.4 PEMs based on polybenzimidazole

Aromatic polybenzimidazole (PBI) is a thermally resistant and chemically stable material with a glass transition temperature of 450 ^{o}C,[72] whose structure is shown in Figure 1.8 (a). Since the polymer chains are linear and the aromatic rings have a marked tendency to be coplanar, the non-modified PBI film contains tightly held water molecules and shows low proton conductivity.[73] Sulfonation of PBI can be accomplished by immersing the polymer film in sulfuric acid and heating the polymer-sulfuric acid complex at 475 ^{o}C so that the sulfonate groups can be covalently bonded to the polymer chain.[72] The chemical structure of the sulfonated PBI is shown in Figure 1.8 (b). However, the conductivity of the sulfonated membranes is barely higher than the non-substituted PBI and varies from 3×10^{-6} S/cm at 40^{o}C to 7.5×10^{-5} S/cm at 160^{o}C in saturated water vapor.[72] These properties seem in contrast to those observed for benzylsulfonate grafted PBI, whose structure is shown in Figure 1.8 (c). Grafting of sulfonated aryl groups onto PBI leads to a proton conducting polymer, displaying a conductivity of 1×10^{-2} S/cm with 75% sulfonation at 50 ^{o}C and 100% relative humidity.[74]

PBI is a basic polymer (pKa = 5.5) and can be readily complexed by a strong acid to give a so-called acid doped system. Phosphoric acid doped PBI films have been widely studied as proton exchange membranes, which can be prepared by immersing a PBI film in aqueous phosphoric acid solution or by casting PBI films directly from a solution containing phosphoric acid. The uptake of phosphoric acid by PBI depends both on the acid concentration and duration of immersion.[75] The proton conductivity of phosphoric acid doped PBI is strongly influenced by the doping level and the temperature, but insensitive to humidity.[76] At a doping level of 450 mol% H_3PO_4, the measured conductivity ranges

between 4.5×10^{-3} S/cm at room temperature and 4.6×10^{-2} S/cm at 165 ^{o}C. At high doping levels between 1300 and 1600 mol% H_3PO_4, the conductivity of PBI films is in the same range as Nafion® at temperature from 25 to 85 ^{o}C. Acid doped PBI membranes having low fuel permeability and low electro-osmotic drag open new opportunities to operate fuel cells at high temperatures without any gas feed humidification and pressure requirements.[77] However, it is pointed out that at high doping levels, the PBI membrane has limited mechanical strength[75,76] and the low molecular weight acid may be leached out over long term fuel cell operation.[78]

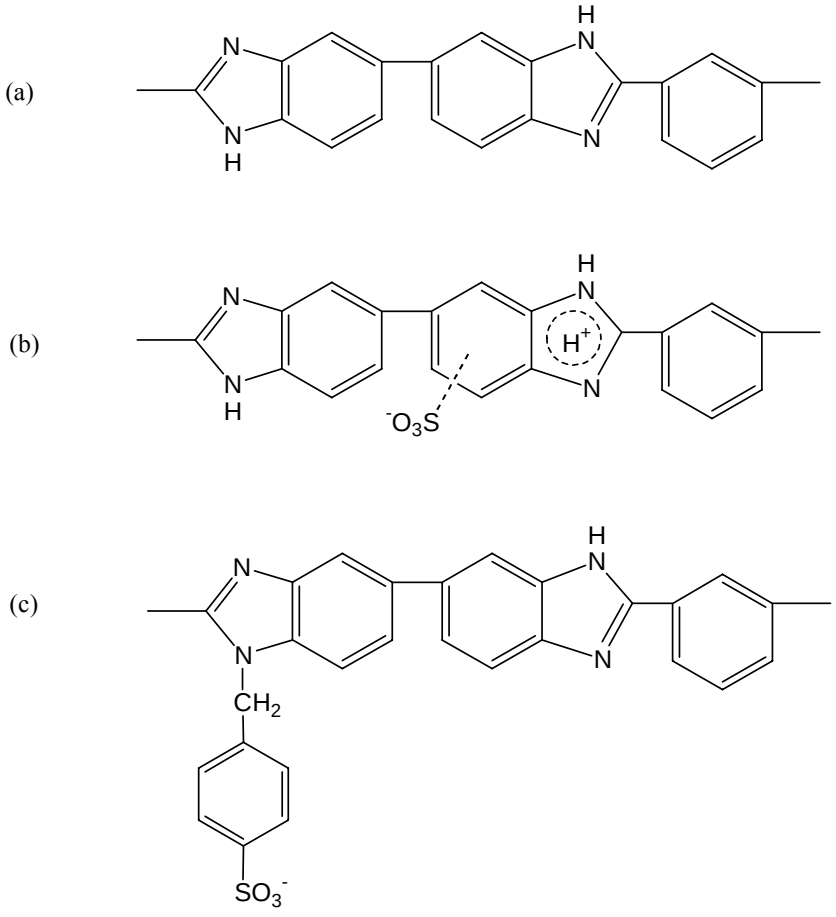

Figure 1.8 Chemical structure of PBIs. (a) Non-modified PBI. (b) Sulfonated PBI. (c) Benzylsulfonate grafted PBI.[74]

1.3.2.5 PEMs containing styrene and its derivatives

Due to low cost, easy synthesis and the flexibility to modify styrenic functionalities, materials based on styrene and its derivatives have been studied as proton exchange membranes. Polystyrene can be partially sulfonated to various extents, obtaining homogeneous distribution of the sulfonic acid groups in the polymer. For un-cross-linked sulfonated polystyrene (SPS), the level of sulfonation should be carefully controlled to maximize the proton conductivity, while preventing the membrane from becoming water soluble. While the membranes are essentially nonconductivie below 10% sulfonation, *i.e.* IEC = 0.93 meq/g, the proton conductivity is reasonably high at sulfonate concentration above 15 mol%. Sulfonated polystyrene with an IEC value of 1.41 meq/g displays a conductivity of 0.05 S/cm at room temperature, which is about half of that of Nafion®.[79] In order to improve the long term stability of nonfluorinated partially aliphatic SPS, Ballard Advanced Materials Corporation developed a novel family of sulfonated copolymers based on α, β, β-trifluorostyrene and substituted α, β, β-trifluorostyrene monomers,[80] whose general structure is given in Figure 1.9 (a).

Due to the unfavorable interaction between the different components, block copolymers tend to phase separate and form ordered microdomain structures. Depending on the relative volume fraction of constituent components, block copolymers can take the form of lamellae, cylinders, spheres, bicontinuous gyroid and other structures. Sulfonated block copolymers based on styrene have been studied as alternative proton exchange membrane materials, including sulfonated poly(styrene-*b*-(ethylene-*co*-butylene)-*b*-styrene),[81,82] sulfonated and selectively hydrogenated poly(butadiene-*b*-styrene),[83] sulfonated

poly(styrene-*b*-isobutylene-*b*-styrene).[84,85] The chemical structures of these block copolymer PEM materials are shown in Figure 1.9.

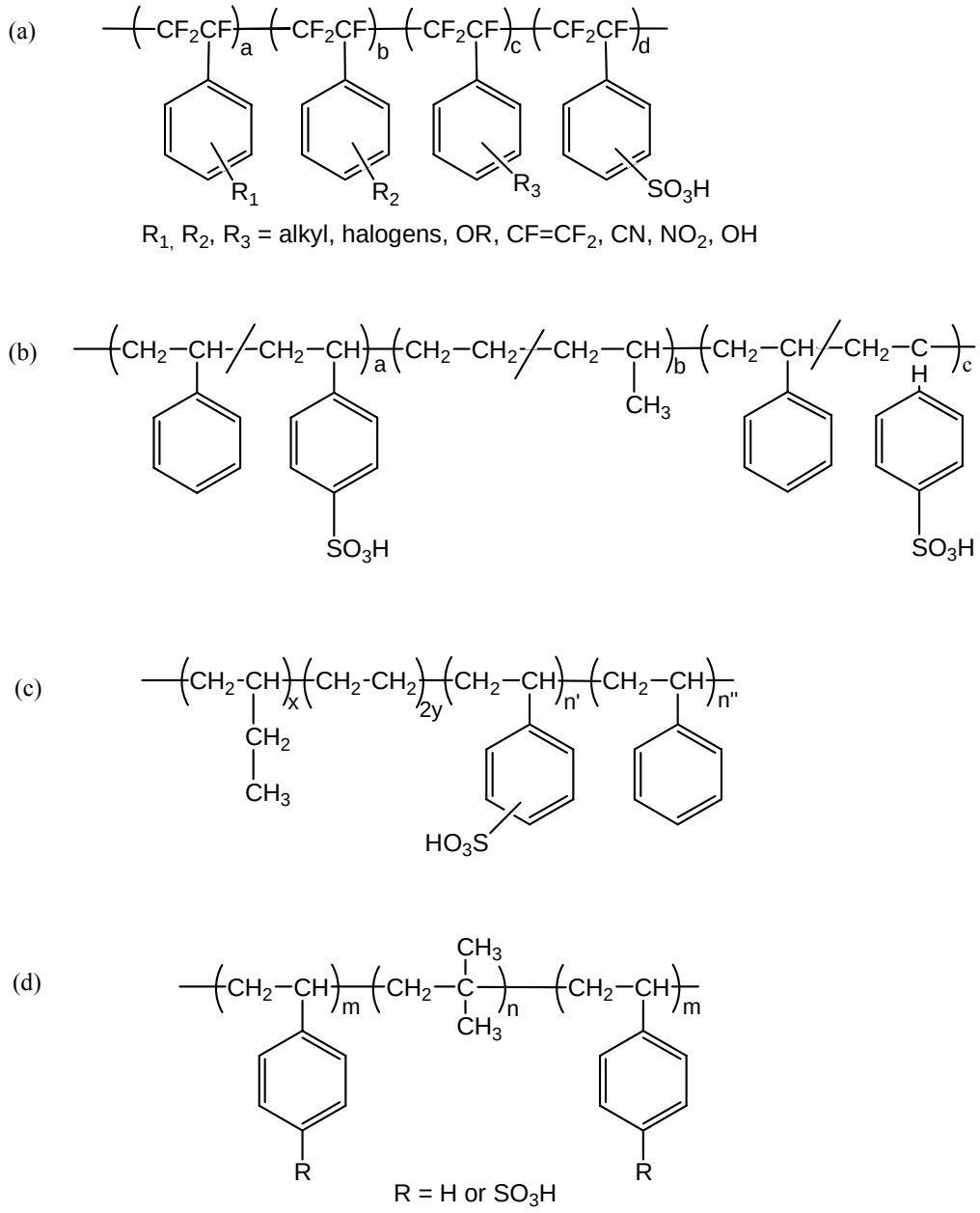

Figure 1.9 Chemical structure of polystyrene based PEM materials. (a) Chemical structure of Ballard PEMs based on α, β, β-trifluorostyrene.[80] (b) Chemical structure of sulfonated sulfonated poly(styrene-*b*-(ethylene-*co*-butylene)-*b*-styrene) block copolymer.[82] (c) Chemical structure of sulfonated and hydrogenated poly(butadiene-*b*-styrene) block copolymer.[83] (d) sulfonated poly(styrene-*b*-isobutylene-*b*-styrene) block copolymer.[84]

It has been demonstrated that the proton conductivity and methanol permeability of the membranes are significantly dependent on the size, shape and ordering direction of the microdomains in the sulfonated block copolymers. For example, the transport of water and methanol through the membranes with a lamellar structure parallel to the plane of the film is difficult and therefore proton conductivity and methanol permeability values are low compared to membranes with disordered morphology.[82]

Synthetic methods have been developed to incorporate ionic components as grafts onto a hydrophobic polymer backbone. Well-defined graft polymers can provide a better understanding of the structure-property relationship of ion conducting membranes. In principle, the length of graft chains would determine the size of ionic domains, and the number density of graft chains would determine the number of ionic domains. Collectively, the length and number density of the hydrophilic graft chains would determine the degree of connectivity between ionic clusters.[9] A series of graft polymers comprising graft chains of a poly(sodium styrenesulfonate) macromonomer (*mac*PSSNa) and a polystyrene (PS) backbone have been prepared using a combination of stable free radical polymerization and emulsion polymerization.[86-88] Well defined PSSNa polymers are prepared by stable free radical polymerization. The pseudo-living chains are terminated with divinylbenzene to afford a macromonomer *mac*PSSNa, which is subsequently copolymerized with styrene by emulsion polymerization to afford PS-*g*-*mac*PSSNa graft polymers. The synthetic scheme is shown in Figure 1.10. By adjusting the feed ratio of macromonomers to styrene, the number density of graft chains can be controlled and a series of polymers with uniform graft length and variable ion content can be obtained. For comparison, random copolymers of styrene and sodium styrene sulfonate (PS-*r*-SSNa) were prepared using conventional emulsion

copolymerization techniques. Compared to membranes prepared from random copolymers, the graft polymer membranes exhibit lower water uptake but much larger proton conductivity for a given ion content. Transmission electron microscopy shows that the graft polymer membranes exhibit a higher degree of phase separation and enhanced connectivity between ionic domains.[86,87] These observations demonstrate unambiguously that polymer morphology can play a strong role in determining the properties of PEM materials and proton conductivity is enhanced by the formation of nanochannels of polyelelctrolyte. Further study of this graft ionomer system also shows that phase separation occurs to a greater extent in membranes prepared from amphiphilic polymers possessing longer graft chains.[88]

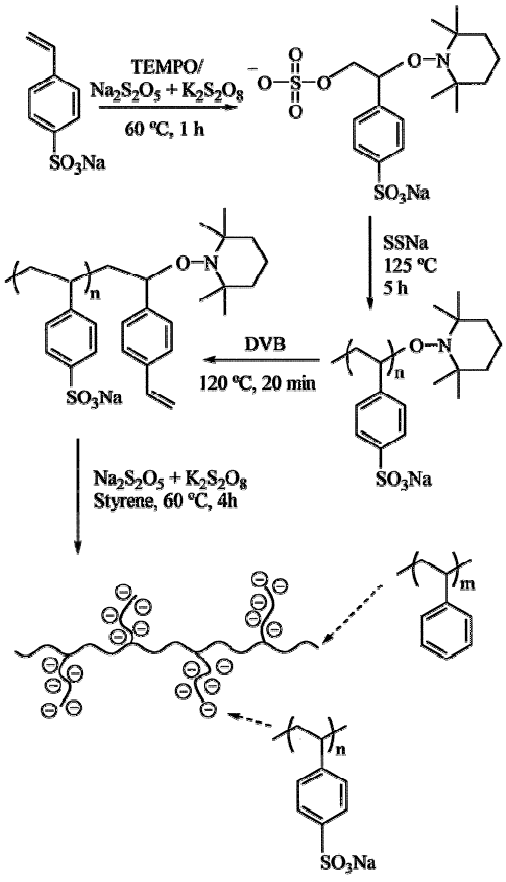

Figure 1.10 Synthetic scheme for PS-*g*-macPSSNa graft polymers.[86]

Poly(styrene sulfonic acid) grafts have also been attached to polymer films made of poly(ethylene-tetrafluoroethylene) (ETFE),[89,90] poly(vinylidene fluoride) (PVDF),[90-92] poly(fluoroethylene-*co*-hexafluoropropylene) (FEP)[93,94] or Nafion®.[95] Preparation of this type of PEMs includes three steps: irradiation of the base polymer; grafting of monomer onto the base polymer; and sulfonation of the grafted film. This process starts with a pre-existing base polymer as a film and PEMs prepared in this way are not homogeneous across the membrane. The thickness of the membrane is somehow fixed by the base polymer film and sulfonation occurs only in the grafted polystyrene layers. The extent of grafting can be controlled by styrene concentration, choice of solvents, grafting temperature and time. In some studies, divinylbenzene is used to copolymerize with styrene in order to create cross-links between grafts and possibly control water swelling and other properties of the membranes.[93-95] Büchi and coworkers[93] studied the radiation grafted FEP-*g*-polystyrene sulfonic acid membranes and found that cross-linking increased the structural density of the membranes and therefore improved the gas separation properties and long term stability of the membranes. On the other hand, the mobility of the protons in the membrane is reduced with increasing degree of cross-linking due to decreasing water uptake. Therefore, the proton conductivity of the membranes decreases with increasing degree of cross-linking.[93]

1.4 Objective and overview

As the preceding sections have illustrated, many families of polymers with differing chemical structures and various strategies for incorporation of sulfonic acid groups have been explored to develop high performance proton exchange membranes. Despite the extensive efforts to develop novel PEM materials, Nafion® is still widely accepted as the industry

standard since its overall performance outperforms most other materials. However, the shortcomings of Nafion® and other conventional PEM materials limit their utility and performance of fuel cells. We will address some of these aspects in this dissertation with an aim to prepare and characterize novel, high performance proton exchange membranes.

To achieve good proton conductivity, especially at low relative humidity conditions, PEMs with high acid-loading are highly desirable. One strategy is to impregnate the membrane with a small molecule strong acid: PBI doped with phosphoric acid[96,97] is the prototypical example of this approach. The conductivity is significantly improved by this approach, but the low molecular weight acid may be leached out over long term operation.[78] A second strategy is to synthesize polymers with high ion exchange capacity by incorporating high levels of sulfonic acid groups into the chemical structure of the polymer. For linear polymers, however, high acid loading leads to compromised mechanical strength and swelling effects. Indeed at sufficiently high ion loading level, acid-containing linear polymers can even become water soluble.[44] In particular, in the synthesis of very high IEC Nafion®, competing β-scission processes during polymerization result in such lower molecular weight materials that they are unusable for PEMs. Unlike linear polymers, chemically crosslinkable ionomeric systems offer the potential of achieving unusually high IECs without the associated challenges for linear polymers. A chemically crosslinked system should provide a way of making PEMs with both very high conductivity and good mechanical integrity. Furthermore, crosslinked membranes may also have the advantage of decreased swelling.[78] In this work, we will present a novel chemically cross-linked fluoropolymer PEM material that is prepared from 100% solventless liquid precursors.

The lack of processability of Nafion® has curtailed fabrication strategies, forcing all conventional PEMs to be flat and therefore lacking enhanced performance in such surface area dependent electrochemical cells. Up to now, Nafion® and other conventional PEM materials are processed into a membrane form either by melt extrusion or by solvent casting. The resulting membranes are flat and smooth at the surface. Such a 2-dimensional configuration restricts the membrane electrode assembly to a flat geometry and sets an upper limit on the active surface area of fuel cells. In addition to other issues such as transport phenomenon, the restricted surface area limits the power density that is ultimately achievable in fuel cells. An increase in the active surface area between a PEM and the catalyst layer without an increase in the geometric volume of the MEA should result in higher power densities, which can lead to the miniaturization of fuel cells. Moreover, it will enable the integration of fuel cells as a desirable power source in the area of microelectronics and portable devices. In order to create high interfacial area between the PEM and catalyst layer, we prepare patterned, 3-dimensional membranes by soft-lithography techniques starting from functionalized liquid precursors. Patterned PEMs with unprecedented levels of morphologic control can be achieved by this approach and increasing surface area can be obtained by simply varying the size and aspect ratios of the patterned features. The high surface area PEMs display increased power density over standard PEMs.

This dissertation consists of six chapters. In Chapter 1, a short introduction to fuel cells is given and current studies of polymer electrolyte membranes are reviewed. In Chapter 2, we describe the synthesis of precursor materials and discuss the thermal, mechanical and surface properties of membranes prepared from these liquid precursors. These membranes can be hydrolyzed to the acid form, displaying excellent properties as proton exchange

membranes. Chapter 3 discusses the preparation and characterization of these novel PEM materials, including thermal and mechanical properties, water uptake, dimensional change, proton conductivity and fuel cell performance. To further improve the thermal and chemical stability of these PEMs, the membranes can be fluorinated by elemental fluorine gas. Properties of the fluorinated PEMs are also studied and compared with the unfluorinated membranes in this chapter. Chapter 4 focuses on the preparation and characterization of patterned, 3-dimensional proton exchange membranes. The influence of surface area on power output of fuel cells is demonstrated in this chapter. By using macromonomer precursors of different molecular weights, cross-link density of the PEMs can be systematically controlled. In Chapter 5, the effects of cross-link density on the properties of PEMs are discussed. Some future directions are discussed in Chapter 6.

1.5 References:

(1) Appleby, A. J.; Foulkes, R. L. *Fuel Cell Handbook*; Van Nostrand Reinhold: New York, **1989**.

(2) Whittingham, M. S.; Savinell, R. F.; Zawodzinski, T. A. *Chem. Rev.* **2004**, *104*, 4243-4244.

(3) Malhotra, S.; Datta, R. J. *J. Electrochem. Soc.* **1997**, *144*, L23-L26.

(4) Scott, K.; Shukla, A. K. *Reviews in Environmental Science and Bio-Technology* **2004**, *3*, 273-280.

(5) Minh, N. Q. In *Electronic Materials Chemistry*; Pogge, H. B., Ed.; Marcel Dekker, Inc: New York, **1996**.

(6) Perry, M. L.; Fuller, T. F. *J. Electrochem. Soc.* **2002**, *149*, S59-S67.

(7) Alkire, R. C.; Gerischer, H.; Kolb, D. M.; Tobias, C. W., Eds. *Advances in Electrochemical Science and Engineering*; Johy Wiley & Sons: New York, **2002.**

(8) www. eere.energy.gov.

(9) Hickner, M. A.; Ghassemi, H.; Kim, Y. S.; Einsla, B. R.; McGrath, J. E. *Chem. Rev.* **2004**, *104*, 4587-4612.

(10) Mauritz, K. A.; Moore, R. B. *Chem. Rev.* **2004**, *104*, 4535-4585.

(11) Heitner-Wirguin, C. *J. Membr. Sci.* **1996**, *120*, 1-33.

(12) Grot, W. G. (E. I. DuPont) US 4,433,082, **1984**.

(13) Steck, A.; Yeager, H. L. *Anal. Chem.* **1979**, *51*, 862-865.

(14) Zawodzinski, T. A.; Derouin, C.; Radzinski, S.; Sherman, R. J.; Springer, T.; Gottesfeld, S. *J. Electrochem. Soc.* **1993**, *140*, 1041-1047.

(15) Zawodzinski, T. A.; Lopez, C.; Jestel, R.; Valerio, J.; Gottesfeld, S. *J. Electrochem. Soc.* **1993**, *140*, 1981-1985.

(16) Pushpa, K. K.; Nandan, D.; Iyer, R. M. *J. Chem. Soc., Faraday Trans 1* **1988**, *84*, 2047-2056.

(17) Zaluski, C.; Xu, G. *Macromolecules* **1994**, *27*, 6750-6754.

(18) Randin, J. P. *J. Electrochem. Soc.* **1982**, *129*, 1215-1220.

(19) Ren, X.; Springer, T. E.; Gottesfeld, S. *J. Electrochem. Soc.* **2000**, *147*, 92-98.

(20) Sone, Y.; Ekdunge, P.; Simonsson, D. *J. Electrochem. Soc.* **1996**, *143*, 1254-1259.

(21) Zawodzinski, T. A.; Neeman, M.; Sillerud, L.; Gottesfeld, S. *J. Phys. Chem.* **1991**, *95*, 6040-6044.

(22) Choi, P.; Jalani, N. H.; Datta, R. *J. Electrochem. Soc.* **2005**, *152*, E123-E130.

(23) Doyle, M.; Lewittes, M. E.; Roelofs, M. G.; Perusich, S. A.; Lowrey, R. E. *J. Membr. Sci.* **2001**, *184*, 257-273.

(24) Doyle, M.; Lewittes, M. E.; Roelofs, M. G.; Perusich, S. A. *J. Phys. Chem. B* **2001**, *105,* 9387-9394.

(25) Hsu, W. Y.; Gierke, T. D. *J. Membr. Sci.* **1983**, *13*, 307-326.

(26) Roche, E. J.; Pineri, M.; Duplessix, R.; Levelut, A. M. *J. Polym. Sci. , Polym. Phys. Ed.* **1981**, *19*, 1-11.

(27) Roche, E. J.; Pineri, M.; Duplessix, R. *J. Polym. Sci. , Polym. Phys. Ed.* **1982**, *20*, 107-116.

(28) Manley, D. S.; Williamson, D. L.; Noble, R. D.; Koval, C. A. *Chem. Mater.* **1996**, *8*, 2595-2600.

(29) Xue, T.; Trent, J. S.; Osseo-Asare, K. *J. Membr. Sci.* **1989**, *45*, 261-271.

(30) Ceynowa, J. *Polymer* **1978**, *19*, 73-76.

(31) Rieberer, S.; Norian, K. H. *Ultramicroscopy* **1992**, *41*, 225-233.

(32) Lehmani, A.; Durand-Vidal, S.; Turq, P. *J. Applied. Polymer. Sci.* **1998**, *68*, 503-508.

(33) McLean, R. S.; Doyle, M.; Sauer, B. B. *Macromolecules* **2000**, *33*, 6541-6550.

(34) James, P. J.; McMaster, T. J.; Newton, J. M.; Miles, M. J. *Polymer* **2000**, *41*, 4223-4231.

(35) Hsu, W. Y.; Gierke, T. D. *Macromolecules* **1982**, *15*, 101-105.

(36) Yeager, H. L.; Steck, A. *J. Electrochem. Soc.* **1981**, *128*, 1880-1884.

(37) Hsu, W. Y.; Barkley, J. R.; Meakin, P. *Macromolecules* **1980**, *13*, 198-200.

(38) Rikukawa, M.; Sanui, K. *Prog. Polym. Sci.* **2000**, *25*, 1463-1502.

(39) Gil, M.; Ji, X.; Li, X.; Na, H.; Hampsey, J. E.; Lu, Y. *J. Membr. Sci.* **2004**, *234*, 75-81.

(40) Savadogo, O. *J. New. Mater. Electrochem. Syst.* **1998**, *1*, 47-51.

(41) Gottesfeld, S.; Zawodzinski, T. A. In *Advances in Electrochemical Science and Engineering*; Alkire, R. C.; Gerischer, H.; Kolb, D. M.; Tobias, C. W., Eds.; Johy Wiley & Sons: New York, **2002**.

(42) Si, Y.; Kunz, H. R.; Fenton, J. M. *J. Electrochem. Soc.* **2004**, *151*, A623-A631.

(43) Cruickshank, J.; Scott, K. *J. Power Sources* **1998**, *70*, 40-47.

(44) Kerres, J.; Cui, W.; Reichle, S. *J. Polym. Sci., Part A: Poly. Chem.* **1996**, *34*, 2421-2438.

(45) Karlsson, L. E.; Jannasch, P. *J. Membr. Sci.* **2004**, *230*, 61-70.

(46) Miyatake, K.; Chikashige, Y.; Watanabe, M. *Macromolecules* **2003**, *36*, 9691-9693.

(47) Chikashige, Y.; Chikyu, Y.; Miyatake, K.; Watanabe, M. *Macromolecules* **2005**, *38,* 7121-7126.

(48) Wang, F.; Hickner, M.; Kim, Y. S.; Zawodzinski, T. A.; McGrath, J. E. *J. Membr. Sci.* **2002**, *197*, 231-242.

(49) Nolte, R.; Ledjeff, K.; Bauer, M.; Mulhaupt, R. *J. Membr. Sci.* **1993**, *83*, 211-220.

(50) Kerres, J.; Cui, W.; Junginger, M. *J. Membr. Sci.* **1998**, *139*, 227-241.

(51) Kerres, J.; Cui, W.; Disson, R.; Neubrand, W. *J. Membr. Sci.* **1998**, *139*, 211-225.

(52) Kim, Y. S.; Wang, F.; Hickner, M.; Zawodzinski, T. A.; McGrath, J. E. *J. Membr. Sci.* **2003**, *212*, 263-282.

(53) Kim, Y. S.; Wang, F.; Hickner, M.; Mccartney, S.; Hong, Y. T.; Harrison, W.; Zawodzinski, T. A.; Mcgrath, J. E. *J. Polym. Sci., Part B: Poly. Phys.* **2003**, *41*, 2816-2828.

(54) Kobayashi, T.; Rikukawa, M.; Sanui, K.; Ogata, N. *Solid State Ionics* **1998**, *106*, 219-225.

(55) Xing, P.; Robertson, G. P.; Guiver, M. D.; Mikhailenko, S. D.; Kaliaguine, S. *Macromolecules* **2004**, *37*, 7960-7967.

(56) Roziere, J.; Jones, D. J. *Annu. Rev. Mater. Res.* **2003**, *33*, 503-555.

(57) Kopitzke, R. W.; Linkous, C. A.; Anderson, H. R.; Nelson, G. L. *J. Electrochem. Soc.* **2000**, *147*, 1677-1681.

(58) Helmer-Metzmann, F.; Osan, F.; Schneller, A.; Ritter, H.; Ledjeff, K.; Nolte, R.; Thorwirth, R.; Hoechst A. US 5,438,082, **1995**.

(59) Mikhailenko, S. D.; Wang, K.; Kaliaguine, S.; Xing, P.; Robertson, G. P.; Guiver, M. D. *J. Membr. Sci.* **2004**, *233*, 93-99.

(60) Zaidi, S. M. J.; Mikhailenko, S. D.; Robertson, G. P.; Guiver, M. D.; Kaliaguine, S. *J. Membr. Sci.* **2000**, *173*, 17-34.

(61) Swier, S.; Ramani, V.; Fenton, J. M.; Runz, H. R.; Shaw, M. T.; Weiss, R. A. *J. Membr. Sci.* **2005**, *256*, 122-133.

(62) Kerres, J.; Ullrich, A.; Meier, F.; Haring, T. *Solid State Ionics* **1999**, *125*, 243-249.

(63) Genies, C.; Mercier, R.; Sillion, B.; Cornet, N.; Gebel, G.; Pineri, M. *Polymer* **2001**, *42*, 359-373.

(64) Yin, Y.; Fang, J.; Watari, T.; Tanaka, K.; Kita, H.; Okamoto, K.-I. *J. Mater. Chem.* **2004**, *14*, 1062-1070.

(65) Einsla, B. R.; Kim, Y. S.; Hickner, M. A.; Hong, Y.-T.; Hill, M. L.; Pivovar, B. S.; McGrath, J. E. *J. Membr. Sci.* **2005**, *255*, 141-148.

(66) Okamoto, K.-I.; Yin, Y.; Yamada, O.; Islam, M. N.; Honda, T.; Mishima, T.; Suto, Y.; Tanaka, K.; Kita, H. *J. Membr. Sci.* **2005**, *258*, 115-122.

(67) Fang, J.; Guo, X.; Harada, S.; Watari, T.; Tanaka, K.; Kita, H.; Okamoto, K. I. *Macromolecules* **2002**, *35*, 9022-9028.

(68) Miyatake, K.; Zhou, H.; Matsuo, T.; Uchida, H.; Watanabe, M. *Macromolecules* **2004**, *37*, 4961-4966.

(69) Asano, N.; Miyatake, K.; Watanabe, M. *Chem. Mater.* **2004**, *16*, 2841-2843.

(70) Miyatake, K.; Asano, N.; Watanabe, M. *J. Polym. Sci. , Part A: Polym. Chem.* **2003**, *41*, 3901-3907.

(71) Einsla, B. R.; Hong, Y.-T.; Kim, Y. S.; Wang, F.; Gunduz, N.; McGrath, J. E. *J. Polym. Sci. , Part A: Polym. Chem.* **2004**, *42*, 862-874.

(72) Staiti, P.; Lufrano, F.; Arico, A. S.; Passalacuqua, E.; Antonucci, V. *J. Membr. Sci.* **2001**, *188*, 71-78.

(73) Hoel, D.; Grunwald, E. *J. Phys. Chem.* **1977**, *81*, 2135-2136.

(74) Glipa, X.; Haddad, M. E.; Jones, D. J.; Roziere, J. *Solid State Ionics* **1997**, *97*, 323-331.

(75) Glipa, X.; Bonnet, B.; Mula, B.; Jones, D. J.; Roziere, J. *J. Mater. Chem.* **1999**, *9*, 3045-3049.

(76) Li, Q.; Hjuler, H. A.; Bjerrum, N. J. *J. Appl. Electrochem.* **2001**, *31*, 773-779.

(77) Xiao, L.; Zhang, H.; Scanlon, E.; Ramanathan, L. S.; Choe, E. W.; Rogers, D.; Apple, T.; Benicewicz, B. C. *Chem. Mater.* **2005**, *17*, 5328-5333.

(78) Chen, S. L.; Krishnan, L.; Srinivasan, S.; Benziger, J.; Bocarsly, A. B. *J. Membr. Sci.* **2004**, *243*, 327-333.

(79) Carretta, N.; Tricoli, V.; Picchioni, F. *J. Membr. Sci.* **2000**, *166*, 189-197.

(80) Wei, J.; Stone, C.; Steck, A. E. (Ballard Power Systems, Inc) US 5,422,411, **1995**.

(81) Edmondson, C. A.; Fontanella, J. J.; Chung, S. H.; Greenbaum, S. G.; Wnek, G. E. *Electrochim. Acta.* **2001**, *46*, 1623-1628.

(82) Kim, J.; Kim, B.; Jung, B.; Kang, Y. S.; Ha, K. Y.; Oh, I.-H.; Ihn, K. J. *Macromol. Rapid Commun.* **2002**, *23*, 753-756.

(83) Mokrini, A.; Acosta, J. L. *Polymer* **2001**, *42*, 9-15.

(84) Elabd, Y. A.; Napadensky, E.; Sloan, J. M.; Crawford, D. M.; Walker, C. W. *J. Membr. Sci.* **2003**, *217*, 227-242.

(85) Elabd, Y. A.; Walker, C. W.; Beyer, F. L. *J. Membr. Sci.* **2004**, *231*, 181-188.

(86) Ding, J.; Chuy, C.; Holdcroft, S. *Chem. Mater.* **2001**, *13*, 2231-2233.

(87) Ding, J.; Chuy, C.; Holdcroft, S. *Macromolecules* **2002**, *35*, 1348-1355.

(88) Ding, J.; Chuy, C.; Holdcroft, S. *Adv. Funct. Mater.* **2002**, *12*, 389-394.

(89) Navessin, T.; Eikerling, M.; Wang, Q.; Song, D.; Liu, Z.; Horsfall, J.; Lovell, K. V.; Holdcroft, S. *J. Electrochem. Soc.* **2005**, *152*, A796-A805.

(90) Shen, M.; Roy, S.; Kuhlmann, J. W.; Scott, K.; Lovell, K.; Horsfall, J. A. *J. Membr. Sci.* **2005**, *251*, 121-130.

(91) Vie, P.; Paronen, M.; Stromgard, M.; Rauhala, E.; Sundholm, F. *J. Membr. Sci.* **2002**, *204*, 295-301.

(92) Soresi, B.; Quartarone, E.; Mustarelli, P.; Magistris, A.; Chiodelli, G. *Solid State Ionics* **2004**, *166*, 383-389.

(93) Büchi, F. N.; Gupta, B.; Hass, O.; Scherer, G. G. *Electrochem. Acta.* **1995**, *40*, 345-353.

(94) Schmidt, T. J.; Simbeck, K.; Scherer, G. G. *J. Electrochem. Soc.* **2005**, *152*, A93-A97.

(95) Bae, B.; Ha, H. Y.; Kim, D. *J. Membr. Sci.* **2006**, *276*, 51-58.

(96) Wainright, J. S.; Wang, J. T.; Weng, D.; Savinell, R. F.; Litt, M. *J. Electrochem. Soc.* **1995**, *142*, L121-L123.

(97) Samms, S. R.; Wasmus, S.; Savinell, R. F. *J. Electrochem. Soc.* **1996**, *143*, 1225-1232.

Chapter 2

SYNTHESIS AND CHARACTERIZATION OF PRECURSOR MATERIALS

2.1 Introduction

Perfluoropolyethers (PFPEs) are low molecular weight highly fluorinated oils which exhibit unique properties. Like many other fluoropolymers, PFPE materials have exceptionally low surface energy and high chemical stability due to the existence of C-F moieties. Moreover, PFPE materials display hydrophobic and lipophobic behavior and outstanding thermal stability. Unlike other fluoropolymers, however, the glass transition temperature of PFPEs is very low, typically in the range of -120 to -70 °C.[1] Therefore, PFPEs are oil-like liquids at room temperature with high spreading ability. Functionalized PFPEs can be thermally or photo-chemically cross-linked[2] to yield highly fluorinated, chemically and thermally robust elastomers. Due to these unique properties, α, ω-methacryloxy functionalized PFPE (PFPE_DMA) has been developed[2,3] and used as high performance materials in microfluidic device,[4] high-resolution soft lithograpy,[5] and fabrication of monodisperse and shape-specific nano-materials.[6]

With exceptionally high thermal stability and chemical resistance, functionalized PFPEs with proton conducting sites are suitable for use as proton exchange membranes. Upon cross-linking, reactive liquid precursors can be easily transformed into solid membranes of desired dimensions. By using soft lithography[7] techniques, patterned membranes with unprecedented levels of morphologic control can be achieved starting from functionalized liquid precursors. In order to obtain a curable PFPE that is stable under hydrolysis and fuel cell operation conditions, a styrenically functionalized perfluoropolyether (sPFPE) is developed (Figure 2.1) and used in conjunction with a precursor containing proton conducting sites.

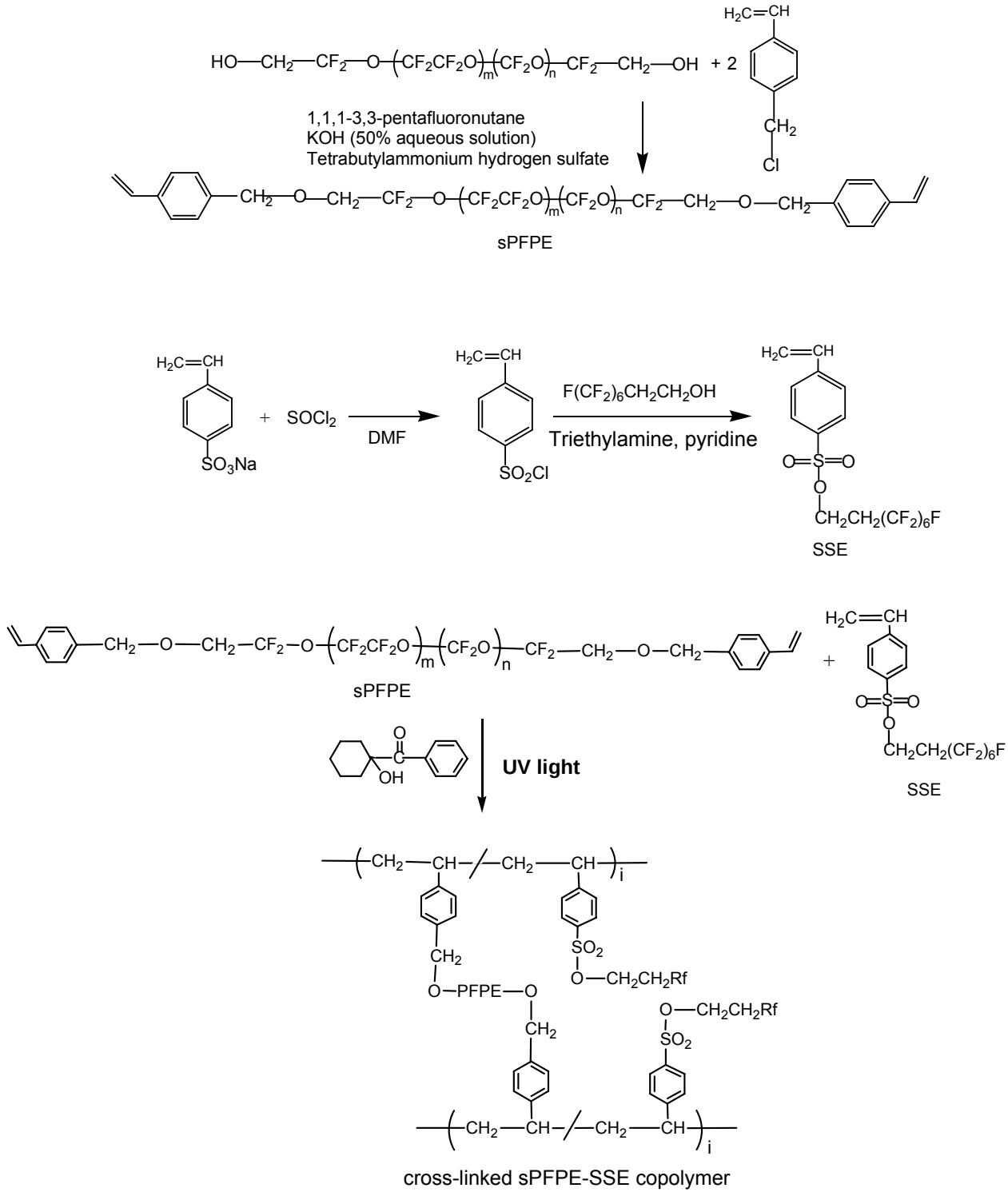

Figure 2.1 Synthesis routes for sPFPE precursor, SSE precursor and cross-linked sPFPE-SSE copolymer membranes.

Aromatic sulfonic acid functionalities are widely used as proton conducting sites in proton exchange membranes.[8] Sodium *p*-styrene sulfonate is commercially available and the reactivity of styrene groups is comparable to that of styrenically functionalized PFPE. However, it is not miscible with PFPE due to their very different chemical natures. In order to make a styrene sulfonic acid precursor that can form a single phase mixture with PFPE, sodium *p*-styrene sulfonate needed to be first converted to 4-vinyl benzenesulfonyl chloride. A fluorinated styrene sulfonate ester (SSE) monomer was then prepared by reacting 4-vinyl benzenesulfonyl chloride with a fluorinated alcohol. The synthesis procedure of sPFPE and SSE are shown in Figure 2.1.

The fluorinated SSE monomer can form single phase mixtures with sPFPE with 30-70 wt% SSE. Upton photo-chemical or thermal curing, the liquid mixtures become chemically cross-linked membranes, which can be hydrolyzed to serve as proton exchange membranes. Without hydrolysis, the sPFPE-SSE membranes are highly fluorinated elastomers with many desirable features for applications as low surface energy, super-hydrophobic materials. This chapter will discuss the synthesis of these precursor materials and the properties of the sPFPE-SSE membranes. The mechanical strength of this network material depends on its composition, with higher SSE content rendering higher modulus. Due to the highly fluorinated nature, the membranes exhibit very low surface energy and high static contact angle with water. Membranes with nano-scale patterned structures on the surface can be prepared by imprint lithography/micro-molding techniques.[5,7] Effects of topographical architectures and surface roughness on the surface properties of the cured membranes were also studied.

2.2 Experimental

2.2.1 Materials

Poly(tetrafluoroethylene oxide-*co*-difluoromethylene oxide) (PFPE) α-, ω- diol with an number average molecular weight of 3800 g/mol was purchased from Solvay Solexis. 1, 1, 1, 3, 3-pentafluorobutane was obtained from Solvay Fluoride. All other chemicals were purchased from Aldrich unless otherwise noted.

2.2.2 Synthesis of sPFPE

In order to incorporate crosslinkable functionality, a styrene linkage was added to both chain ends of PFPE α-, ω- diol by a phase transfer catalyzed reaction. In a typical synthesis, PFPE α-, ω- diol (30 g, 7.89 mmol), 1, 1, 1, 3, 3-pentafluorobutane (30 mL), and tetrabutylammonium hydrogensulfate (1.5g, 4.42 mmol) were added into a round bottom flask. KOH (15g, 0.27 mol) dissolved in deionized water (30 mL) was then added under stirring. After addition of 4-vinylbenzyl chloride (3 mL, 17.2 mmol), the reaction mixture was allowed to stir vigorously at 45 ^{o}C for 48 h. The product was filtered to remove the brown solid, and the resulting solution was washed with deionized water three times and stirred with carbon black for 10 h. The mixture was passed through a 0.22 μm filter to remove the carbon black and vacuum dried at room temperature to remove the solvent. The resulting product (sPFPE) is a clear viscous liquid, whose structure is shown in Figure 2.1.

2.2.3 Synthesis of SSE

4-Vinyl benzenesulfonyl chloride was synthesized by the following procedure.[9] Sodium *p*-styrene sulfonate (26.3g, 128 mmol) was added to thionyl chloride (70 mL) under

Ar flow in small portions with stirring. Dry *N*, *N*-dimethylformamide (35 mL) was added to the resulting suspension dropwise. The reaction mixture became homogeneous, and it was stirred for 6 h at room temperature. The reaction mixture was kept in a refrigerator overnight and poured into ice water to quench unreacted thionyl chloride. The aqueous solution was extracted three times with diethyl ether, and the combined ether layer was washed with 10% NaCl solution 3 times and then dried over $MgSO_4$ for 1 h. $MgSO_4$ was then filtered out and diethyl ether was removed by vacuum evaporation. The resulting product is a yellow liquid and not miscible with PFPE.

In order to make a styrene sulfonic acid precursor that is miscible with sPFPE, a fluorinated styrene sulfonate ester was synthesized by reacting 4-vinyl benzenesulfonyl chloride with a fluorinated alcohol. To a round bottom flask, 4-vinyl benzenesulfonyl chloride (7.6 g, 37.5 mmol), 3,3,4,4,5,5,6,6,7,7,8,8,8-tridecafluoro-1-octanol (13.66 g, 37.5 mmol), triethylamine (10 mL), and pyridine (20 mL) were added under Ar flow. The resulting slurry was stirred at room temperature for 20 h. The reaction mixture was then poured into excess hydrochloric acid-ice bath to quench the triethylamine. The aqueous solution was extracted with diethyl ether three times, and the combined ether layer was washed sequentially with water, 10% NaOH solution, and 10% NaCl solution. The ether solution was then dried over $MgSO_4$ for 1 h. $MgSO_4$ was filtered out, and diethyl ether was removed by vacuum evaporation. The resulting product, a fluorinated styrene sulfonate ester, is a waxy yellow solid whose structure is shown in Figure 2.1.

2.2.4 Membrane preparation by UV/thermal curing

To make a cross-linked membrane, sPFPE with 1wt% photo-initiator (1-hydroxycyclohexyl phenyl ketone) or thermal initiator (perkadox) and SSE were mixed in the desired ratio. The mixture was heated above 40 ^{o}C to form a homogeneous yellow liquid. The liquid precursor was poured onto a preheated glass slide and then chemically cross-linked by irradiation with UV light (λ=365 nm) for 40 min or heat treatment at 80 ^{o}C for 1 h under inert atmosphere. The resulting solid membrane sPFPE-SSE is in the ester form, transparent and slightly yellow.

2.2.5 Preparation of sPFPE-SSE nanopillars

In order to make membranes with high aspect ratio nano-structures, sPFPE (40 wt%) and SSE (60 wt%) with 1 wt% photo-initiator (1-hydroxycyclohexyl phenyl ketone) were mixed at 80 ^{o}C. The liquid precursor was then transferred on top of a porous anodic aluminum oxide (p-AAO) template with different aspect ratios that was prepared by Dr. Lei Zhang. The liquid precursor was cured by exposing to UV light (λ=365 nm) for 40 min under nitrogen purge. The resulting solid membrane was peeled off the p-AAO template.

2.2.6 Characterization techniques

Nuclear Magnetic Resonance (NMR) spectra were taken using a Bruker 400 MHz DRX spectrometer. Samples of sPFPE were dissolved in 1, 1, 1, 3, 3-pentafluorobutane with a few percent of added $CDCl_3$ (Cambridge Isotope Labs). Other samples were prepared by dissolving in $CDCl_3$.

The thermal stability of the membranes was measured by a Perkin-Elmer Pyris 1 thermogravimetric analyzer (TGA). All the samples were heated from room temperature to 500 ^{o}C in a nitrogen atmosphere with a heating rate of 10 ^{o}C/min. The onset of rapid weight loss was defined as the decomposition temperature.

Dynamic mechanical and thermal analysis (DMTA) measurements were performed with a 210 Seiko dynamic mechanical spectroscopy (DMS) instrument, operating at fixed frequency and film tension mode. The frequency used was 1 Hz and the temperature was varied from –140 to 350 ^{o}C at a heating rate of 2 ^{o}C/min. The mechanical properties of the cross-linked membranes were measured by an Instron 5566 instrument at ambient conditions.

Static contact angles were measured using a KSV Instrument LTD CAM 200 Optical Contact Angle Meter. A screw-top syringe (Fisher) was used to deposit a small drop of fluid onto a substrate. Contact angles were then calculated using the instrument software.

Scanning electron microscope (SEM) images were taken by a Hitachi S4700 SEM. In order to obtain high quality images, samples were coated with a thin layer of gold (around 10 nm) using a standard sputter-coater (Cressington 108 auto).

2.3 Results and discussion

2.3.1 Synthesis

In order to incorporate crosslinkable functionality that was deemed to be more robust than methacryloxy groups, a styrene linkage was added to both chain ends of PFPE α-, ω-diol by a phase transfer catalyzed reaction. The ^{1}H NMR spectrum of the styrenically functionalized PFPE (sPFPE) is shown in Figure 2.2. As shown in this figure, the peak at 3.82 ppm corresponds to the methylene protons from PFPE next to the ether linkage (2H, -

CF_2-C***H***$_2$-O-). The peak at 4.65 ppm corresponds to the methylene protons in between the ether linkage and the aromatic ring structure (2H, -O-C***H***$_2$-ϕ-). The vinyl protons appeared at 5.25 ppm, 5.80 ppm (vinyl, =C***H***$_2$) and 6.75 ppm (vinyl, -C***H***=CH_2), respectively. The peaks between 7.25 and 7.45 ppm (4H, aromatic) correspond to protons on the aromatic ring.

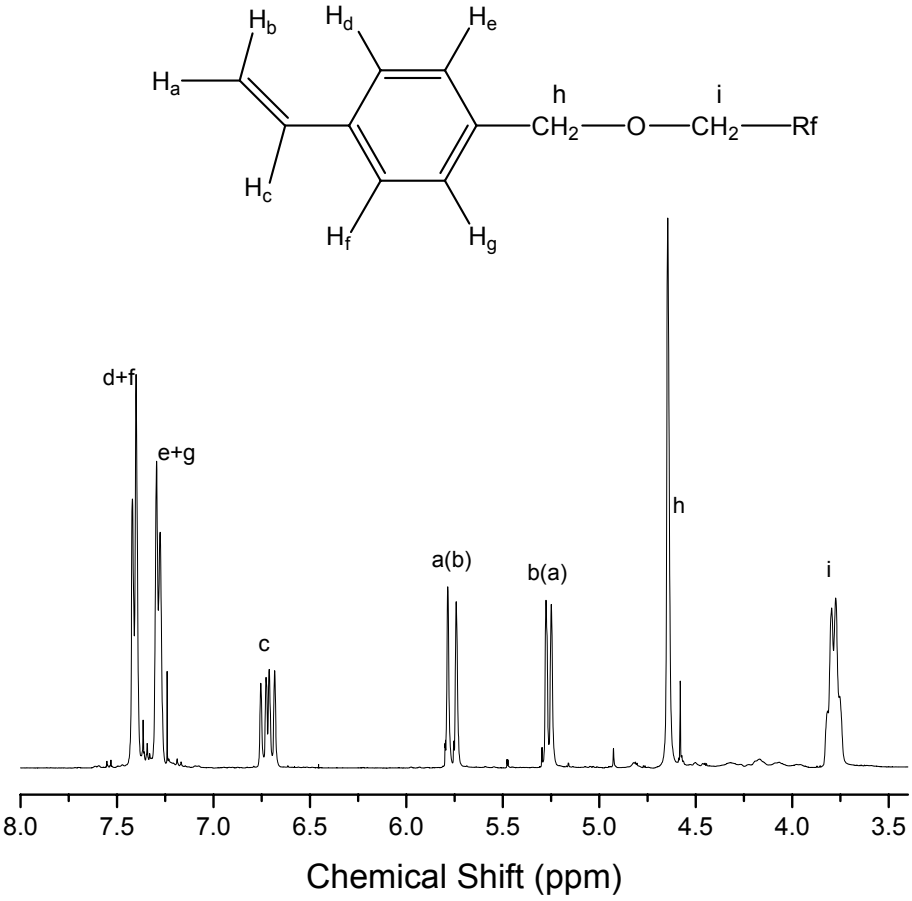

Figure 2.2 ^{1}H NMR spectrum of styrenically functionalized PFPE (sPFPE)

In order to make a styrene sulfonic acid precursor that can form a single phase mixture with PFPE, sodium *p*-styrene sulfonate was first converted to 4-vinyl benzenesulfonyl chloride by reacting with thionyl chloride. The ^{1}H NMR spectra of sodium

p-styrene sulfonate and 4-vinyl benzenesulfonyl chloride are shown in Figure 2.3. Compared to sodium *p*-styrene sulfonate, the peaks of 4-vinyl benzenesulfonyl chloride shift downfield. The vinyl protons shift from 5.30 ppm, 5.85 ppm (vinyl, =C***H***$_2$) and 6.73 ppm (vinyl, -C***H***=CH_2) in sodium *p*-styrene sulfonate to 5.55 ppm, 5.96 ppm (vinyl, =C***H***$_2$) and 6.80 ppm (vinyl, - C***H***=CH_2), respectively. The aromatic protons also shift downfield to 7.55-8.05 ppm (4H, aromatic).

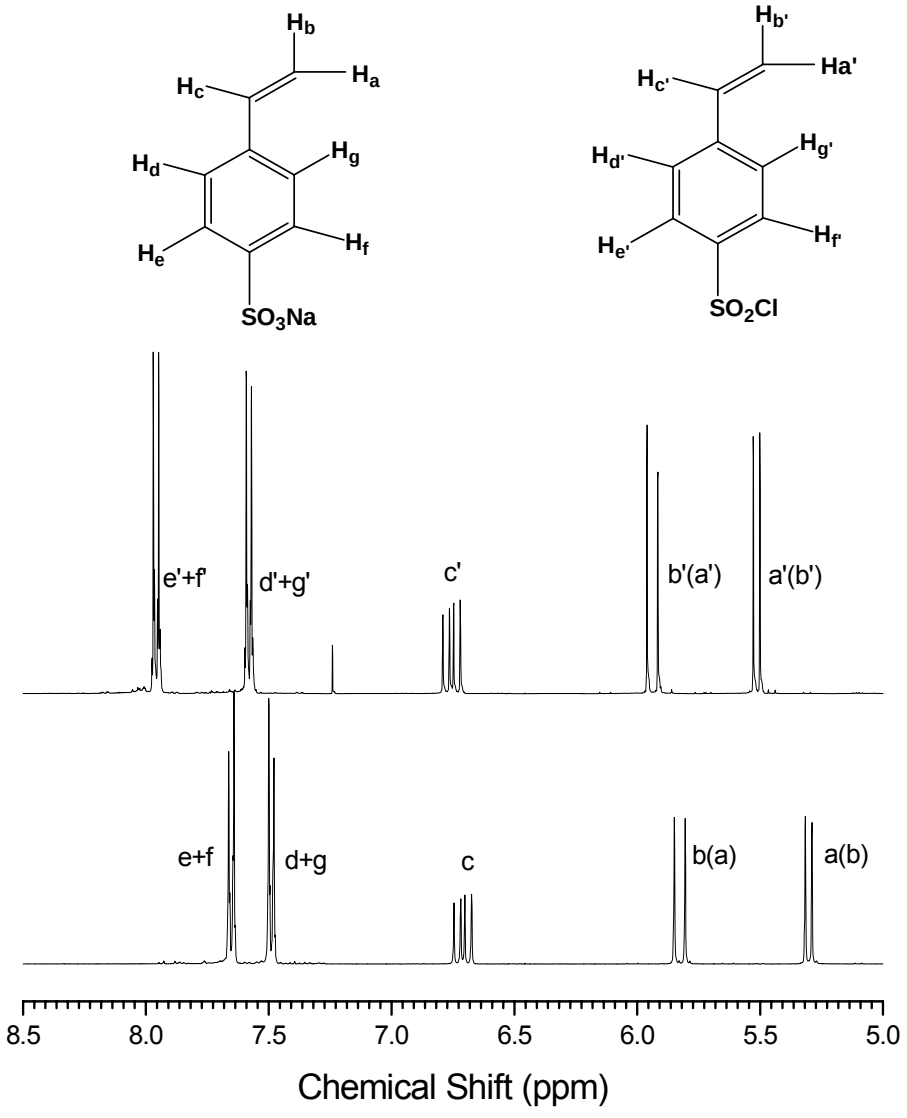

Figure 2.3 ^{1}H NMR spectra of sodium *p*-styrene sulfonate and styrene sulfonyl chloride

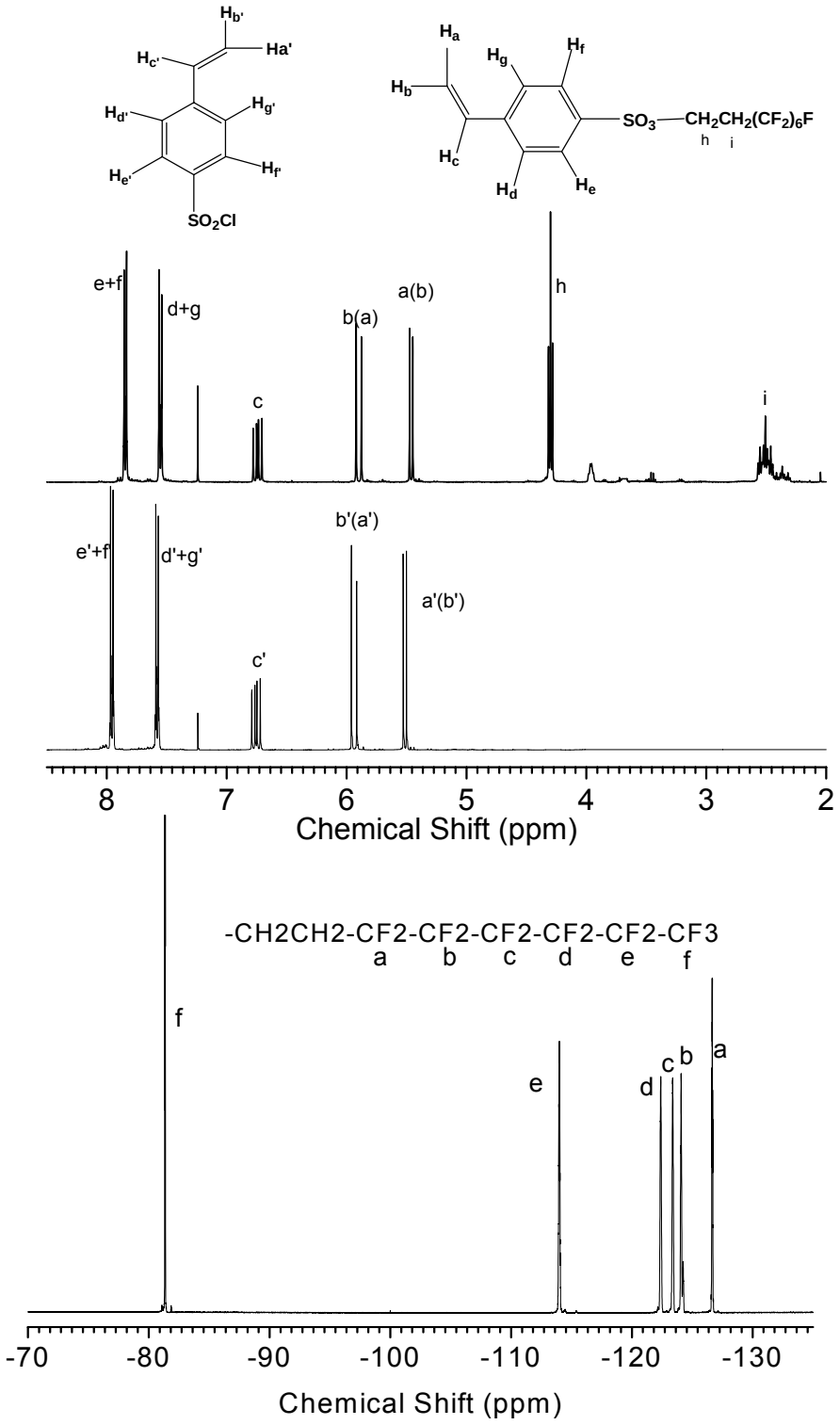

Figure 2.4 ^{1}H and ^{19}F NMR spectra of fluorinated styrene sulfonate ester (SSE) monomer

However, the 4-vinyl benzenesulfonyl chloride was found to not be miscible with sPFPE either, and some fluorocarbon moiety was necessary to form a homogeneous mixture with sPFPE. This was achieved by reacting 4-vinyl benzenesulfonyl chloride with a fluorinated alcohol to afford a fluorinated styrene sulfonate ester (SSE) monomer as shown in Figure 2.1. The ^{1}H NMR spectra of SSE and 4-vinyl benzenesulfonyl chloride are compared in Figure 2.4. Due to the formation of ester functionality, the resonance peaks of the vinyl protons and aromatic protons slightly shift to upfield. Moreover, two more peak are observed at 4.30 ppm (2H, -O-C***H***$_2$-CH_2-) and 2.50 ppm (2H, -O-CH_2-C***H***$_2$-CF_2-), respectively, corresponding to the methylene protons from the fluorinated alcohol. The ^{19}F NMR spectrum of the fluorinated SSE is also shown in Figure 2.4.

SSE and sPFPE was found to form a homogeneous single phase mixture with 30-70 wt% SSE. At temperature above 40 ^{o}C, the mixture is a clear yellow liquid. Cross-linked membranes were prepared by curing the mixtures photochemically or thermally under inert atmosphere. Since the polymerization functionalities were styrenic groups for both sPFPE and SSE precursors, their reactivity ratio should be around one and the composition of the cured membrane should be the same as that of the liquid precursor mixture. Five samples with 30 wt%, 40 wt%, 50 wt%, 60wt%, and 70wt% sPFPE were prepared and their thermal, mechanical and surface properties are discussed below.

2.3.2 Thermal and mechanical properties

The thermal stability of the cured sPFPE-SSE membranes was tested by TGA and the result is shown in Figure 2.5. Independent of the membrane composition, all five samples

displayed a decomposition temperature (5wt% weight loss) at 301 ^{o}C, indicating good thermal stability of the cross-linked sPFPE-SSE copolymers.

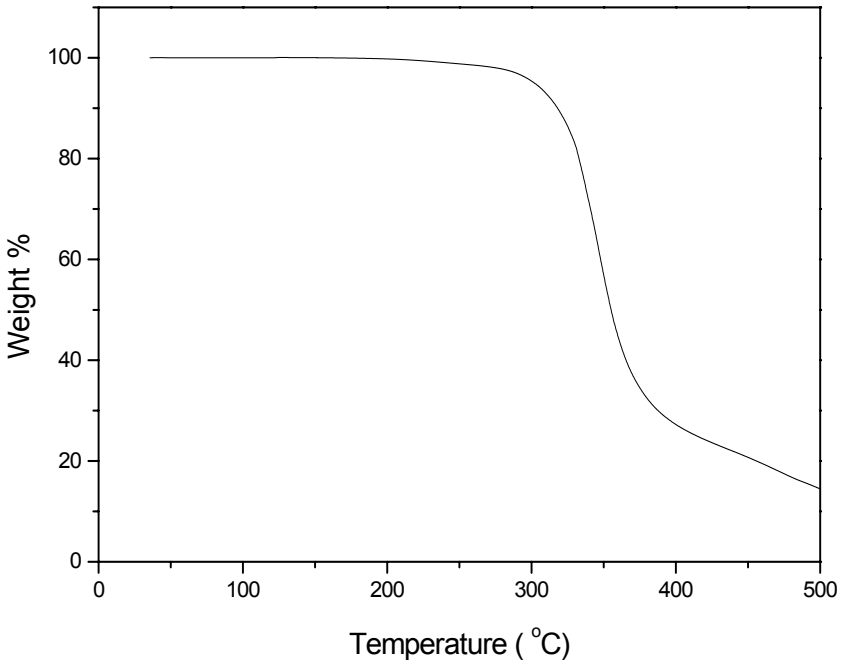

Figure 2.5 TGA curve of the cross-linked sPFPE-SSE membranes

DMTA methods have been very useful for the analysis of the phase behavior of the polymer studied. While phase separation of cross-linked materials is hard to detect as separate glass transitions by differential scanning calorimetry (DSC), it usually corresponds with clear thermo-mechanical transitions in DMTA measurements. The DMTA curves of cross-linked sPFPE-SSE membranes are shown in Figure 2.6. The glass transition temperature (Tg) of polystyrene is 100 ^{o}C.[10] Due to the longer side chain and larger barrier to rotation, the glass transition temperature of SSE homopolymer should be higher than 100 ^{o}C,

while the Tg of sPFPE is -120 ^{o}C. As shown in Figure 2.6, a broad transition was observed for all the samples at temperatures between -85 to 100 ^{o}C, which is between the glass transition temperatures of sPFPE and SSE homopolymers. The presence of only one transition in DMTA measurements that was in between the glass transition temperatures of the precursor materials confirmed that sPFPE and SSE were miscible with each other and formed homogeneous mixtures at various ratios. As the content of SSE increased, the transition temperature of the cured membrane increased due to the bigger molecular rotation barrier.

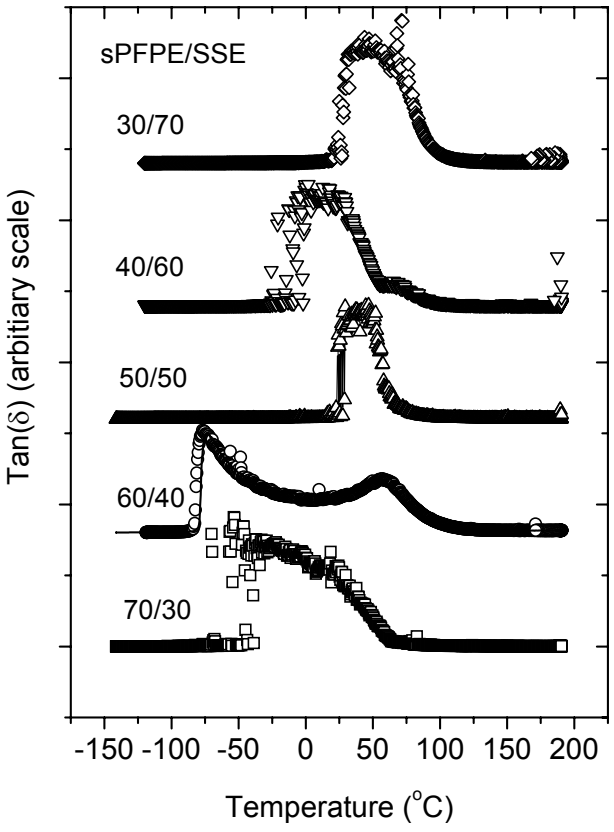

Figure 2.6 DMTA spectra of the cross-linked sPFPE-SSE membranes

The mechanical properties of the membrane materials were characterized by an Instron instrument. Figure 2.7 shows the stress-strain curves of the cured membranes. The membranes displayed elastomeric properties, elongating to a significant extent after yield, and typically breaking above 12% tensile strain. The Young's modulus, tensile stress (σ) and tensile strain (γ) of the cross-linked membranes are summarized in Table 2.1. The cured sPFPE homopolymer displayed typical properties of an elastomer, having a Young's modulus of 2 MPa and a tensile strain of 43% at break. When SSE monomer was included in the network, the cured membranes started to lose their elastomeric features and showed a higher modulus. As the SSE content increased from 30 wt% to 70 wt%, the Young's modulus increased from 15 MPa to 144 MPa, while the tensile strain at break decreased from 23% to 12%.

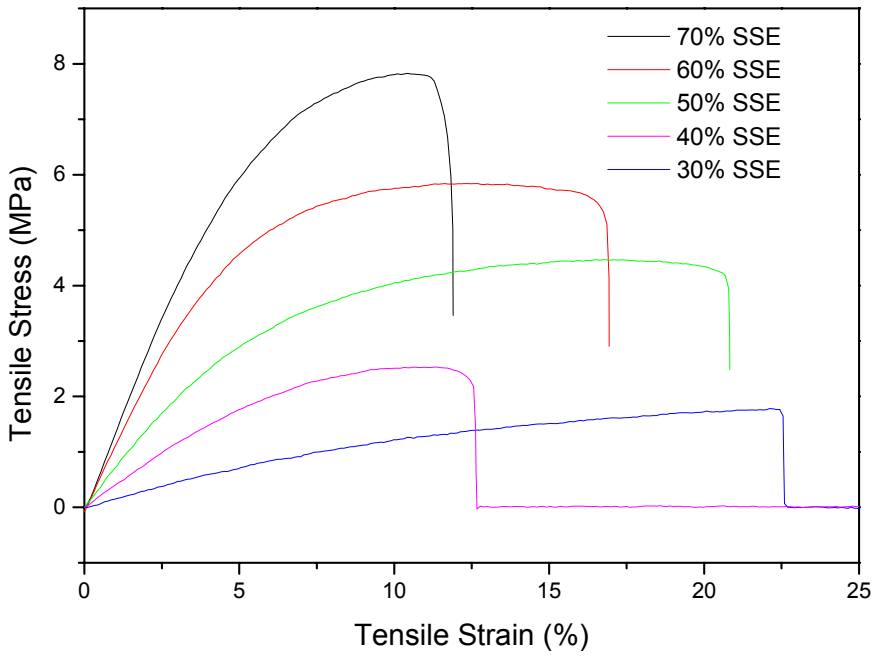

Figure 2.7 Stress-Strain curves of cross-linked sPFPE-SSE membranes

Sample	sPFPE (wt%)	SSE (wt%)	E (MPa)	σ at break (MPa)	γ at break (%)
1	100	0	2	0.13	43
2	70	30	15	1.78	23
3	60	40	39	2.53	13
4	50	50	66	4.47	21
5	40	60	114	5.84	17
6	30	70	144	7.83	12

Table 2.1 Mechanical properties of cross-linked sPFPE-SSE membranes

2.3.3 Surface properties

The surface properties of the cured sPFPE homopolymer and sPFPE-SSE membranes were characterized by static contact angle measurements. Tests were performed with a series of *n*-alkanes having a variety of surface tensions. Six different *n*-alkanes were used and the number of carbons equaled to 6, 8, 10, 12, 14, and 16, respectively. The surface energy of the cured sPFPE homopolymer and sPFPE-SSE membranes was quantified by using Zisman analysis.

In preparing the membrane samples by UV-curing, one surface of the sample was in contact with nitrogen while the other surface was in contact with a glass slide. In order to understand the effect of contacting surfaces on the properties of the resulting samples, both surfaces of the cured sPFPE homopolymer were characterized. Table 2.2 lists the static contact angle results for the fully cured sPFPE surfaces in contact with nitrogen and glass

during curing. By Zisman analysis (Figure 2.8), the surface energies (γ_c) of the fully cured sPFPE were 13.45 mN/m and 13.80 mN/m, respectively, for surfaces in contact with nitrogen and glass. These surface energies were significantly lower than silicon based elastomer poly(dimethylsiloxane) (~22 mN/m) and even lower than that of Teflon® (18 mN/m).[11] The remarkable low surface energy of this material can be attributed to its highly fluorinated nature and low roughness of the fully cured membrane. The residual surfactant left from Teflon® synthesis and the roughness of the samples may contribute to its higher surface energy. For the sPFPE surfaces in contact with nitrogen and glass during curing, the static contact angles with water were measured to be 120^o and 104^o, respectively, although their surface energies were about identical (13.45 vs. 13.80 mN/m). The surface in contact with nitrogen was more hydrophobic than that in contact with glass during curing. The difference of sPFPE surfaces is probably caused by molecular motion and rearrangement during polymerization. When in contact with a more polar surface like glass, the polar groups of the molecules would try to move toward the contacting interface and be locked at the surface due to cross-linking. Therefore, the resulting sample surface was more polar than that prepared in contact with nitrogen and displayed a smaller contact angle with water.

contacting surface	hexane	octane	decane	dodecane	tetradecane	hexadecane	water
nitrogen	42	53	63	67	68	77	120
glass	38	50	58	62	67	70	104

Table 2.2 Static contact angles of cured sPFPE homopolymers

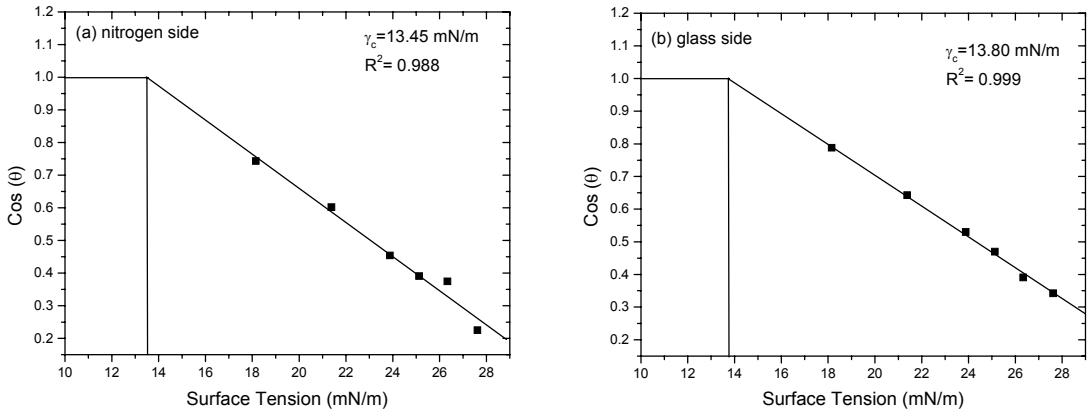

Figure 2.8 Critical surface tension of cross-linked sPFPE homopolymers. (a) nitrogen side; (b) glass side.

The surface properties of the cured sPFPE-SSE copolymers were also characterized by contact angle measurements and Zisman analysis. The surface in contact with nitrogen during UV-curing was analyzed for all samples. Table 2.3 lists the surface energies (γ_c) of the fully cured membranes with different compositions and their static contact angles with water (θ_w). Due to the additions of SSE component, the percentage of the hydrocarbons increased in the sPFPE-SSE copolymers. As a result, the surface energies of the copolymer films were higher than that of sPFPE homopolymer. As the SSE content increased from 30 wt% to 70 wt%, the surface energy of the copolymer membranes increased from 15.0 mN/m to 18.5 mN/m. Moreover, the copolymer surfaces were less hydrophobic than the that of sPFPE homopolymer and their static contact angles with water were in the range of 107^o to 113^o, while that of cured sPFPE was 120^o.

SSE content	30 wt%	40 wt%	50 wt%	60 wt%	70 wt%
γ_c (mN/m)	15.0	15.8	16.7	17.0	18.5
θ_W	113	109	109	107	113

Table 2.3 Surface energies of cured sPFPE-SSE films and their static contact angle with water

2.3.4 Super-hydrophobic behavior of sPFPE-SSE nanopillars

Topographical architectures and surface roughness have been found to have substantial impact on the surface properties of a given material. The lotus leaf, consisting of micrometer and nanometer-scaled structures, exhibits a self cleaning effect[12-14] in which a water droplet rolling down its surface and removing superficial dirt particles along its way. This effect has attracted a lot of attention due to their potential applications in making self-cleaning surfaces for building materials, windshields,[15,16] and microfluodic channels.[17] Low contact angle hysteresis and super-hydrophobicity are necessary[18-21] to obtain a surface with the self-cleaning effect. Both a rough surface and a low surface energy material are required to obtain a super-hydrophobic surface with a water contact angle in excess of 150^o. Patterned structures of sPFPE homopolymer and sPFPE-SSE copolymers can be easily prepared by micro-molding and soft lithography techniques. The low surface energy of these materials and ease for engineering patterning make them suitable for preparing super-hydrophobic surfaces. Moreover, the resulting materials are flexible due to their elastomeric nature.

In order to obtain patterned nano-structures with high aspect ratios, a high modulus material is needed. For this purpose, a copolymer with 40 wt% sPFPE and 60 wt% SSE with a modulus of 114 MPa was used in preparation of the super-hydrophobic surfaces. Patterned

sPFPE-SSE nanopillars were fabricated by using porous anodic aluminum oxide (p-AAO) membranes as the mold. The pores of the p-AAO templates are parallel to each other and approximately hexagonally packed with uniform diameter. The height of the pores was controlled by anodizing time.

Figure 2.9 shows the SEM images of sPFPE-SSE nanopillars peeled off the p-AAO membranes with different aspect ratios. Figure 2.9 (a) shows the image of sPFPE-SSE nanopillars with an aspect ratio of 10. The nanopillars, with diameter of 70 nm and length around 0.7 μm, were found to be straight and parallel to each other. The tips of the nanopillars were hemispherical, which was the negative replica of the pore bottom in the p-AAO template. A static contact angle with water of 164^{o} was observed for this patterned membrane. Figure 2.9 (b) shows the SEM image of sPFPE-SSE nanopillars with an aspect ratio of 15 and length of 1.5 μm. Due to the higher aspect ratio and the elasticity of the polymeric material, some of the nanopillars were aggregated into bundles while others were straight and separate. The static contact angle with water was measured to be 167^{o}. The nanopillars in Figure 2.9 (c) have an aspect ratio of 20 with lengths of 3 μm, and they all collapse into conical bundles. Patterned sPFPE-SSE membrane with such a high aspect ratio gave a static contact angle with water as high as 171^{o}. While the static contact angle with water of the flat sPFPE-SSE membranes with the same composition was only 107^{o}, the nanopillar surfaces displayed contact angles far above 150^{o}, confirming their super-hydrophobic properties and demonstrating the effects of topographical architectures and surface roughness.

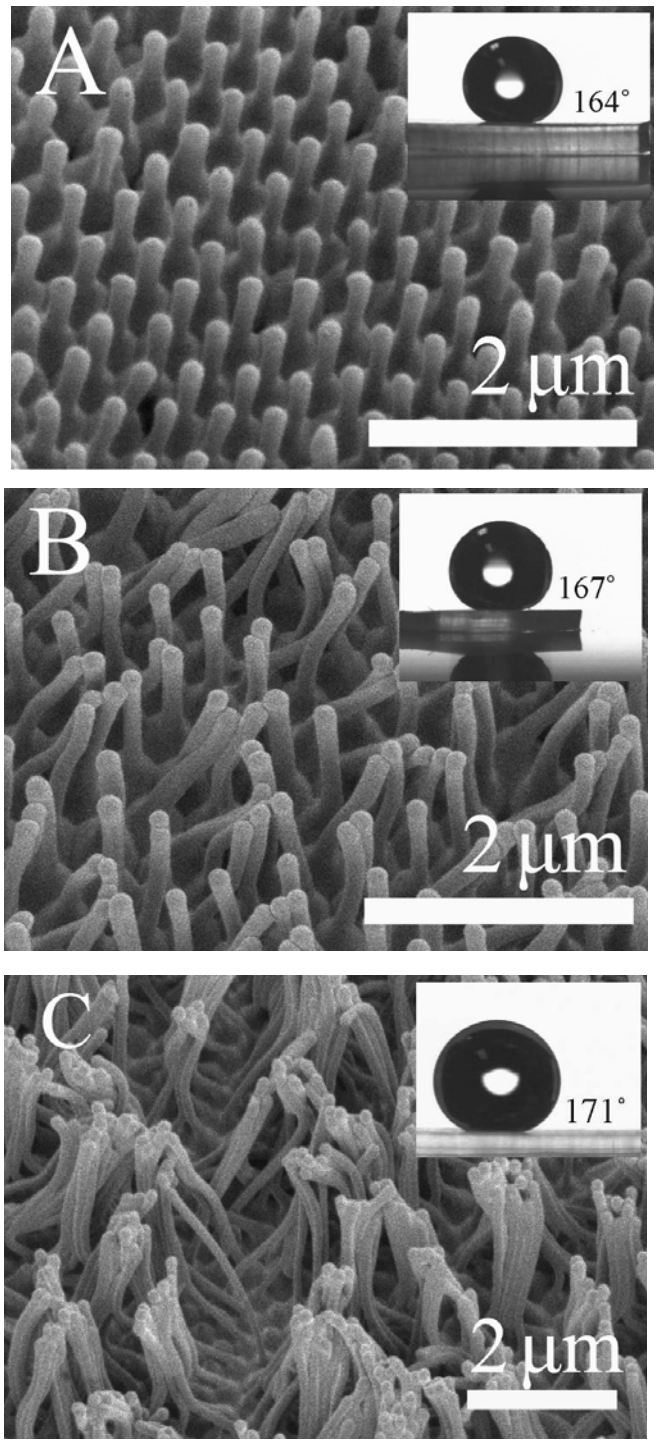

Figure 2.9 SEM images of sPFPE-SSE nanopillar films with aspect ratios of 10, 15 and 20. The inset in the top right of each image is the water droplet on such as-prepared surfaces during static contact angle measurements.

The dynamic behavior of water on a sPFPE-SSE film with high aspect ratio nanopillars was also studied. The dynamics of a water droplet falling on such a surface mimics rain falling on a lotus leaf. Figure 2.10 shows the dynamic behavior of a water droplet with a diameter of 2.2 mm on a sPFPE-SSE nanopillar film with an aspect ratio of 20 (Figure 2.9 (c)). The sPFPE-SSE surface had a tilt angle of about 0.5^{o} and the pictures were taken at a rate of 25 frames per second. As shown in Figure 2.10, the water droplet rolled down the sPFPE-SSE nanopillar surface with no hesitation. Fine fibrous debris on the surface could be removed by the moving water droplet. These observations are reminiscent of the water repellant lotus leaf and its self-cleaning property.

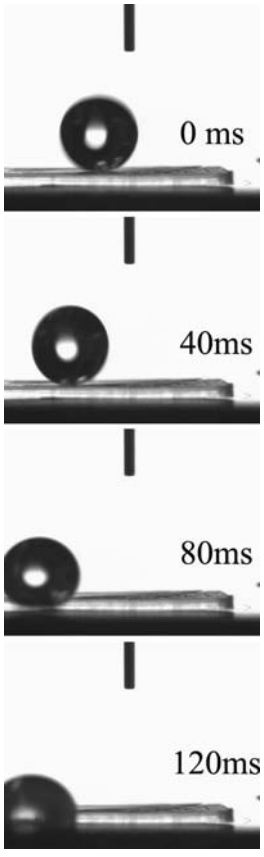

Figure 2.10 Motion of water droplet on the sPFPE-SSE nanopillar film with an aspect ratio of 20 (Figure 2.9 (c)).

2.4 Conclusions

Liquid precursors of styrenically functionalized perfluopolyether sPFPE and a fluorinated styrene sulfonate ester SSE were successfully prepared. They form single phase mixtures at various ratios and can be easily cured by exposing to UV-light or thermal treatment under inert atmosphere. Upon curing, the cross-linked copolymer membranes are stable at temperatures up to 301^{o}C. By DMTA analysis, single broad transitions were observed for sPFPE-SSE copolymer films with various compositions, which occurred in between the glass transition temperatures of sPFPE and SSE homopolymers. The cured films displayed elastomeric behavior, and the modulus of the membrane increased with increasing SSE ratio. The cross-linked sPFPE homopolymer and sPFPE-SSE copolymer films had very low surface energy. Topographical architectures and surface roughness had strong effect on the surface properties of the sPFPE-SSE copolymers. The high aspect ratio patterned nanopillars, made from cured sPFPE-SSE films displayed super-hydrophobic behavior. Self-cleaning effect of the as-prepared surface was also demonstrated.

2.5 References:

(1) Scheirs, J. *Modern Fluoropolymers*; John Wiley & Sons: New York, **1997**.

(2) Priola, A.; Bongiovanni, R.; Malucelli, G.; Pillicino, A.; Tonelli, C.; Simeone, G. *Macromol. Chem. Phys.* **1997**, *198*, 1893-1907.

(3) Sianesi, D.; Pasetti, A.; Fontanelli, R.; Bernardi, G. C.; Caporiccio, G. *Chim. Ind.* **1973**, *55*, 208-221.

(4) Rolland, J. P.; Dam, R. M. V.; Schorzman, D. A.; Quake, S. R.; DeSimone, J. M. *J. Am. Chem. Soc.* **2004**, *126*, 2322-2323.

(5) Rolland, J. P.; Hagberg, E. C.; Denison, G. M.; Carter, K. R.; DeSimone, J. M. *Angew. Chem. Int. Ed.* **2004**, *43*, 5796-5799.

(6) Rolland, J. P.; Maynor, B. W.; Euliss, L. E.; Exner, A. E.; Denison, G. M.; DeSimone, J. M. *J. Am. Chem. Soc.* **2005**, *127*, 10096-10100.

(7) Xia, Y.; Whitesides, G. M. *Angew. Chem. Int. Ed.* **1998**, *37*, 550-575.

(8) Hickner, M. A.; Ghassemi, H.; Kim, Y. S.; Einsla, B. R.; McGrath, J. E. *Chem. Rev.* **2004**, *104*, 4587-4612.

(9) Ishizone, T.; Tsuchiya, J.; Hirao, A.; Nakahama, S. *Macromolecules* **1992**, *25*, 4840-4847.

(10) Brandrup, J.; Immergut, E. H., Eds. *Polymer Handbood*, 3rd Edition; Johy Wiley & Sons: New York, **1989**.

(11) Rossier, J.; Reymond, F.; Michel, P. E. *Electrophoresis* **2002**, *23*, 858-867.

(12) Barhlott, W.; Neinhuis, C. *Planta* **1997**, *202*, 1-8.

(13) Otten, A.; Herminghaus, S. *Langmuir* **2004**, *20*, 2405-2408.

(14) Patankar, N. A. *Langmuir* **2004**, *20*, 8209-8213.

(15) Callies, M.; Quere, D. *Soft Matter* **2005**, *1*, 55-61.

(16) Quere, D. *Nature Mater.* **2005**, *1*, 14-15.

(17) Choi, C.-H.; Kim, C.-J. *Phys. Rev. Lett.* **2006**, *96*, 066001-066004.

(18) Oner, D.; McCarthy, T. J. *Langmuir* **2000**, *16*, 7777-7782.

(19) Chen, W.; Fadeev, A. Y.; Hsieh, M. C.; Oner, D.; Youngblood, J.; McCarthy, T. J. *Langmuir* **1999**, *15*, 3395-3399.

(20) Krupenkin, T. N.; Taylor, J. A.; Schneider, T. M.; Yang, S. *Langmuir* **2004**, *20*, 3824-3827.

(21) Quere, D.; Lafuma, A.; Bico, J. *Nanotechnology* **2003**, *14*, 1109-1112.

Chapter 3

CHEMICALLY CROSS-LINKED, FLUOROPOLYMER PROTON EXCHANGE MEMBRANES FROM LIQUID PRECURSORS

3.1 Introduction

Fuel cells are devices that convert the chemical energy stored in a fuel directly into electricity. As a potential candidate for environmentally benign and highly efficient power generation technology, fuel cells are attracting increasing interest.[1-3] The simplicity in design and in operational properties, makes polymer electrolyte membrane fuel cells ideal as power sources for portable electronic devices, passenger vehicles and distributed power generation. The polymer electrolyte membrane (PEM), serves as the electrolyte for transport of protons from the anode to the cathode while maintaining a barrier to keep the fuel and the oxidant separate.[4] For a fuel cell to work effectively and to be widely adapted, the PEM must have a portfolio of properties including acceptable costs, high proton conductivity, good chemical and thermal stability, good mechanical strength and low fuel crossover.[5]

The current bench mark PEM material is Nafion®, a perfluorinated ionomer membrane developed by DuPont. Nafion® has many desirable properties including good chemical and thermal stability, high proton conductivity under conditions of high water availability and reasonable mechanical properties. However, Nafion® has several shortcomings which limit its utility and performance such as high synthesis and processing costs,[6] diminished proton conductivity under conditions of low water availability,[7-9] and high fuel crossover when used in direct methanol fuel cells (DMFC).[10] As summarized in Chapter 1, significant efforts have been devoted worldwide to develop high performance and reliable proton exchange membranes. Some of the polymer electrolytes investigated to date, include sulfonated poly(arylene ether)s,[11] graft[12] or block copolymers[13] based on sulfonated polystyrene (PS), acid doped polybenzimidazole (PBI),[14] sulfonated poly(imides)[15] and polyphosphazene.[16] Even though each of these materials has their own advantages, most of

them do not possess both high proton conductivity and good chemical and mechanical stabilities under fuel cell operation conditions. As a result, Nafion® still stands as the bench mark PEM material.

In order to achieve good proton conductivity, especially at low relative humidity conditions, PEMs with high acid-loading are desirable. Various approaches have been applied to obtain high proton conductivity. One strategy is to impregnate the membrane with a small molecule strong acid: PBI doped with phosphoric acid[17,18] is the prototypical example of this approach. The conductivity is significantly improved by this approach, but some suggest that the low molecular weight acid may be leached out over long term operation.[19] A second strategy is to incorporate sulfonic acid sites along the polymer chain, either by post-sulfonation of the parent polymer, or by direct copolymerization of sulfonated monomers. For linear polymers, however, high acid loading does yield better conductivities, but also leads to compromised mechanical strength and swelling effects.

To achieve high proton conductivity without the associated challenges for linear polymers, chemically cross-linkable ionomeric systems were proposed and several systems were studied. Important cross-linking methods include electron beam[20] or γ irradiation[21] of preformed membranes, and cross-linking by inter/intra chain bridging links[22] through the sulfonic acid groups. However, irradiation cross-linking can result in PEMs with non-uniform properties and consumption of sulfonic acid groups results in decrease in ion content of the membrane and therefore lower proton conductivity.

In this work, we present a new strategy for making highly proton conductive, chemically cross-linked PEMs from easily processable, 100% curable, low molecular weight reactive liquid precursors. Highly fluorinated liquid precursors based on styrenically

functionalized reactive perfluoropolyethers (sPFPE) were used in conjunction with a fluorinated derivative of sulfonated styrenic (SS) monomers. Chemically cross-linked membranes are prepared by photochemically or thermally induced free radical polymerization of these liquid precursors. The synthesis of the precursor materials, sPFPE and a fluorinated styrene sulfonate ester (SSE), and the characterization of the cross-linked membranes were discussed in Chapter 2. Upon hydrolysis, the fluorinated styrene sulfonate ester (SSE) is converted to styrene sulfonic acid (SSA) functionalities, which serve as proton conducting sites in the membranes. Due to the similar reactivity of styrene functionalities in sPFPE and SS, the IEC of the membranes can be easily controlled by polymerizing mixtures of sPFPE and SSE at desired ratios and subsequent hydrolysis. Covalent cross-linking occurs through the styrene groups at both chain ends of the sPFPE precursor (functionality = 4) and is uniform across the membrane. By employing such a cross-linked system, high proton conductivity and good mechanical integrity are obtained at the same time. Furthermore, cross-linked membranes have the advantages of decreased swelling.[19]

In order to fabricate proton exchange membranes, Nafion® is typically extruded in the melt processable sulfonyl fluoride form to form a membrane with certain thickness, which is later converted to the acid form by base hydrolysis and acid treatment. In an alternative approach, dispersions of Nafion® can be obtained by heating the polymer in mixtures of water and alcohol at 240 ^{o}C in an autoclave under pressure.[23] Such dispersions can be dried to form so called "recast" Nafion® membranes, whose morphology and physical properties are different from the extruded membranes. Similar to Nafion®, all conventional PEM materials are processed into a membrane form either by melt extrusion or solvent casting. These processes are energy-consuming and expensive.

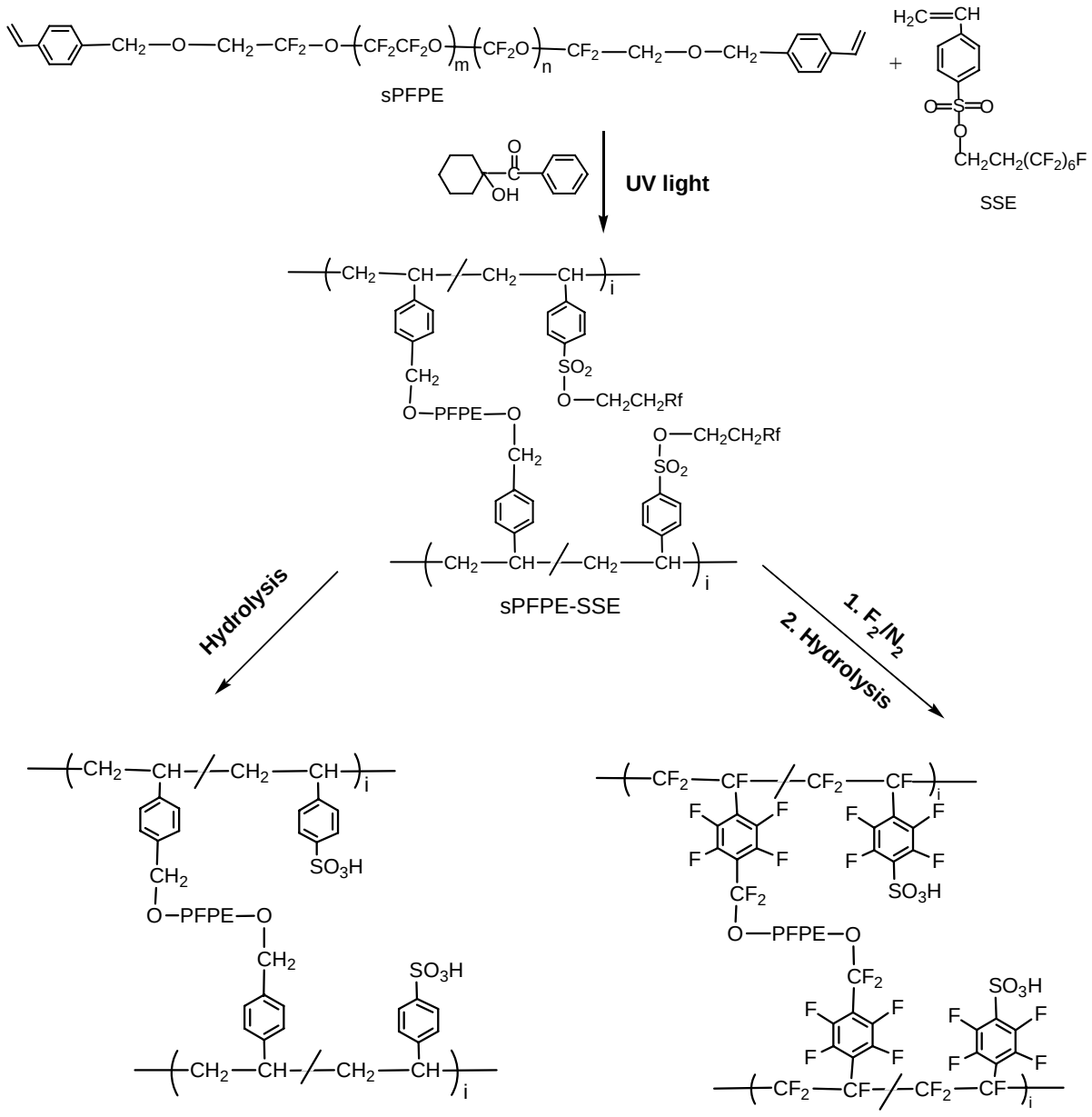

Figure 3.1 Chemical structures of the precursor materials, the cross-linked sPFPE-SSE membranes and the cross-linked sPFPE-SSA PEMs.

For our sPFPE-SSA PEM system, liquid precursors are directly cured into solid membranes of desired form and thickness. This process is solvent free and no further

processing steps are necessary. This liquid precursor to PEM approach also provides many opportunities for fuel cell development that would be otherwise impossible, which will be discussed in Chapter 4. In this chapter, the properties of the sPFPE-SSA PEMs are discussed, including their thermal and mechanical properties, water uptake, dimensional change, proton conductivity and fuel cell performance. To further improve the thermal and chemical stability of the sPFPE-SSA system, the membranes were fluorinated by elemental fluorine gas before hydrolysis (Figure 3.1). Properties of the fluorinated membranes were also studied and compared with the unfluorinated sPFPE-SSA PEMs.

3.2 Experimental

3.2.1 Membrane preparation

To make a membrane, sPFPE with 1wt% photo-initiator (1-hydroxycyclohexyl phenyl ketone) and SSE monomer were mixed in the desired ratio. The mixture was heated above 40 ^{o}C to form a homogeneous yellow liquid. The liquid precursor was poured onto a preheated substrate and then chemically cross-linked by irradiation with UV light (λ=365 nm) for 40 min under nitrogen purge. The resulting solid membrane in the ester form is transparent and slightly yellow.

To further improve the thermal and chemical stability of the partially fluorinated materials, membranes were fluorinated by elemental fluorine gas before hydrolysis (Exfluor, TX). This fluorination process can replace both aliphatic and aromatic hydrogen with fluorine atoms. Cross-linked sPFPE-SSE membranes were treated sequentially with N_2 at room temperature for 24 h, 1% F_2 in N_2 at room temperature for 24 h, and N_2 at room temperature for 24 h. The fluorinated membranes are yellow-brown in color.

To convert the SSE groups into SSA, the sPFPE-SSE membranes were soaked in a 5:6 (v/v) mixture of 30% NaOH aqueous solution and methanol for 12 h and then refluxed in the same mixture for an additional 10 h. After rinsing with distilled water, the membranes were stirred for a total of 24 h in fresh 20 wt% HCl solution, which was refreshed four times. The resulting sPFPE-SSA membranes were in the acid form. Residual HCl was removed by washing with distilled water.

3.2.2 Ion exchange capacity measurement

Sulfur content of the membranes in the ester and sodium salt forms was determined by elemental analysis (Atlantic Microlab). Ion exchange capacity (IEC) and equivalent weight (EW) of the membranes were calculated from the weight percentage of the sulfur and compared with those determined by titration of the sulfonic acid groups. In a titration measurement, a piece of sPFPE-SSA membrane (typically 0.2~0.3g) was stirred with saturated NaCl solution overnight; the resulting solution was then titrated with standardized 0.01 mol/L NaOH solution using phenolphthalein as the indicator. The titrated membrane was in the salt form and dried over phosphorus pentaoxide (P_2O_5) for a week at room temperature, at which point it was accurately weighed. The EW and IEC of the membranes were calculated as follows:

$$EW\ (H^+,\ g\ mol^{-1}) = [Dry\ weight\ /(V_{NaOH}*[NaOH])] - 22$$

$$IEC\ (meq\ g^{-1}) = 1000/EW$$

3.2.3 Thermal and mechanical analysis

The thermal stability of the membranes was measured by a Perkin-Elmer Pyris 1 thermogravimetric analyzer (TGA). All the samples were heated from room temperature to 120 ^{o}C and kept at 120 ^{o}C for 1 h to remove residual water. The samples were then cooled down to room temperature and heated to 500 ^{o}C in a nitrogen atmosphere with a heating rate of 10 ^{o}C/min. The onset of rapid weight loss was defined as the decomposition temperature.

Dynamic mechanical and thermal analysis (DMTA) measurements were performed with a 210 Seiko dynamic mechanical spectroscopy (DMS) instrument, operating at fixed frequency and film tension mode. The frequency used was 1 Hz and the temperature was varied from –140 to 350 ^{o}C at a heating rate of 2 ^{o}C/min. The mechanical properties of the PEM materials were measured by Instron 5566 at ambient conditions (20 ^{o}C and 35% relative humidity).

3.2.4 Water uptake

After hydrolysis, the membranes were kept in water for at least 24 h at room temperature. The wet membranes were blotted dry and quickly weighed. The membranes were then dried over P_2O_5 for at least a week at room temperature and the dried membranes were weighed again. The water uptake of the membranes expressed as a weight percentage was calculated as follows:

$$\text{Water uptake (wt\%)} = (W_{wet} - W_{dry})/ W_{dry} * 100$$

The effect of relative humidity on water uptake was also studied. Typically, the membranes were placed in a humidity chamber at the targeted temperature and relative humidity for at least 14 h and then weighed using an analytical balance in the chamber.

3.2.5 Proton conductivity

Proton conductivity was measured by AC Impedance over the frequency range of 1Hz – 1MHz. Impedance spectra were recorded using Solartron 1287 Impedance and Solartron 1255 HF frequency response analyzer. The conductivity cell was designed to ensure that the membrane resistance dominated the response of the system.[24] The membrane resistance was taken at the frequency of zero phase angle. The proton conductivity (σ) was calculated using $\sigma = l/(RS)$, where l, R, S denoted the distance of the two electrodes, the measured resistance, and the cross-section area of the membrane perpendicular to proton transport direction, respectively.

3.2.6 Fuel cell performance

To evaluate the fuel cell performance of the sPFPE-SSA membranes, LT 140E-W low temperature ELAT® gas diffusion electrodes (E-TEK, NJ) with a Pt catalyst loading of 5 g/m^2 painted with 5 wt% Nafion dispersion were used to achieve the most reproducible results. Membrane electrode assembly (MEA) was fabricated by sandwiching the PEM and a piece of painted electrode on each side into the fuel cell testing hardware. MEA containing Nafion® 117 membrane was prepared and investigated under the otherwise identical conditions for comparison. The MEAs were tested under atmospheric pressure using

hydrogen and oxygen as the fuel and the oxidant. A flow rate of 0.1 L/min was used for all the experiments.

3.3 Results and discussion

3.3.1 Preparation of chemically cross-linked PEMs

In order to make fluorinated PEM materials, highly fluorinated liquid precursors based on styrenically functionalized reactive perfluoropolyethers (sPFPE) were used in conjunction with a fluorinated derivative of sulfonated styrenic (SS) monomers (Figure 3.1). The detailed procedures for the synthesis of these liquid precursors were discussed in Chapter 2. In order to form a homogeneous single phase mixture with sPFPE, it was necessary to use the fluorinated derivates of the sulfonated styrenic monomers as opposed to using the acid form or the sulfonyl chloride form of the styrenic monomer otherwise single phase mixtures were not achievable.

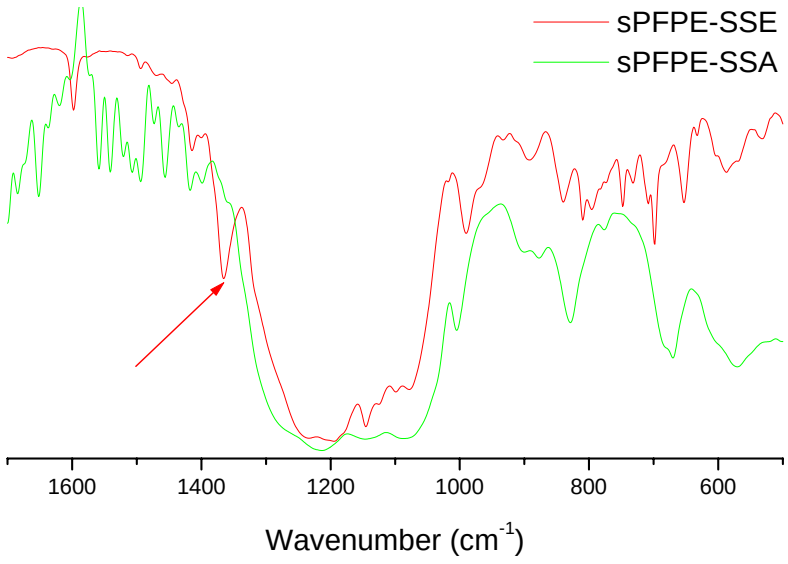

Figure 3.2 IR spectra of sPFPE-SS membranes before and after hydrolysis

During membrane preparation, the sPFPE and SSE precursors were mixed in a certain weight ratio and directly cured into a membrane with desired dimensions. No melt extrusion or solvent casting process is necessary. The membrane was then converted to the acid form sPFPE-SSA by hydrolysis. Figure 3.2 shows the IR spectra of a cross-linked membrane before and after hydrolysis. A peak at 1365 cm^{-1} was observed for the ester form sPFPE-SSE membrane, corresponding to asymmetric stretch of SO_2 groups in sulfonate ester. After hydrolysis, this peak completely disappeared, confirming that the cross-linked membrane was fully hydrolyzed to the acid form (sPFPE-SSA).

Ion exchange capacity (IEC) is an absolute measure of the number of reactive acid sites per unit mass or volume of the materials studied. In most fuel cell literatures, IEC is defined based on the mass of the membrane and expressed in units of milliequivalents per gram (meq/g). This is appropriate in most cases which discuss the properties of one particular ionomeric system, and we will use this expression in most of our discussions. Due to the similar reactivity of styrene functionalities in sPFPE and SSE, IEC of the membranes can be easily controlled by polymerizing mixtures of sPFPE and SSE at desired ratios and subsequent hydrolysis. Based on the precursor feed ratio, the theoretical IEC of the PEMs can be calculated and is plotted as the solid line as shown in Figure 3.3. The experimental IEC values were measured by titration or calculated from the membrane sulfur content by elemental analysis. As shown in Figure 3.3, the IEC values from the titration and elemental analysis were in good agreement with each other and with the theoretical calculated values, confirming that the ester groups were completely converted to the acid form. It may be worth noting that the only deviation of measured IEC values from the theoretically predicted one was at the higher IEC end of the IEC range. As IEC increases, the crosslink density is

expected to decrease since sPFPE is the source of cross-links. As a result, there is an increased possibility that for the higher IEC samples, some of the styrene sulfonic acid units may not be incorporated in the cross-linked network by covalent bonds and some of sol fractions may dissolve during hydrolysis. As shown in Figure 3.3, the experimental IEC values of membranes with IEC 1.52 meq/g and 1.82 meq/g are only slightly lower than the theoretical values, indicating that most of the SSA units are chemically incorporated into the network.

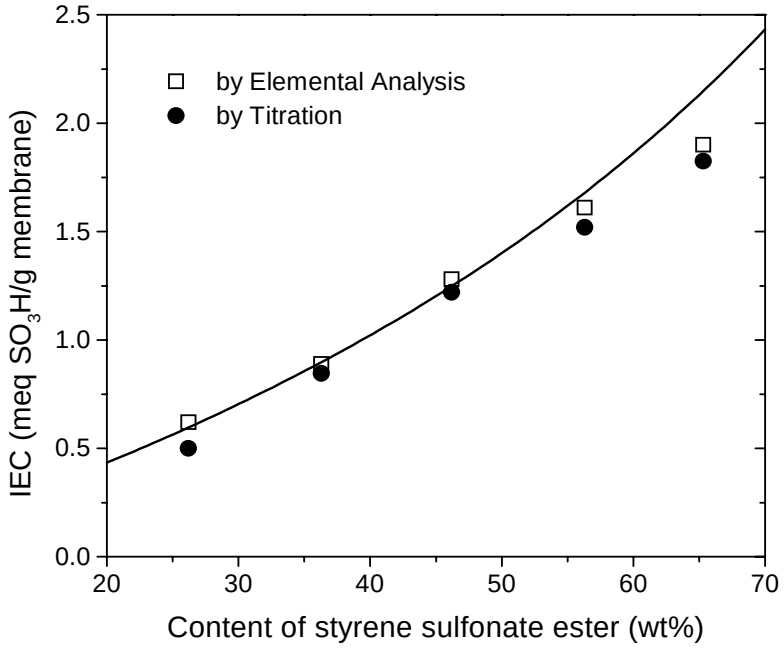

Figure 3.3 IEC of sPFPE-SSA membranes measured by titration and elemental analysis

A series of chemically cross-linked sPFPE-SSA membranes were prepared with IEC ranging from 0.50 meq/g to 1.82 meq/g. It is common for linear PEM materials to dissolve in water if they contain a significant amount of acid groups.[25] In particular, in the synthesis of

very high IEC Nafion®, competing β-scission processes during polymerization results in such lower molecular weight materials that they are unusable for PEMs. The high ion concentration (IEC>1.2 meq/g) polymers are soluble in many polar solvents.[26] Due to the cross-linked nature, sPFPE-SSA PEM with IEC as high as 1.82 meq/g remained intact after refluxing in methanol-water mixture for 10 h during hydrolysis.

Hydrocarbon based linear PEM materials with IEC larger than 2.0 meq/g has been reported[11] that does not dissolve in water. However, in comparison of the ion concentration of hydrocarbon and fluorocarbon based materials, the density effect should be considered. The density of hydrocarbon based polymeric materials is typically around 1 g/cm^3 or smaller, while the density of most fluorocarbon materials is larger than 1.5 g/cm^3. For PEM materials, the swelling effect of the membrane and the formation of a continuous hydrophilic domain for good proton conduction are both based on volume. In this case, it is more appropriate to use IEC based on volume expressed in units of milliequivalents per cubic centimeter (meq/cm^3). An IEC based on mass can be converted to volume based IEC by simply multiplying the density of the PEM material. The density of PFPE is 1.8 g/cm^3, and the density of sPFPE-SS membranes is about 1.7 g/cm^3 by a rough mass-volume measurement. Therefore, the IEC range of 0.50-1.82 meq/g for the sPFPE-SSA membranes corresponds to ion concentration range of 0.9-3.1 meq/cm^3 based on volume.

Due to the presence of aliphatic hydrocarbon moieties, the long-term stability of the cross-linked sPFPE-SSA PEMs may be questionable. In an effort to improve the long term stability of these materials, some membranes were treated with elemental fluorine gas (Figure 3.1) before hydrolysis to exhaustively fluorinate the membrane. The fluorination condition was described in the experimental section. Before fluorination, the ester form

membranes contained 1-1.5 wt% hydrogen atoms, and the hydrogen atom content was in the range of 0.5-1 wt% after fluorination. By elemental analysis, the degree of fluorination would be 75%, 57%, 40% and 35%, respectively, for sPFPE-SSE membranes with 30wt%, 50wt%, 60wt% or 70wt% SSE. As the SS content increased, the degree of fluorination decreased under the current reaction conditions. This may be related to the higher glass transition temperature of sPFPE-SSE samples with higher SSE content. For future directions, higher fluorine concentration, higher reaction temperature and longer reaction time could be used for samples with higher SS content in order to achieve complete fluorination.

3.3.2 Thermal and mechanical properties

The thermal stability of the membranes was investigated by TGA. As shown in Figure 3.4, the acid (H) form of the membranes displayed a thermal decomposition temperature of 290 ^{o}C independent of IEC. This is believed to be associated mainly with the loss of sulfonic acid groups.[11,27-29] Compared with the acid form membranes, samples in sodium (Na) form showed higher thermal stability with a decomposition temperature of 322 ^{o}C. It should be noted that the thermal stability observed under non-equilibrium conditions of TGA experiments might be overestimated to some extent. However, these results suggest that the sPFPE-SSA membranes are sufficiently stable within the conceivable temperature range of PEM fuel cell applications up to 120 ^{o}C. In order to improve the long-term stability of these partially fluorinated materials, the membranes were exhaustively fluorinated by elemental fluorine gas. The fluorinated materials exhibited a significant improvement in thermal stability, with a decomposition temperature of 354 ^{o}C in the sodium form.

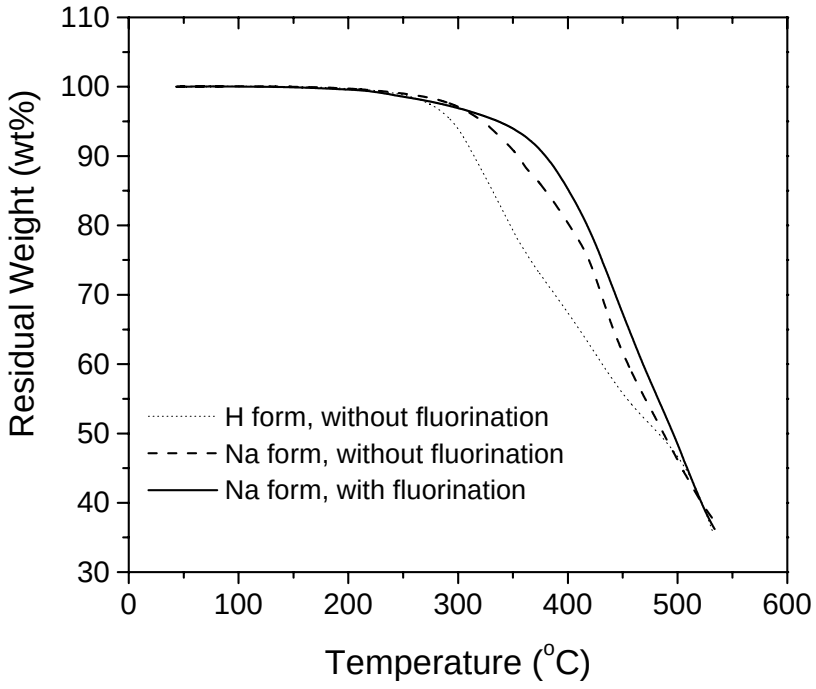

Figure 3.4 TGA curves of sPFPE-SSA membranes in H and Na forms

DMTA methods have been very useful for the analysis of phase behavior of the polymer studied. While phase separation of cross-linked materials is hard to detect as separate glass transitions by differential scanning calorimetry (DSC), it usually corresponds with clear thermo-mechanical transitions in DMTA measurements. As shown in Figure 3.5, two transitions were observed for the acid (H) form of the sPFPE-SSA PEMs, one at 200~250 ^{o}C (α transition) and the other at -80 ~ -45 ^{o}C (γ transition). The α relaxation is presumably due to chain motions within or/and near the ion-rich domains formed by styrene sulfonic acid, and the γ relaxation corresponds to chain motions in the sPFPE rich domains. Compared to typical phase separated systems such as block copolymers, the sPFPE/SSA segment lengths are very short but these two components would tend to be strongly

segregated from each other due to their very different natures. It was found that both IEC values and residual water content affected the peak positions and relative intensities of these two transitions.

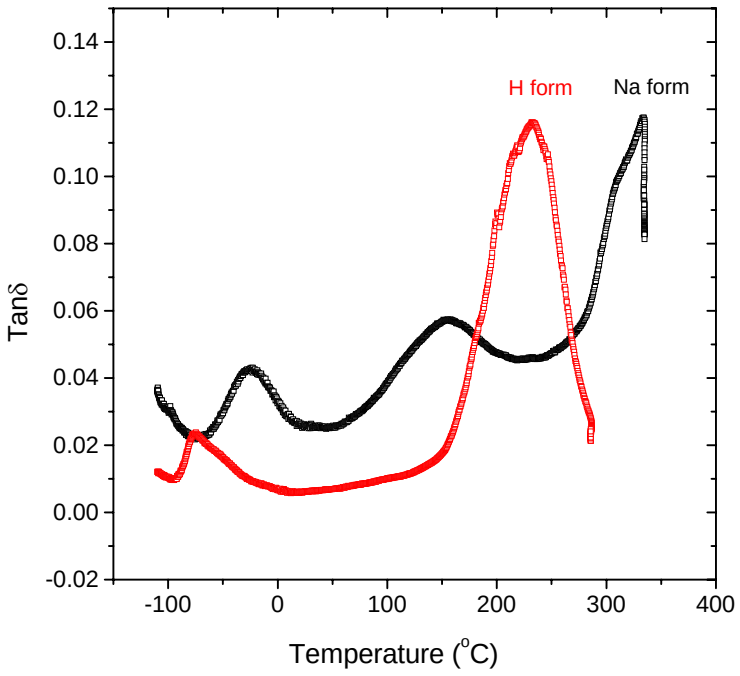

Figure 3.5 DMTA spectra of sPFPE-SSA membranes in H and Na forms

As shown in Figure 3.5, the type of counter-ion has a very strong effect on the dynamic mechanical properties of the membrane. When converted to the Na form, the γ relaxation shifted to slightly higher temperature, and the α transition shifted significantly to higher temperatures. Since thermal decomposition was observed at 322 °C, we are not sure if the peak observed at 310~330 °C is the actual α transition or an artificial peak caused by decomposition. However, an α transition at higher temperature is expected since the dipole-dipole interactions between the sodium sulfonate groups is much stronger than the hydrogen

bond interactions between the SO_3H groups. In addition, another relaxation near 150 ^oC was observed for the sodium form membranes; and this may be associated with the hydrocarbon domains formed mainly by aromatic groups. In the H form, these two transitions combined together and occurred in the 200~250 ^oC temperature range.

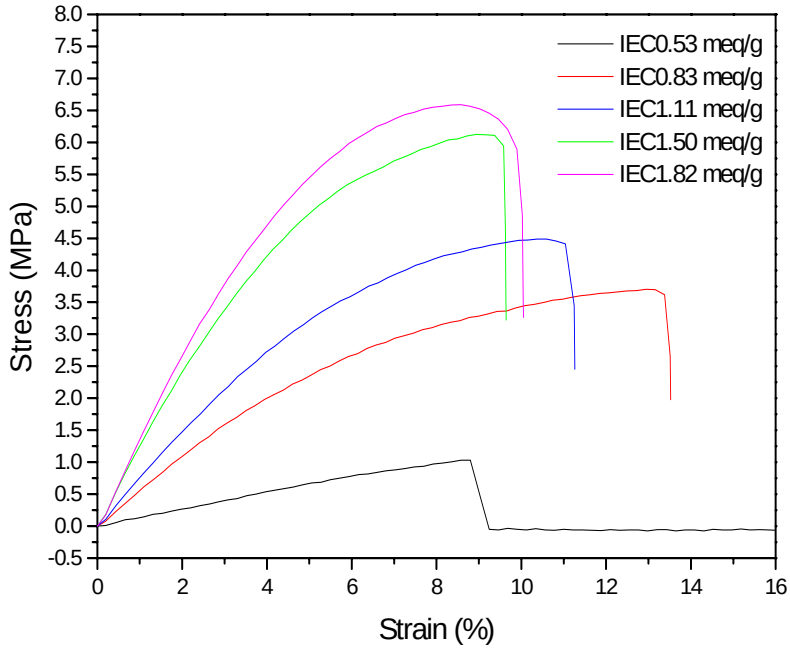

Figure 3.6 Stress-Strain curves of sPFPE-SSA membranes in H form under ambient conditions (20 ^oC, 35% RH).

The mechanical properties of the PEM materials were characterized by an Instron instrument under ambient conditions. Figure 3.6 shows the stress-strain curves of the membranes in H form. While the ester form sPFPE-SSE membranes were elastomeric, the acid form sPFPE-SSA membranes lost their elasticity. As the ion content increased, the membranes became stronger. As IEC increased from 0.53 to 1.82 meq/g, the moduli of the membranes increased from 15 MPa to 126 MPa.

3.3.3 Water uptake and dimensional change

The water sorption of the polymeric materials has profound effect on the proton conductivity and mechanical properties of the PEMs. Water uptake of sPFPE-SSA membranes from liquid water is presented in Table 3.1 as the weight percentage of the dry samples and as the number of water molecules per sulfonic acid (λ). The IEC had a strong effect on water uptake. As the IEC changed from 0.53 to 1.82 meq/g, the water uptake increased from 14 wt% to 121 wt%. As IEC increased, there were more ionic groups to interact with water. Furthermore, as IEC increased, each ionic group interacted with more water molecule as indicated by λ. This number increased from 15 water molecules for the IEC 0.53 meq/g sample to 37 water molecules for the IEC 1.82 meq/g membrane. Without any thermal treatment, Nafion® 117 (IEC 0.91 meq/g) absorbed 34 wt% water from liquid water, corresponding to 21.5 water molecules per acid group.[30]

IEC (meq/cm^3)	IEC (meq/g)	EW (g/mol)	water uptake (wt%)	λ (H_2O/SO_3H)	dimensional change (%)	σ at R. T. (S/cm)
0.90	0.53	1900	14	15	9	0.025
1.41	0.83	1200	26	17	17	0.042
1.89	1.11	900	54	25	24	0.087
2.55	1.50	670	76	28	32	0.134
3.09	1.82	550	121	37	44	0.254

Table 3.1 Characterization of the sPFPE-SSA PEM materials

The membrane's dimensional change along the length/width direction of the sample due to water sorption at fully hydrated conditions is given in Table 3.1. Analogous to water uptake, dimensional change also strongly depended on IEC values and almost linearly correlated with the water uptake of the membrane. As IEC increased from 0.53 to 1.82 meq/g, the swelling ratio increased from 9% to 44%. Compared with linear PEM materials, the degree of swelling is much lower for such crosslinked PEMs. For example, the swelling of Nafion® 117 (IEC 0.91 meq/g) is about 85% and the swelling of sulfonated poly(vinyl fluoride) PEMs (IEC 1.5 meq/g) is about 93% under similar conditions,[31] whereas even for our IEC 1.82 meq/g cross-linked PEM, the swelling was only 44%. Therefore, chemical cross-linking can dramatically decrease the degree of swelling, which can have a significant impact on retaining good interfacial contact between the catalyst layer and the membrane.

It is desirable for fuel cells to operate under low relative humidity (RH) conditions. Therefore, sorption of water from water vapor at 25 ^{o}C under controlled RH environments was investigated. As shown in Figure 3.7 (a), all the membranes displayed increased water uptake in a higher RH environment. In the low RH region (RH = 20-65%), there was a relatively small increase in water content with RH. In the high RH region (RH = 65-100%), the increase in water content was steeper than in the low RH region. The low RH region corresponds to uptake of water vapor by the ions in the membrane, while the high RH region corresponds to water that fills the ionic domain and swells the polymer. Similar to water uptake from liquid water, high IEC membranes tend to take more water from vapor than low IEC ones under the same conditions. For example, while the IEC 0.53 meq/g membrane took 13 wt% water at 100% RH, IEC 1.82 meq/g membrane took as much as 50 wt% water at 100% RH. As indicated by Figure 3.7 (b), it can be seen that differences in water uptake

between different IEC samples, expressed in terms of weight percentage of the membrane dry weight, are almost completely explained by the difference in ion concentration. When water uptake is expressed as the number of water molecules per sulfonate group, the uptake looks essentially the same for all the samples.

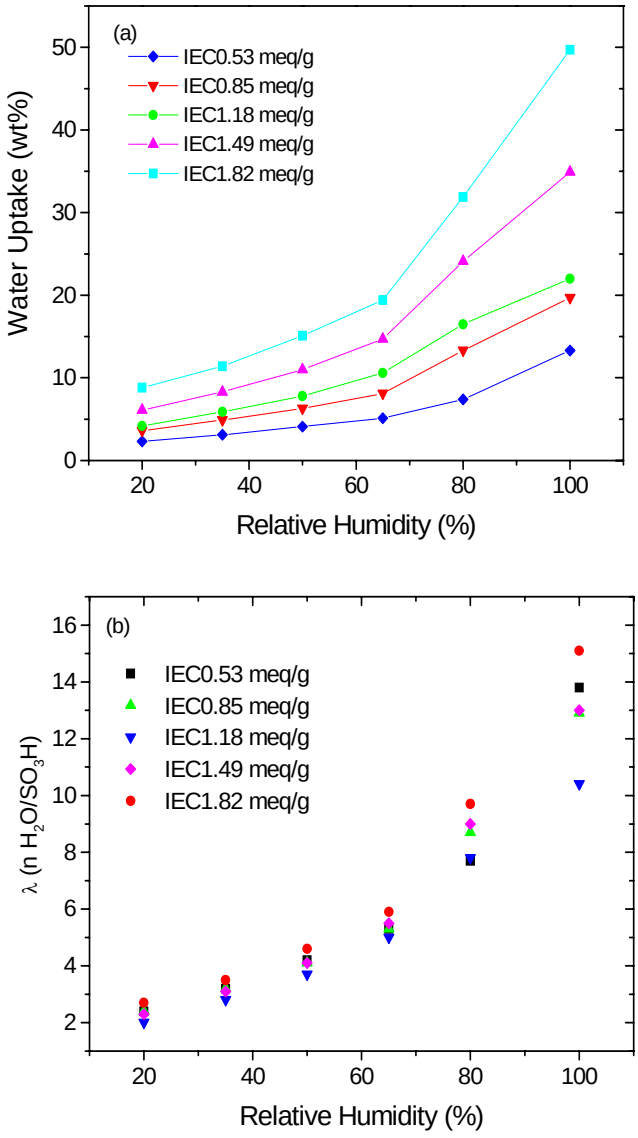

Figure 3.7 Water uptake of sPFPE-SSA membranes from vapor phase with controlled relative humidity: (a) in terms of weight percentage; (b) in terms of number of water molecules per acid group.

Comparison of water uptake from liquid water and from saturated water vapor (RH = 100%) reveals an apparent paradox. The water sorption of the membrane in equilibrium with water vapor (RH = 100%) is not the same as the water sorption of the same membrane in contact with liquid water. For example, the membrane with IEC=1.82 meq/g adsorbed 15 water molecules per sulfonate group from saturated vapor phase vs. 37 from liquid phase. A difference in water uptake by polymers from liquid versus saturated water vapor has been observed for several polymer/solvent systems including Nafion®,[8] and is referred to Schroeder's paradox. One explanation is that the polymer surface is more hydrophobic when exposed to water vapor, but more hydrophilic when in contact with liquid water. Therefore, water sorption from vapor phase is less favorable.

3.3.4 Proton Conductivity

In PEM fuel cells, the proton conductivity of the membrane is particularly important since it plays a significant role in the performance of fuel cells. To achieve good conductivity, high acid loading is desirable. However, for linear PEM materials, this is achieved at the expense of compromised mechanical integrity and excessive swelling. By employing chemically cross-linked systems, we have maximized the acid loading of the PEM materials to achieve higher proton conductivity. Table 3.1 lists the proton conductivity (σ) of the sPFPE-SSA PEMs at room temperature under fully hydrated conditions. As IEC increased from 0.53 to 1.82 meq/g, the proton conductivity of the membranes increased by an order of magnitude from 0.025 S/cm to 0.254 S/cm. This is reasonable since proton conductivity is determined by the product of charge carrier density and charge carrier mobility and high ion content PEMs have more proton carriers. Nafion®117 has a

conductivity of 0.095 S/cm under this condition by our measurement, which agrees well with the literature value.[32] Compared with Nafion®, the conductivity of sPFPE-SSA membrane with the same IEC is lower. This may relate to the lower pKa of the sulfonic acid in Nafion® and difference in the morphology and proton mobility of the corresponding PEMs. But the ion loading of Nafion® is limited by β scission during polymerization and the resulting problems with mechanical strength and dissolution in water. By employing a chemically cross-linked system, we can maximize the ion content of membranes and still maintain decent mechanical integrity. The IEC1.82 meq/g membrane has a conductivity of 0.254 S/cm, which is almost 3 times higher than Nafion®. Many researchers try to design PEM materials that have higher conductivity than Nafion®, but not many succeed. For many aromatic-based ionomers, low proton conductivity is observed[33] due to the lack of the formation of properly ordered microphase separation as compared to perfluorinated ionomers.[34] The lower acidity of hydrocarbon based SO_3H than that of fluorocarbon based SO_3H may also be responsible. The strong hydrophobicity of PFPE in our system may contribute to the formation of microphase separated nanochannels and a membrane with conductivity 270% higher than Nafion® is achieved.

Figure 3.8 shows the temperature dependence of the proton conductivity and the resultant activation energies for the sPFPE-SSA membranes. Similar to many other PEM materials, the proton conductivity of these cross-linked PEMs increased with temperature. According to our measurements, the proton conductivity of both Nafion® and the cross-linked sPFPE-SSA membranes exhibited Arrhenius behavior. The activation energy (E_a) for the proton conduction in Nafion® was measured to be 10.5 kJ/mol, which agrees well with literature values.[35] The activation energy of our cured membranes was found to depend on

the IEC values. As shown in Figure 3.8 (b), once the ion content increased above a certain threshold, the activation energy started to decrease as the IEC increased. Although the proton conduction mechanism and the morphology of the sPFPE-SSA PEMs are not well understood, we suspect the decreasing activation energy may be caused by the larger volume fraction of the hydrophilic styrene sulfonic acid component for higher IEC membranes, and the easier formation of a continuous network of the ionic domains. Further studies on the membrane morphology by scattering and microscopy techniques are planned for future directions.

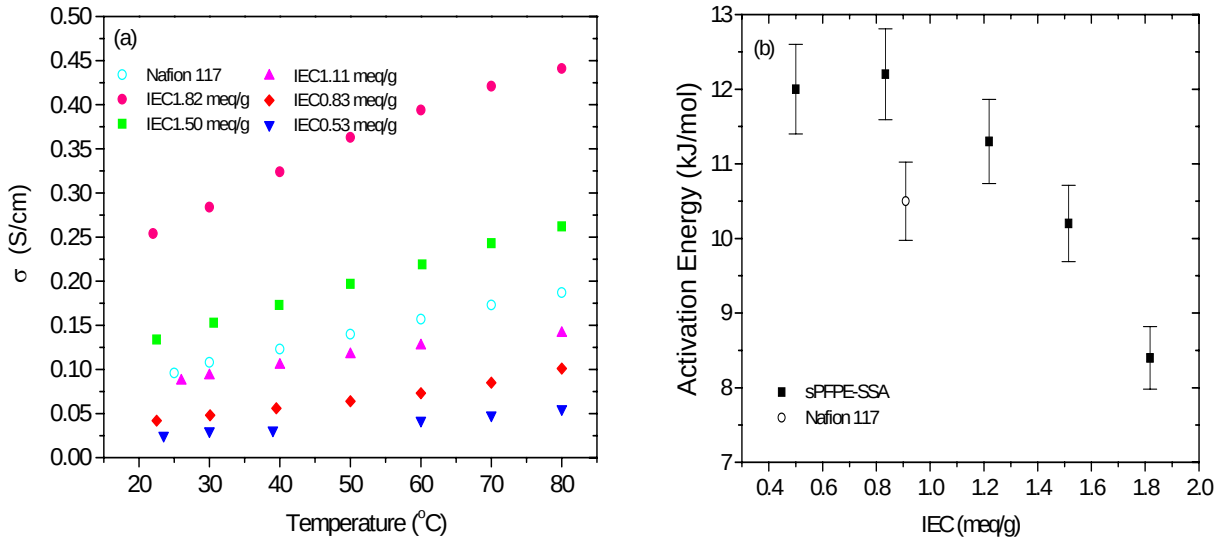

Figure 3.8 (a) Proton conductivity of sPFPE-SSA membranes at different temperatures under fully hydrated conditions; and (b) their activation energies for proton conduction.

3.3.5 MEA performance

To investigate the effect of highly proton conductive PEMs on fuel cell performance, MEAs were prepared from our cured PEMs and were compared with MEAs fabricated from Nafion® 117 membranes. Gas diffusion electrodes (LT 140E-W low temperature ELAT®,

E-TEK, NJ) with a Pt catalyst loading of 5 g/m^2 were used for all of the MEAs in order to make comparisons between the tested systems.

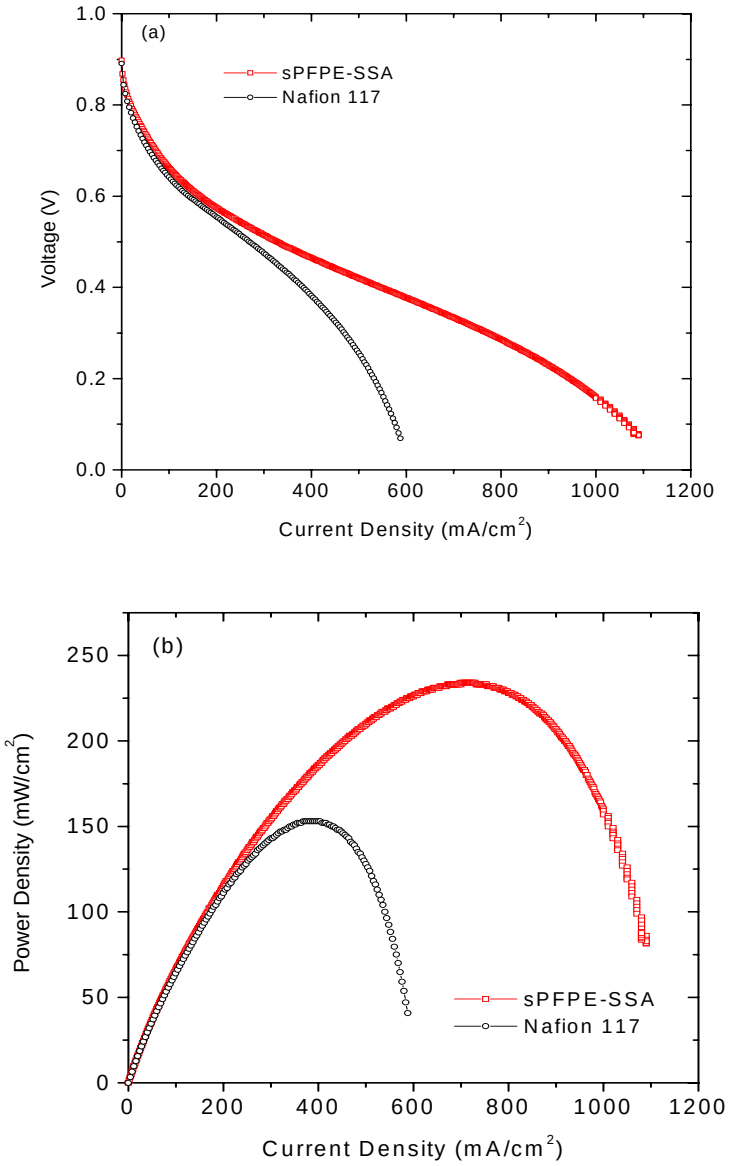

Figure 3.9 MEA performance of Nafion®117 (175μm in thickness) and sPFPE-SSA membrane with a IEC value of 1.67 meq/g (190μm in thickness) at 50 ^{o}C and 75% RH: (a) polarization curves and (b) power output curves.

Figure 3.9 shows the MEA performance of Nafion® 117 (175 μm thick) and a cured sPFPE-SSA membrane with an IEC value of 1.67 meq/g (190μm thick) at 50 ^{o}C and 75% RH. Even though the tested sPFPE-SSA membrane is thicker than Nafion® 117, and the ELAT electrodes were developed and optimized for Nafion® based systems, the MEA made from sPFPE-SSA membrane having a higher IEC value and hence higher proton conductivity showed significantly better fuel cell performance without any optimization. The achievable power density of the sPFPE-SSA membrane outperformed Nafion ® by 150% under the testing conditions. This is presumably due to the higher proton conductivity of the sPFPE-SSA membrane under the testing conditions, which helps to decrease the overall resistance of the MEA. Under this operation condition, the availability of water was very important and played a different role for these two membranes. Nafion® 117 did not have enough water to be highly proton-conductive and effective for the MEA operation. However, high levels of hydration were not as necessary for the MEA fabricated from the high IEC sPFPE-SSA membrane since the ionic domains start to overlap with each other without much swelling.

A sPFPE-SSA membrane with 5wt% trifluorovinyl benzene as external cross-linker was prepared to further decrease swelling and improve mechanical properties of the membrane. This membrane had a IEC of 1.50 meq/g and a thickness of 190 μm. Similar to the previous membrane (IEC 1.67 meq/g), the MEA performance of this membrane was significantly better than Nafion® 117 at 50 ^{o}C and 75% RH, as shown in Figure 3.10. When the fuel cell was tested at 80 ^{o}C and 100% RH, the MEA made of Nafion® showed significant improvement. On the other hand, the performance of this sPFPE-SSA MEA displayed some improvement at higher temperature and better humidified environments, but the improvement was not as dramatic as for Nafion®. As discussed earlier, water availability

is very important for low IEC PEMs such as Nafion® to form continuous ionic domains and to have high proton conductivity. Therefore the MEA performance of Nafion® 117 showed a strong dependence on operation conditions. However, much less water is needed for high IEC PEMs to form continuous ionic domains, and the presence of large amount of water is not very important for them to have good proton conductivity. Therefore, the MEA performance of sPFPE-SSA was not strongly dependent on the operation conditions and displayed acceptable performance under mild conditions. This is especially beneficial for applications in portable devices.

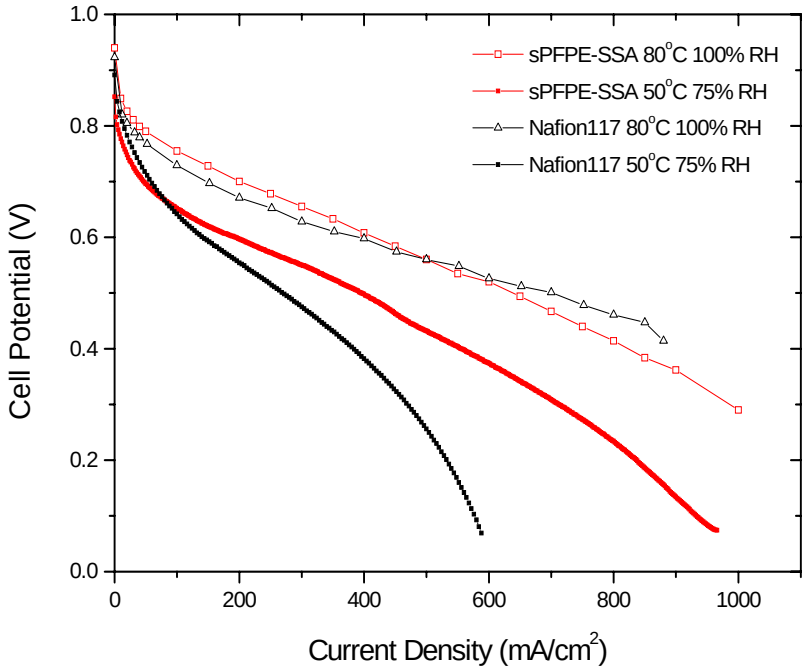

Figure 3.10 MEA performance of a sPFPE-SSA membrane with external cross-linker (IEC 1.50 meq/g, 190 µm) and Nafion® 117 (IEC 0.91 meq/g, 175 µm) at different conditions.

3.3.6 Effect of Fluorination

The sPFPE-SSA PEMs are partially fluorinated materials. The presence of aliphatic units may result in long-term instability during fuel cell operation. To further improve their thermal and chemical stability, some initial efforts were taken to fluorinate the sPFPE-SSE membranes by elemental fluorine gas before hydrolysis. According to elemental analysis, it was found that the degree of fluorination depended on the SSE content of the samples under current reaction conditions. Higher SSE content resulted in lower degree of fluorination, presumably due to the higher glass transition temperature of the higher SSE content samples. The effect of fluorination on thermal stability was studied by TGA. Since the decomposition of acid form polymers was mainly associated with the loss of sulfonic acid group, PEMs in Na form were compared before and after fluorination. As shown in Figure 3.4, the decomposition temperature increased from 322 to 354 ^{o}C after fluorination.

Due to the replacement of H with F, the density of the membranes increased after fluorination and the IEC values of the membranes decreased if we use mass based IEC with units of meq/g. However, the number of ion conducting sites per unit volume of the membrane is essentially the same before and after fluorination assuming no volume change and no loss of functional groups during fluorination. Therefore, it is more appropriate to use volume based IEC values to compare properties of the unfluorinated and fluorinated membranes.

Water uptake and dimensional change of the fluorinated membranes were measured and compared with the unfluorinated PEMs. As shown in Figure 3.11 (a), the fluorinated membranes took slightly more water than the unfluorinated samples with the same ion concentration. However, the dimensional change of fluorinated membranes was essentially

the same as the unfluorinated samples, as shown in Figure 3.11 (b). This may relate to the stronger segregation of hydrophobic and hydrophilic domains upon fluorination and decrease of the interfacial regions. A possible explanation is that the ionoic cluster domains can interact with more water while the more hydrophobic fluorocarbon domains prevent the membrane from swelling.

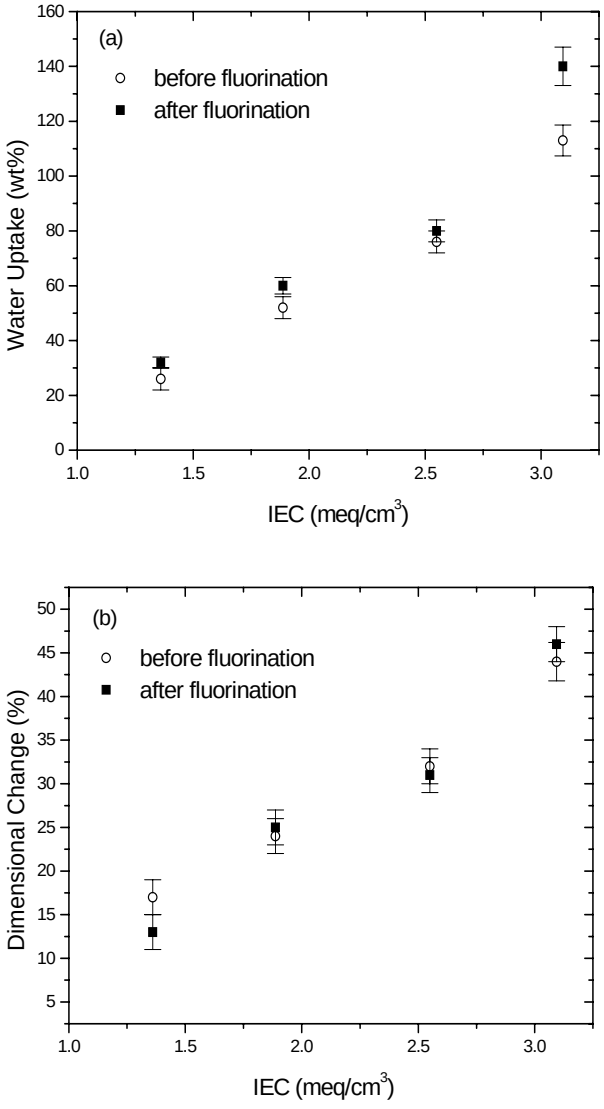

Figure 3.11 Effect of fluorination on: (a) water uptake and (b) dimensional change of sPFPE-SSA PEMs.

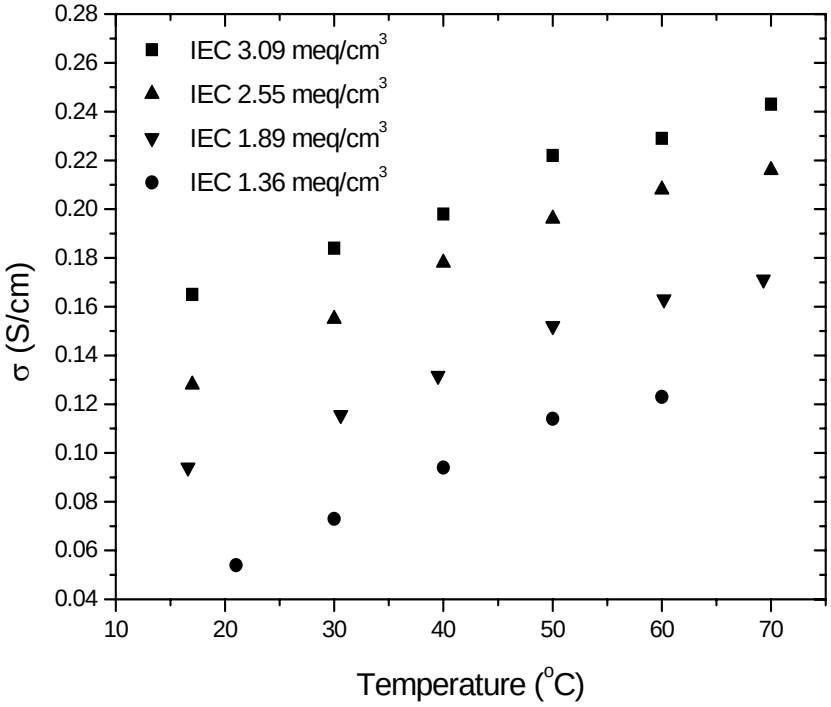

Figure 3.12 Proton conductivity of fluorinated sPFPE-SSA membranes at different temperatures under fully hydrated conditions.

The proton conductivity of the fluorinated PEMs are shown in Figure 3.12. Similar to unfluorinated PEMs, the conductivity of the fluorinated membranes increased with temperature and membranes with higher IEC showed higher conductivity. Due to the strong electron-withdrawing effect of fluorine, the fluorinated styrene sulfonic acid is expected to be a stronger acid. The lower pKa of the sulfonic acid combined with possible morphology changes due to fluorination could potentially affect the proton conductivity of the resulting PEMs. In Figure 3.13, the conductivity of fluorinated PEMs is compared with those of the unfluorinated ones at room temperature and fully hydrated conditions. For membranes with IEC values of 1.36 and 1.89 meq/cm^3, fluorination resulted in higher proton conductivity. As

IEC increased, different effects were observed. For the IEC 2.55 meq/cm^3 sample, the conductivity of the fluorinated membrane was slightly lower than the unfluorinated one. For the IEC 3.09 meq/^{3} sample, the conductivity of the fluorinated membrane was much lower than that of the unfluorianted one.

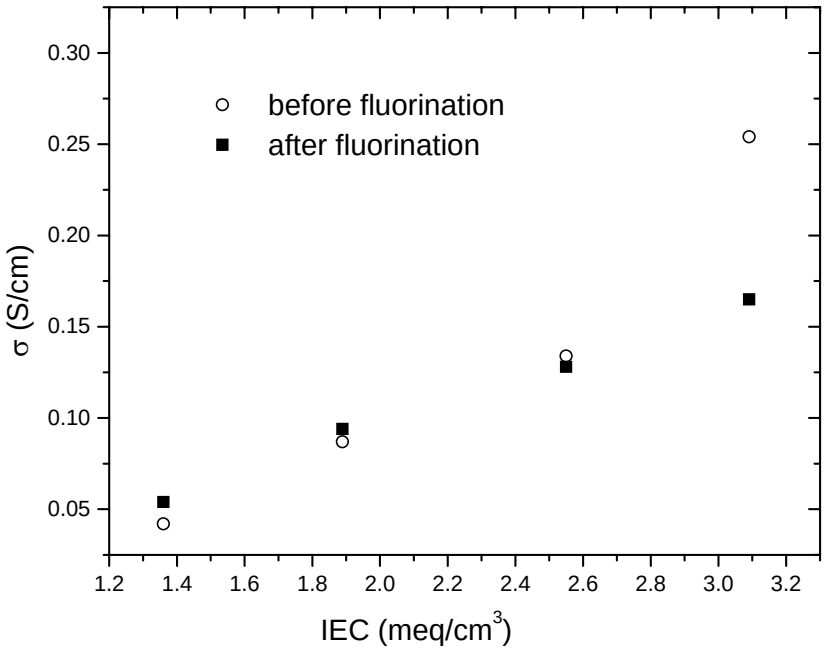

Figure 3.13 Comparison of proton conductivity of sPFPE-SSA PEMs before and after fluorination at room temperature and fully hydrated conditions.

Table 3.2 compares the proton conductivity of the membranes before and after fluorination at temperatures between 20 ^{o}C to 70 ^{o}C under fully hydrated conditions. Similar to Figure 3.13, fluorination had different effects on conductivity for different IEC samples for this entire temperature range studied.

		60 wt% sPFPE		50 wt% sPFPE		40 wt% sPFPE		30 wt% sPFPE	
		b. f.*	a. f.*	b. f.	a. f.	b. f.	a. f.	b. f.	a. f.
IEC	meq/g	0.8	0.68	1.11	0.92	1.50	1.39	1.82	1.64
	meq/cm^3	1.36	1.36	1.89	1.89	2.55	2.55	3.09	3.09
σ (S/cm)	20 °C	0.042	0.054	0.087	0.094	0.134	0.128	0.254	0.165
	30 °C	0.048	0.073	0.093	0.116	0.153	0.155	0.284	0.184
	40 °C	0.056	0.094	0.105	0.132	0.173	0.178	0.324	0.198
	50 °C	0.064	0.114	0.117	0.152	0.197	0.196	0.363	0.222
	60 °C	0.073	0.123	0.127	0.163	0.219	0.208	0.394	0.229
	70 °C	0.085	N/A	N/A	0.171	0.243	0.216	0.421	0.243

Table 3.2 Effect of fluorination on the proton conductivity of sPFPE-SSA PEMs at different temperatures under fully hydrated conditions. (*: b. f. before fluorination; a. f. after fluorination).

These observations are complicated and hard to explain from these limited initial results. We suspect that several factors can play important roles and should be considered: extent of fluorination, possible loss of proton conducting sites or partial breaking of network structures during fluorination, acidity of the acid groups, and morphology changes before and after fluorination. As discussed before, the degree of fluorination is lower for higher IEC membranes. By elemental analysis, some loss of sulfer was observed after fluorination, which indicated some loss of proton conducting sites. To better understand these effects, spectroscopic investigation and morphology studies by scattering and transmission electron microscopy are planned as future directions.

3.4 Conclusions

A series of novel fluoropolymer PEMs sPFPE-SSA have been prepared from 100% solventless liquid precursors that are chemically cured into a network. By employing chemical cross-linking, high acid containing PEMs with proton conductivity much higher than Nafion® have been obtained without the loss of mechanical integrity typical with linear polymers. Thermal stability of these materials is expected to be sufficient for fuel cell operations. The thermal and mechanical behavior of the sPFPE-SSA PEMs were studied by DMTA and instron. Water content, dimensional change, and proton conductivity of the sPFPE-SSA membranes were strongly related to the IEC of the materials. High acid content results in higher water uptake, higher dimensional change and better conductivity. The sPFPE-SSA membranes showed better MEA performance than Nafion®117 under low water availability and mild operation conditions.

To improve the long term stability of the partially fluorinated material, sPFPE-SS membranes were fluorinated by elemental fluorine gas. Fluorination of the membranes resulted in improvement of thermal stability, as displayed by TGA measurements. However, the effects of fluorination on proton conductivity and other properties of the sPFPE-SSA PEMs are complicated and not well understood. More studies in this area are needed in the future for better understanding the structure-property relationships of this PEM system.

3.5 References:

(1) Appleby, A. J.; Foulkes, R. L. *Fuel Cell Handbook*; Van Nostrand Reinhold: New York, **1989**.

(2) Whittingham, M. S.; Savinell, R. F.; Zawodzinski, T. A. *Chem. Rev.* **2004**, *104*, 4243-4244.

(3) Malhotra, S.; Datta, R. J. *J. Electrochem. Soc.* **1997**, *144*, L23-L26.

(4) Minh, N. Q. In *Electronic Materials Chemistry*; Pogge, H. B., Ed.; Marcel Dekker, Inc: New York, **1996**.

(5) Hickner, M. A.; Ghassemi, H.; Kim, Y. S.; Einsla, B. R.; McGrath, J. E. *Chem. Rev.* **2004**, *104*, 4587-4612.

(6) Gil, M.; Ji, X.; Li, X.; Na, H.; Hampsey, J. E.; Lu, Y. *J. Membr. Sci.* **2004**, *234*, 75-81.

(7) Savadogo, O. *J. New. Mater. Electrochem. Syst.* **1998**, *1*, 47-51.

(8) Gottesfeld, S.; Zawodzinski, T. A. In *Advances in Electrochemical Science and Engineering*; Alkire, R. C., Gerischer, H., Kolb, D. M., Tobias, C. W., Eds.; Johy Wiley & Sons: New York, **2002**.

(9) Si, Y.; Kunz, H. R.; Fenton, J. M. *J. Electrochem. Soc.* **2004**, *151*, A623-A631.

(10) Cruickshank, J.; Scott, K. *J. Power Sources* **1998**, *70*, 40-47.

(11) For example: (a)Wang, F.; Hickner, M.; Kim, Y. S.; Zawodzinski, T. A.; McGrath, J. E. *J. Membr. Sci.* **2002**, *197*, 231-242; (b) Kim, Y. S.; Wang, F.; Hickner, M.; Mccartney, S.; Hong, Y. T.; Harrison, W.; Zawodzinski, T. A.; Mcgrath, J. E. *J. Polym. Sci., Part B: Poly. Phys.* **2003**, *41*, 2816-2828; (c) Kerres, J.; Cui, W.; Reichle, S. *J. Polym. Sci., Part A: Poly. Chem.* **1996**, *34*, 2421-2438.

(12) For example: (a)Ding, J.; Chuy, C.; Holdcroft, S. *Macromolecules* **2002**, *35*, 1348-1355; (b) Ding, J.; Chuy, C.; Holdcroft, S. *Adv. Funct. Mater.* **2002**, *12*, 389-394.

(13) For example: (a)Kim, J.; Kim, B.; Jung, B.; Kang, Y. S.; Ha, K. Y.; Oh, I.-H.; Ihn, K. J. *Macromol. Rapid Commun.* **2002**, *23*, 753-756; (b) Mokrini, A.; Acosta, J. L. *Polymer* **2001**, *42*, 9-15; (c) Elabd, Y. A.; Walker, C. W.; Beyer, F. L. *J. Membr. Sci.* **2004**, *231*, 181-188.

(14) For example: (a) Xiao, L.; Zhang, H.; Scanlon, E.; Ramanathan, L. S.; Choe, E.-W.; Rogers, D.; Apple, T.; Benicewicz, B. C. *Chem. Mater.* **2005**, *17*, 5328-5333; (b) Samms, S. R.; Wasmus, S.; Savinell, R. F. *J. Electrochem. Soc.* **1996**, *143*, 1225-

1232; (c) Wainright, J. S.; Wang, J. T.; Weng, D.; Savinell, R. F.; Litt, M. *J. Electrochem. Soc.* **1995**, *142*, L121-L123.

(15) For example: (a) Asano, N.; Aoki, M.; Suzuki, S.; Miyatake, K.; Uchida, H.; Watanabe, M. *J. Am. Chem. Soc.* **2006**, *128*, 1762-1769; (b) Miyatake, K.; Zhou, H.; Watanabe, M. *Macromolecules* **2004**, *37*, 4956-4960; (c) Miyatake, K.; Zhou, H.; Matsuo, T.; Uchida, H.; Watanabe, M. *Macromolecules* **2004**, *37*, 4961-4966.

(16) For example: (a) Carter, R.; Wycisk, R.; Yoo, H.; Pintauro, P. N. *Electrochem. Solid-State Lett.* **2002**, *5*, A195-A197; (b) Guo, Q. H.; Pintauro, P. N.; Tang, H.; O'Connor, S. *J. Membr. Sci.* **1999**, *154*, 175-181.

(17) Wainright, J. S.; Wang, J. T.; Weng, D.; Savinell, R. F.; Litt, M. *J. Electrochem. Soc.* **1995**, *142*, L121-L123.

(18) Samms, S. R.; Wasmus, S.; Savinell, R. F. *J. Electrochem. Soc.* **1996**, *143*, 1225-1232.

(19) Chen, S.-L.; Krishnan, L.; Srinivasan, S.; Benziger, J.; Bocarsly, A. B. *J. Membr. Sci.* **2004**, *243*, 327-333.

(20) Miyatake, K.; Zhou, H.; Watanabe, M. *Macromolecules* **2004**, *37*, 4956-4960.

(21) For example: (a) Chen, J.; Asano, M.; Yamaki, T.; Yoshida, M. *J. Membr. Sci.* **2005**, *256*, 38~45; (b) Schmidt, T. J.; Simbeck, K.; Scherer, G. G. *J. Electrochem. Soc.* **2005**, *152*, A93-A97; (c) Bae, B.; Ha, H. Y.; Kim, D. *J. Membr. Sci.* **2006**, *276*, 51-58.

(22) For example: (a) Kerres, J.; Cui, W.; Disson, R.; Neubrand, W. *J. Membr. Sci.* **1998**, *139*, 211-225; (b) Mikhailenko, S. D.; Wang, K.; Kaliaguine, S.; Xing, P.; Robertson, G. P.; Guiver, M. D. *J. Membr. Sci.* **2004**, *233*, 93-99; (c) Kerres, J.; Cui, W.; Reichle, S. *J. Polym. Sci., Part A: Poly. Chem.* **1996**, *34*, 2421-2438.

(23) Grot, W. G. (E. I. DuPont) US 4,433,082, **1984**.

(24) Zawodzinski, T. A.; Neeman, M.; Sillerud, L. O.; Gottesfeld, S. *J. Phys. Chem.* **1991**, *95*, 6040-6044.

(25) Kerres, J.; Cui, W.; Reichle, S. *J. Polym. Sci., Part A: Poly. Chem.* **1996**, *34*, 2421-2438.

(26) Heitner-Wirguin, C. *J. Membr. Sci.* **1996**, *120*, 1-33.

(27) Kerres, J.; Cui, W.; Junginger, M. *J. Membr. Sci.* **1998**, *139*, 227-241.

(28) Zaidi, S. M. J.; Mikhailenko, S. D.; Robertson, G. P.; Guiver, M. D.; Kaliaguine, S. *J. Membr. Sci.* **2000**, *173*, 17-34.

(29) Xing, P.; Robertson, G. P.; Guiver, M. D.; Mikhailenko, S. D.; Kaliaguine, S. *Macromolecules* **2004**, *37*, 7960-7967.

(30) Zawodzinski, T. A.; Derouin, C.; Radzinski, S.; Sherman, R. J.; Springer, T.; Gottesfeld, S. *J. Electrochem. Soc.* **1993**, *140*, 1041-1047.

(31) Vie, P.; Paronen, M.; Stromgard, M.; Rauhala, E.; Sundholm, F. *J. Membr. Sci.* **2002**, *204*, 295-301.

(32) Zawodzinski, T. A.; Neeman, M.; Sillerud, L.; Gottesfeld, S. *J. Phys. Chem.* **1991**, *95*, 6040-6044.

(33) For example: (a) Kopitzke, R. W.; Linkous, C. A.; Anderson, H. R.; Nelson, G. L. *J. Electrochem. Soc.* **2000**, *147*, 1677-1681. (b) Kerres, J.; Cui, W.; Reichle, S. *J. Polym. Sci., Part A: Poly. Chem.* **1996**, *34*, 2421-2438.

(34) Kreuer, K. D. *J. Membr. Sci.* **2001**, *185*, 29-39.

(35) Kim, Y. S.; Wang, F.; Hickner, M.; Mccartney, S.; Hong, Y. T.; Harrison, W.; Zawodzinski, T. A.; Mcgrath, J. E. *J. Polym. Sci., Part B: Poly. Phys.* **2003**, *41*, 2816-2828.

Chapter 4

APPLYING NANO-TECHNOLOGY TO FUEL CELLS:

MOLDED, HIGH SURFACE AREA PROTON EXCHANGE MEMBRANES

4.1 Introduction

Fuel cells will be one of the most important technologies in the 21st century. They can not only provide pollution-free clean energy, but also give high quality and more reliable power. Of various types of fuel cells, the technology based on polymer electrolyte membrane fuel cells is most attractive for various applications, especially for transportation, portable electronic devices, and distributed power generation where high power-to-weight ratios and fast start-up times are needed.[1-3] The most important component of the polymer electrolyte membrane fuel cells is the membrane electrode assembly (MEA), at the heart of which is a polymeric, proton-conductive membrane. The key functions of this proton exchange membrane (PEM) are to transport protons from the anode to the cathode and to separate the fuel and the oxidant. As discussed in Chapter 1 and Chapter 3, significant resources have been devoted to develop high performance and reliable membranes. Of the various PEM systems studied, the perfluorinated ionomer Nafion® stands as the current bench mark material.

Conventionally, Nafion® and most other PEM materials are processed into a membrane form by melt extrusion or solvent casting and employed as pre-formed membranes in MEA fabrication. However, the requirement of using pre-formed membranes may restrict new fuel cell designs and developments. Holdcroft and coworkers[4] proposed the concept of making PEMs from curable liquid precursors and pointed out that such a liquid to PEM approach may enable the formation of PEMs to be conformable by injection molding, formed as micro-channels and unique shapes, or strongly adhering to the catalyst layer without hot pressing. They dissolved a preformed linear proton conducting polymer, sulfonated poly(ether ether ketone) (SPEEK) in a mixture of vinyl monomer and cross-

linking agent and polymerized this composition to form a semi-interpenetrating network in which SPEEK stayed as a guest polymer in a statistically cross-linked host polymer matrix. By doing so, they demonstrated the fabrication of 1 mm features using photolithographic techniques. However, such big features are essentially no use for many fuel cell developments since the thickness of most components in fuel cells are in the range of tens of microns. Moreover, the guest SPEEK is not chemically attached to the network and can be leached out.

In Chapter 3, we presented a new strategy for making highly proton conductive PEMs from easily processable, 100% curable, low molecular weight reactive liquid precursors. Highly fluorinated liquid precursors based on styrenically functionalized reactive perfluoropolyethers (sPFPE) were used in conjunction with a fluorinated derivative of sulfonated styrenic (SS) monomers. Chemically cross-linked PEMs with desired shape and thickness can be easily prepared from the liquid precursors and no further processing steps are needed. Application of highly fluorinated liquid precursors and the liquid precursor to PEM approach will provide many opportunities for fuel cell development that would be otherwise impossible.

The lack of processability of commercially available PEMs has curtailed fabrication strategies forcing all conventional PEMs to be flat and smooth at the surface. Such a 2-dimensional configuration sets an upper limit on the active surface area of fuel cells and therefore limits the power density that is ultimately achievable in fuel cells in addition to other issues such as transport phenomenon. Therefore, a high surface area 3-dimensional interface between the PEM and catalyst layer is highly desirable. Due to the highly fluorinated nature, the sPFPE and styrene sulfonate ester (SSE) liquid precursors have very

low surface energy and good spreading ability. By using imprint lithography/micro-molding techniques,[5,6] 3-dimensional, patterned PEMs with micron sized features can be easily fabricated with high fidelity. The patterned membranes can provide much larger active surface area between the proton conducting membrane and the catalyst layer, and a fuel cell based on such membranes can generate more power compared to those based on flat membranes with the same geometric size. This will be beneficial for the miniaturization of fuel cells and the integration of fuel cells as a desirable power source in the area of microelectronics and portable devices.

4.2 Experimental

4.2.1 Preparation of patterned membranes

The procedure of making patterned membranes is shown in Figure 4.1. A patterned perfluoropolyether (PFPE) mold was first generated by pouring α, ω-methacryloxy functionalized PFPE (PFPE-DMA) liquid precursor containing 1 wt% 1-hydroxycyclohexyl phenyl ketone over a patterned silicon master. The apparatus was degassed by nitrogen for 5 minutes and then exposed to UV light (λ = 365 nm) for 10 minutes under a nitrogen purge. The fully cured PFPE-DMA mold was then released from the silicon master and had the negative image of the silicon master.

The as prepared PFPE-DMA mold was cut to match the size of a glass substrate. Liquid cyano methyl acrylate (CMA) monomers were transferred onto the glass substrate and the PFPE-DMA mold was quickly placed on top of the CMA monomers. Air bubbles in the CMA liquid layer were carefully removed. The apparatus was kept at ambient conditions for 24 hr in order for the CMA monomers to polymerize. After the reaction was complete, the

poly(cyano methyl acrylate) (PCMA) became a solid polymer, having the negative image of the PFPE-DMA mold.

The PFPE-DMA mold was then removed from PCMA and the glass substrate. At this point, the patterned PCMA polymers were adhered to the glass substrate. This was used as a template to make patterned PEMs. A standard steel spacer with a thickness of 190 μm was attached to this template. Liquid precursors of sPFPE and SSE were then transferred onto the PCMA template and another glass slide was placed on top of the liquid precursors to obtain a membrane of uniform thickness. A mixture of 40: 60 (by weight) sPFPE and SSE liquid precursors was used to achieve highly proton conductive PEMs with good mechanical properties after hydrolysis.

The apparatus was then exposed to UV light (λ = 365 nm) for 40 minutes under a nitrogen purge. After the sPFPE-SSE membrane was fully cured, the top glass slide was first removed. The cured membrane and the PCMA template were then immersed in acetone, where PCMA polymer was dissolved and the cured sPFPE-SSE membrane was released.

To convert the SSE groups into styrene sulfonic acid (SSA), the patterned sPFPE-SSE membranes were soaked in a 5:6 (v/v) mixture of 30% NaOH aqueous solution and methanol for 12 h and then refluxed in the same mixture for an additional 10 h. After rinsing with distilled water, the membranes were stirred for a total of 24 h in fresh 20 wt% HCl solution, which was refreshed four times. The resulting sPFPE-SSA membranes were in the acid form. Residual HCl was removed by washing with distilled water.

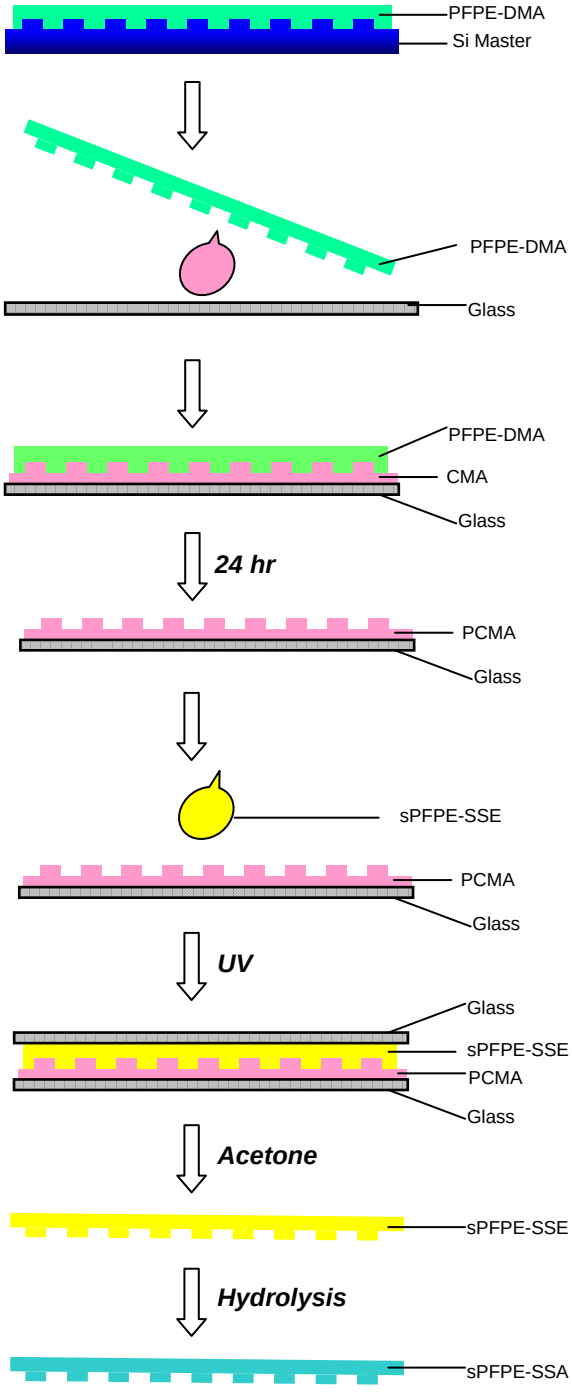

Figure 4.1 Fabrication of patterned membranes

4.2.2 Microscopy characterization

Scanning electron microscope (SEM) images were performed on a Hitachi S4700 SEM. In order to obtain high quality images, samples were coated with a thin layer of gold (around 10 nm) using a standard sputter-coater (Cressington 108 auto).

Atomic force microscopy (AFM) images were taken in the tapping mode using a Multimode Atomic Force Microscope from Veeco Metrology group. The instrument was equipped with Nanoscope IIIA control station and silicon cantilevers from Mikromasch USA with resonance frequencies of about 160 kHz, spring constants of 5.0 N/m, and radii less than 10 nm.

4.2.3 Ion exchange capacity measurement

Ion exchange capacity (IEC) and equivalent weight (EW) of the membranes were determined by titration of the sulfonic acid groups. In a typical titration measurement, a piece of sPFPE-SSA membrane (typically 0.2~0.3g) was stirred with saturated NaCl solution overnight, the resulting solution was then titrated with standardized 0.01 mol/L NaOH solution using phenolphthalein as the indicator. The titrated membrane was in the salt form and dried over phosphorus pentaoxide (P_2O_5) for a week at room temperature, at which point it was accurately weighed. The EW and IEC of the membranes are calculated as follows:

$$EW\ (H^+,\ g\ mol^{-1}) = [Dry\ weight\ /(V_{NaOH}*[NaOH])] - 22$$

$$IEC\ (meq\ g^{-1}) = 1000/EW$$

4.2.4 Fuel cell performance

To evaluate the fuel cell performance of the patterned sPFPE-SSA membranes and study the effect of surface area, catalyst ink was formulated in house. In a typical ink formulation, distilled water (0.192 g) was added drop-wise to 0.2 g carbon supported catalyst (ETEK, 20wt% Pt on C) to wet the catalyst. Nafion® dispersion (5wt%, 2.56 g) was then added to the catalyst drop by drop. The mixture was stirred for several hours to obtain a well dispersed ink like mixture. Ultra-sonication could be applied to get better dispersion.

Membrane electrode assembly (MEA) was prepared by painting the catalyst ink onto both sides of the membrane. The catalyst loading was about 0.2 $mgPt/cm^2$ based on the geometrical surface area of the membranes. The painted membrane was then sandwiched between two pieces of ELAT® gas diffusion substrates (ETEK, NJ) and fixed in the fuel cell testing hardware. The MEAs were tested at 50 ^oC and 75% relative humidity under atmospheric pressure using hydrogen and oxygen as the fuel and the oxidant. A flow rate of 0.1 L/min was used for all the experiments.

4.3 Results and discussion

4.3.1 Preparation of patterned membranes

Due to the lack of processability, conventional PEM materials are processed into a membrane form by melt extrusion or solvent casting and the resulting membranes are flat and smooth at the surface. Patterned membranes with micro-scale or below features at the surface are desired for fuel cell development. Starting from easily processable, 100% curable, highly fluorinated liquid precursors provides a feasible approach to make patterned membranes. Due to their highly fluorinated nature, the sPFPE and SSE liquid precursors have high spreading

and wetting ability. Once chemically cross-linked, the cured solid membranes display relatively low surface energy compared to most hydrocarbon materials. As discussed in Chapter 2, the surface energy of cured sPFPE homopolymer is 13.5 mN/m, and the surface energies of cured sPFPE-SSE membranes with 30 wt% to 70 wt% SSE are in the range of 15.0 to 18.5 mN/m. These surface energies are significantly lower than silicon-based elastomer poly(dimethylsiloxane) (~22 mN/m) and comparable or even lower than that of Teflon® (18 mN/m).[7] As a result, the cured PFPE homopolymer or sPFPE-SSE copolymer membranes can be easily released from the contacting surface.

In order to obtain high proton conductivity and good mechanical integrity after hydrolysis, a homogeneous mixture of 40 wt% sPFPE and 60 wt% SSE were used in preparing patterned membranes. For this particular composition, the fully cured sPFPE-SSE membranes displayed a surface energy of 17.0 mN/m and a tensile modulus of 114 MPa. After hydrolysis, the resulting sPFPE-SSA PEMs had an ion exchange capacity (IEC) of 1.5 meq/g and a proton conductivity of 0.13 S/cm at room temperature under fully hydrated conditions. The thermal, mechanical, and other properties of the sPFPE-SSA PEMs with this composition have been discussed in detail in Chapter 3.

In our initial efforts of making 3-dimensional patterned PEMs, liquid precursors of sPFPE and SSE were transferred onto a patterned silicon master and cured under nitrogen purge. The resulting solid sPFPE-SSE membrane was then released from the silicon master and had the negative image of the master. By this approach, membranes with micron sized features and high fidelity could be obtained. Figure 4.2 shows some examples of patterned membranes prepared in this way. Figure 4.2 (a) shows the image of a membrane with “shark-skin” pattern, which has features of 2 micron in width and 6 micron in height. Figure 4.2 (b)

displays the image of a membrane with 3 micron posts on surface. Figure 4.2 (c) shows a patterned membrane with nano-pillars of diameter around 200 nm. While high fidelity patterned membranes could be obtained by this approach, the silicon master was broken after repeated use (typically 10-20 times).

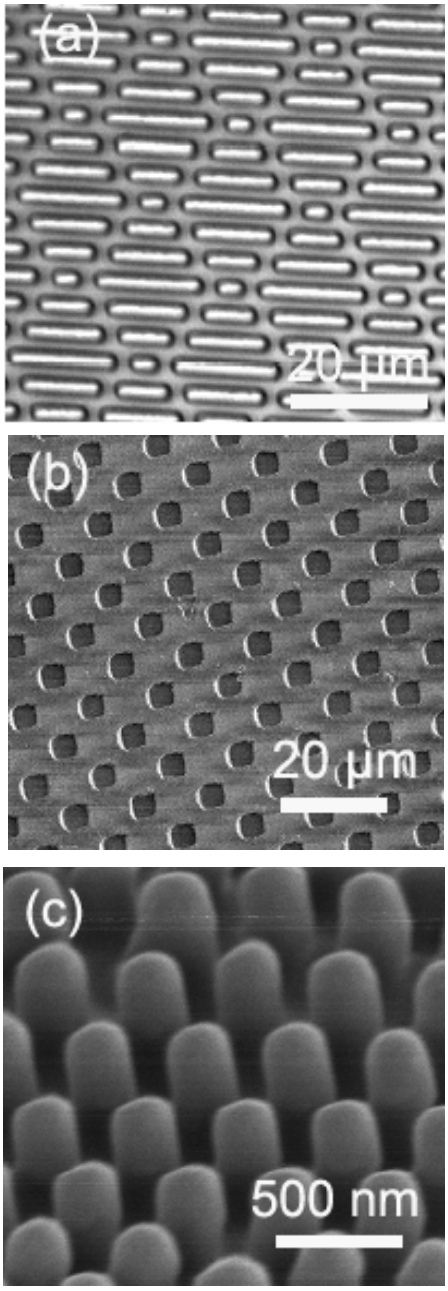

Figure 4.2 Examples of patterned membranes prepared by directly molding the permanent master.

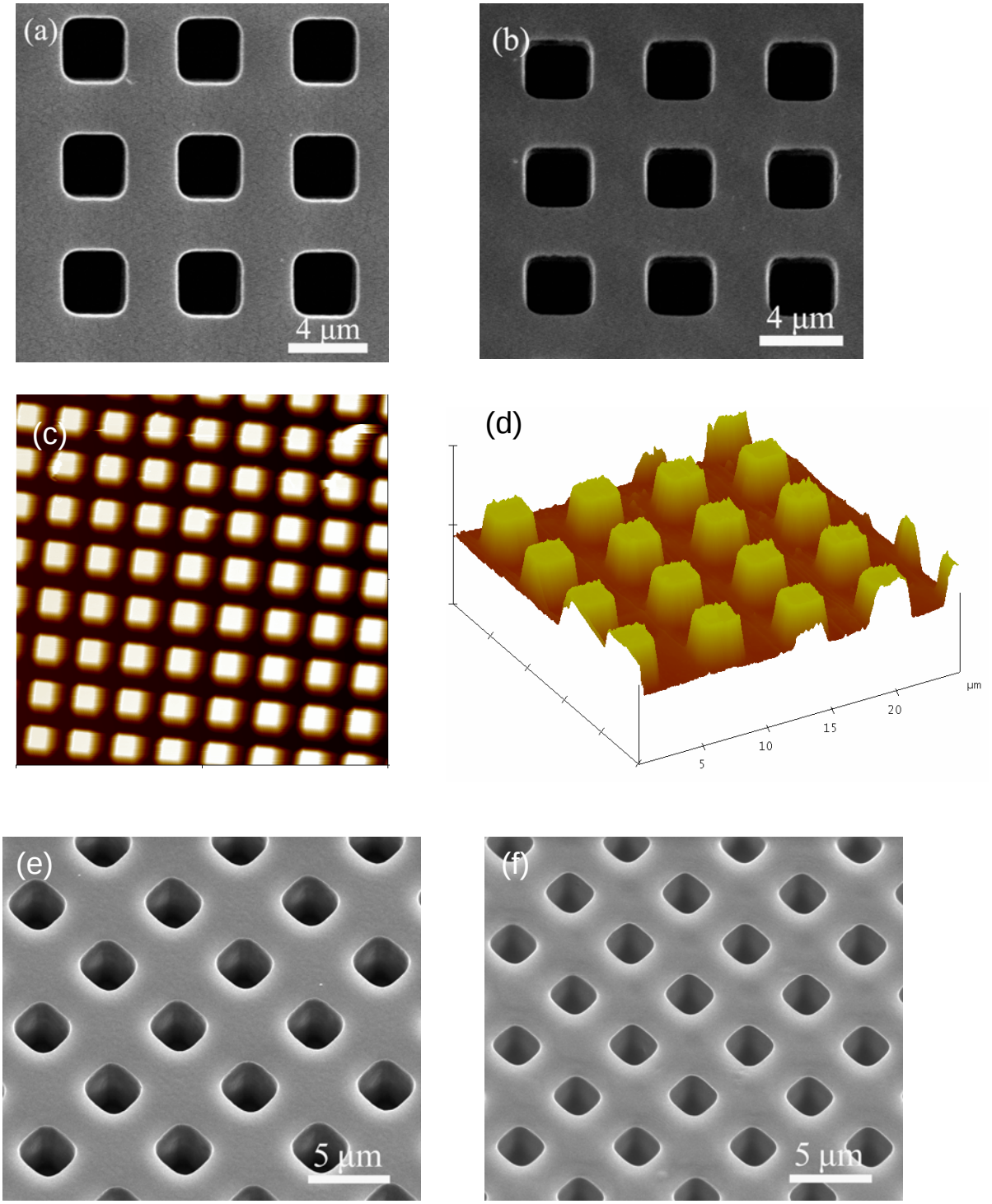

Figure 4.3 (a) SEM image of PFPE-DMA mold taken directly above the sample; (b) SEM image of PFPE-DMA mold taken at a 30 degree angle; (c) 2-dimensional AFM image of PCMA template; (d) 3-dimensional AFM image of PCMA template; (e) SEM image of sPFPE-SSE membrane and (f) SEM image of sPFPE-SSA membrane taken at a 30 degree angle.

In order to prepare patterned membranes without potentially breaking the expensive silicon master, a fabrication method based on imprint lithography/micro-molding techniques was developed as described in Figure 4.1. The detailed fabrication procedures are given in the experimental section. In order to minimize any potential stress build-up in the silicon master and maximize its lifetime, a high fidelity PFPE-DMA mold was first prepared having the negative image of the silicon master. Figure 4.3 (a) and (b) shows the SEM images of a PFPE-DMA mold taken directly above the sample or at a 30 degree angle. The fully cured PFPE-DMA has a tensile modulus of 3.9 MPa[8] and a surface energy of 8.6 mN/m. With such low surface energy and modulus, cured PFPE-DMA membranes can be easily released from the patterned silicon master without any damage to the master.

Due to the low modulus of PFPE-DMA and its similar chemical nature with sPFPE/SSE, it is not easy to use the PFPE-DMA mold to make patterned sPFPE-SSE membranes of uniform thickness. Therefore, a poly(cyano methyl acrylate) (PCMA) template was prepared on a glass substrate using the PFPE-DMA mold. Figure 4.3 (c) and (d) show the 2-dimensional and 3-dimensional AFM images of the PCMA template.

Liquid precursors of sPFPE and SSE were then transferred on to the PCMA template equipped with a standard steel spacer, which was used to control the membrane thickness. Another glass slide was placed on top of the liquid precursors and the apparatus was exposed to UV light for 40 minutes under nitrogen purge. After curing, the top glass slide and the spacer were removed and the rest of the apparatus was immersed in acetone. After PCMA dissolved in acetone, the patterned sPFPE-SSE membranes were released and hydrolyzed. Figure 4.3 (e) shows the SEM image of a patterned sPFPE-SSE membrane taken at a 30 degree angle. As demonstrated by the figure, high fidelity patterns with micron sized features

were obtained. Figure 4.3 (f) shows the SEM image of the corresponding sPFPE-SSA membrane after hydrolysis. As demonstrated by the figure, the micron-scale features were well maintained during the hydrolysis process. The high IEC, acid form membrane absorbed some water from the vapor phase under ambient conditions. As a result, the membrane was swelled and the patterned features looked smaller than those in the ester form membrane. Nonetheless, patterned PEMs with high fidelity features and unprecedented levels of morphologic control can be achieved by this approach.

4.3.2 Effect of surface area on power output of fuel cells

The lack of processability of Nafion® has curtailed fabrication strategies forcing all conventional PEMs to be flat and smooth at the surface. Such a 2-dimensional configuration sets an upper limit on the active surface area of fuel cells and therefore limits the power density that is ultimately achievable in fuel cells in addition to other issues such as transport phenomenon. Therefore, a high surface area 3-dimensional interface between the PEM and catalyst layer is highly desirable. Starting from easily processable, 100% curable, highly fluorinated liquid precursors, patterned PEMs with unprecedented levels of morphologic control can be achieved by micro-molding / imprint lithography techniques.

The surface area of the patterned membrane can be controlled by varying the size and aspect ratio of the features, or the distance between separated features. In general, higher aspect ratio and smaller distance between features correlate with larger active surface area and the actual surface area of the patterned membrane can be easily calculated. For example, if a membrane surface is covered with $a \times a \times h$ squares and the distance between these squares is also a, the ratio of the actual surface area and the geometric surface area of the patterned

membrane is given by (1+h/a). Therefore, the actual surface area of the membrane is directly related to the aspect ratio h/a of the patterned features. To obtain the same actual surface area, for example, 10 times increase in surface area, square features with a height of 100 μm are required if the length of the squares is 10 μm. If the length of the squares is 1 μm, features with a height of 10 μm are needed to obtain the same 10 times increase in surface area. This is important since the height of the features is directly related to the thickness of the membrane, which has significant impact on the fuel cell performance. The thickness of current proton exchange membranes is typically in the range of 25-200 μm, and therefore patterned features in micron or below scale are needed.

While smaller features are good for increasing the surface area of thin membranes, they have to be big enough in order to obtain good contact with the catalyst. Figure 4.4 displays the SEM images of some aggregated catalyst particles. As shown in the figure, the diameter of Pt/carbon catalyst particles is typically around 50-100 nm. Therefore, patterned membranes with micron scale features are probably most appropriate for effective catalyst loading as well as reasonable membrane thickness.

During fuel cell operation, the fuel and the oxidant are supplied to the fuel cell as gases and water is generated as by-product of this electro-chemical process. While a certain amount of water is necessary to partially hydrate the proton exchange membrane, extra water has to be removed from the system for effective gas supply to the fuel cell. Excess water can result in flooding of the electrodes and mass transport limitation of the running fuel cells. The feature shape, size and aspect ratio of the patterned membranes will couple with these complicated transport issues and affect the performance of the fuel cells.

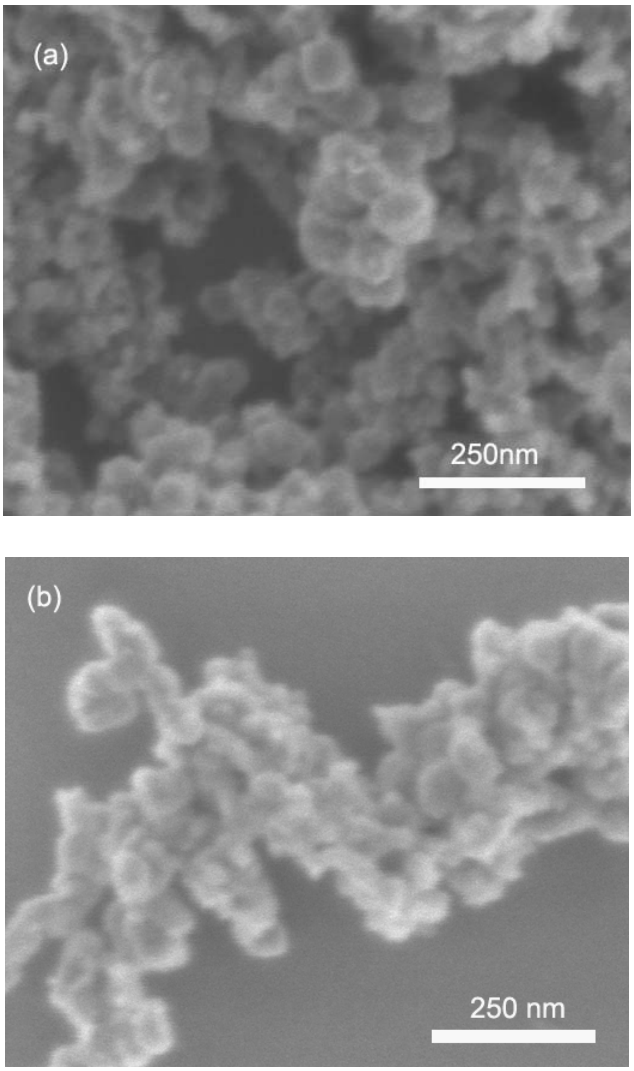

Figure 4.4 SEM images of aggregated catalyst particles

In an effort to minimize uncontrolled parameters and to study the effect of surface area on the power generation of fuel cells, patterned membranes with 3 μm square features were fabricated that differ only in the aspect ratios of the features. Figure 4.5 (a)-(c) shows the SEM images of the patterned membranes with aspect ratios of 0.47, 0.63 and 1.23, respectively. By employing soft lithographic techniques, the surface area of the patterned

PEMs can be increased in a systematic manner through the generation of high fidelity patterned membranes.

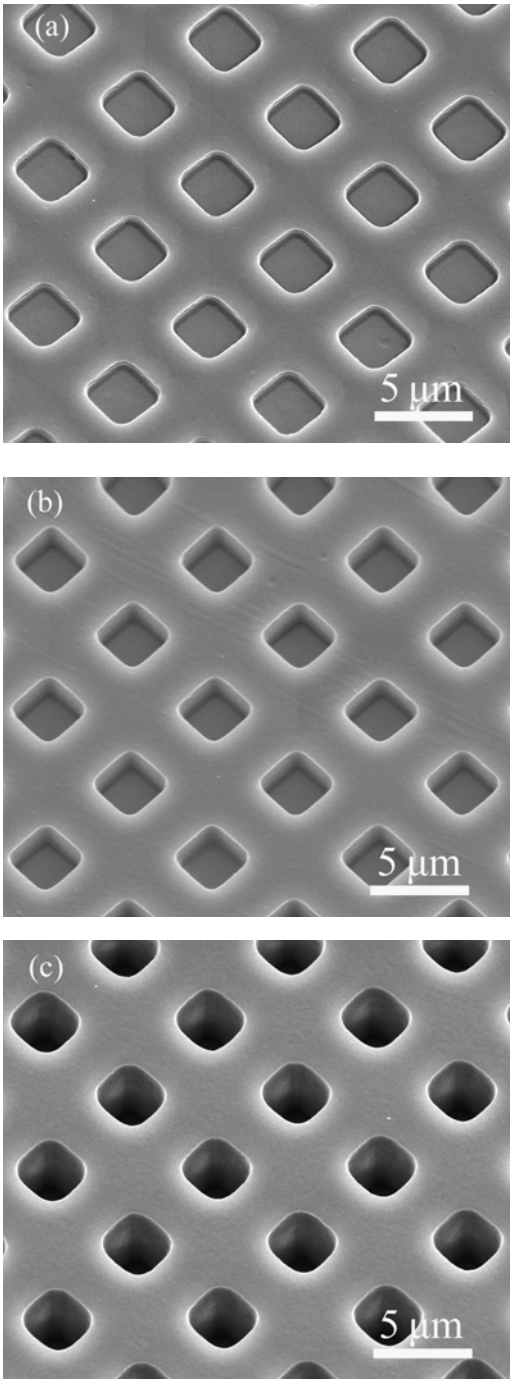

Figure 4.5 SEM images of patterned membranes with 3 μm square features and height of 1.4 μm, 1.9 μm and 3.7 μm, respectively.

To investigate the effect of surface area on the power output of fuel cells, MEA performance was evaluated for both the flat as well as for the patterned PEMs with an IEC value of 1.50 meq/g and a thickness of 190 μm under identical test conditions. A 5 cm^2 test fixture was used in the fuel cell test system and as such the flat membrane system had an identical surface area to the test cell but the patterned PEMs had calculated surface areas of 7.3, 8.3 and 11 cm^2, respectively, all within the 5 cm^2 test cell area. A catalyst ink was formulated based on 20 wt% Pt/C catalyst, 5 wt% Nafion® dispersion and water. Based on the geometric surface area, a Pt loading of 0.2 mg/cm^2 was applied to all the membranes. For the flat membranes, the actual Pt loading was also 0.2 mg/cm^2 since the actual surface area was equal to the geometrical area. For the patterned membranes, the actual Pt loading was much lower at 0.13, 0.12, 0.09 mg Pt/cm^2, respectively.

The MEA performance of the flat and patterned membranes was measured at 50 $^{\circ}C$ and 75 % relative humidity (RH) and the results are compared in Figure 4.6 (a) and (b). As shown in Figure 4.6 (a), all of the patterned membranes displayed much better performance than the flat PEMs. When the cell potential was greater than 0.5 V, the MEA performance was found to be closely proportional to the surface area of the membranes, with the higher surface area PEMs displaying better performance. At the higher current density region where the cell potential was lower than 0.5 V, a mass transfer limitation was observed, presumably due to flooding, which diminished the value of enhancing the PEM surface area. Under the test conditions, a power density as high as 225 mW/cm^2 was obtained for the patterned PEM, while that of the flat one was only 127 mW/cm^2. At a current density of 360 mA/cm^2, the MEA made from a flat PEM displayed a power density of 127 mW/cm^2, while the power

density of MEAs made from patterned PEMs was measured to be 188, 199 and 204 mW/cm^2, respectively, which was 1.48, 1.57 and 1.61 times of the flat one.

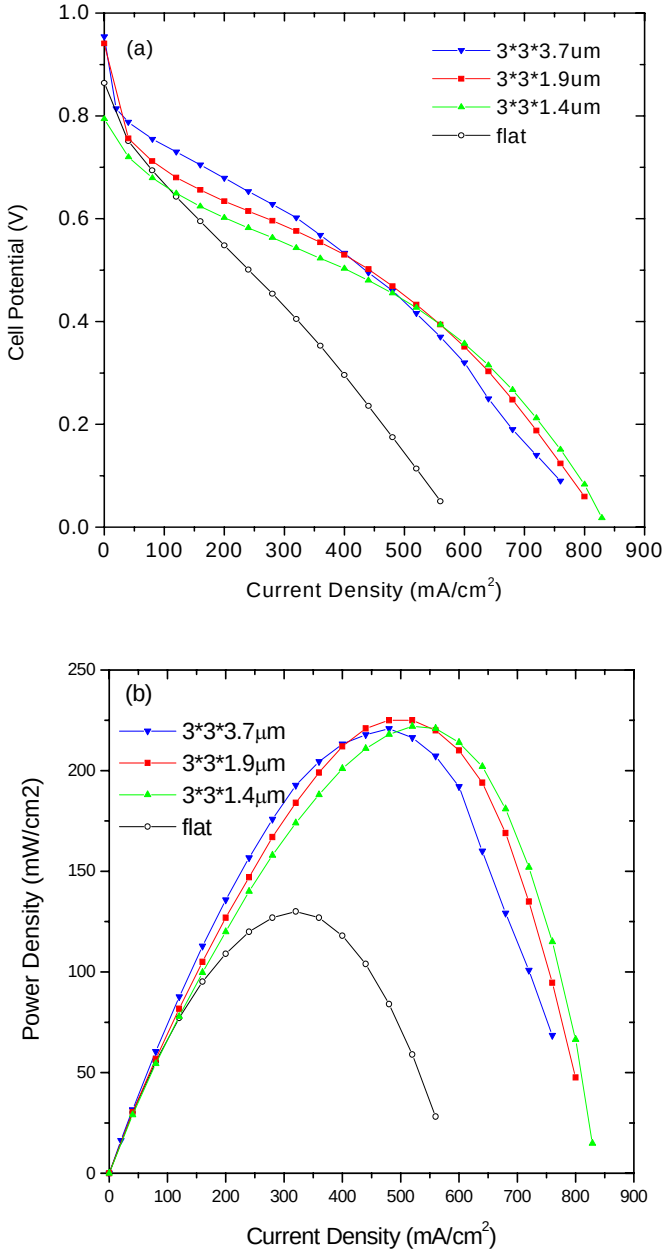

Figure 4.6 MEA performance of patterned and flat sPFPE-SSA membranes with an IEC value of 1.50 meq/g and a thickness of 190 μm at 50 ^{o}C and 75% RH: (a) polarization curves and (b) power output curves.

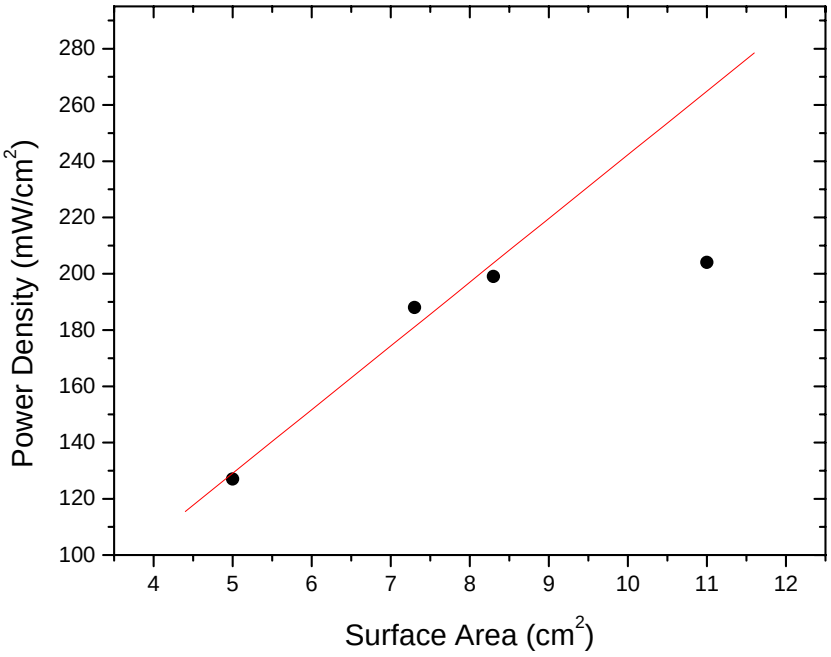

Figure 4.7 Power densities of fuel cells based on sPFPE-SSA membranes as a function of surface area.

Due to the higher membrane thickness, un-optimized electrodes preparation, and milder operation conditions, such power densities are not as high as some published results for thinner membranes, but it is important as a proof of concept. Figure 4.7 shows the power density of the fuel cells based on the flat and patterned membranes as a function of the active surface area of the membranes. The power density obtainable increased in an almost linear fashion as a function of surface area except for the membrane with a surface area of 11 cm^2. We believe the nonlinear relationship seen is due to the lower catalyst loading for the higher surface area membranes. Nonetheless, the higher surface area PEMs clearly results in higher power output of the fuel cells with the same geometric size. Therefore, the same power generation requirement can be achieved from a much smaller fuel cell stack composed of the

patterned membranes than that composed of conventional flat membranes. This can potentially miniaturize fuel cells and promote their application in portable devices.

4.4 Conclusions

Starting from easily processable, 100% curable, highly fluorinated liquid precursors, 3-dimensional, patterned PEMs with an unprecedented level of morphological control can be fabricated by using imprint lithography/micro-molding techniques. The as-prepared patterned PEMs are chemically cross-linked and highly proton conductive. The surface area of the patterned membranes can be systematically controlled by varying the size and aspect ratio of the patterned features. A series of patterned membranes with micron scale features and surface area 1~2.3 times that of the flat membrane were prepared with high fidelity. Fuel cell performance of the patterned membranes demonstrated that high surface area patterned PEMs resulted in higher power output of the fuel cells within the same geometric size. This is potentially beneficial for the miniaturization of fuel cells and the integration of fuel cells as a desirable power source in the area of microelectronics and portable devices.

This liquid precursor to PEM approach also provides many opportunities for fuel cell development that would be otherwise impossible. To improve the performance of direct methanol fuel cells, tri-layer membranes with centered methanol barrier layers has been proposed.[9] By spin-coating and curing sPFPE-SSE precursors with different IECs layer by layer, PEMs with controllable gradient in ion content and virtually continuous changing properties can be obtained with good adherence between the layers. Highly proton conductive liquid precursors may also be used to replace solvent based Nafion® dispersions used for catalyst inks with enhanced interfacial contact. Moreover, the liquid precursors to

PEM approach provides the possibility to fabricate MEAs with tailored interfacial properties by injection molding of liquid PEM precursors between pre-assembled electrodes. These possibilities are planned to study for future directions.

4.5 References

(1) Appleby, A. J.; Foulkes, R. L. *Fuel Cell Handbook*; Van Nostrand Reinhold: New York, **1989**.

(2) Whittingham, M. S.; Savinell, R. F.; Zawodzinski, T. A. *Chem. Rev.* **2004**, *104*, 4243-4244.

(3) Malhotra, S.; Datta, R. J. *J. Electrochem. Soc.* **1997**, *144*, L23-L26.

(4) Schmeisser, J.; Holdcroft, S.; Yu, J.; Ngo, T.; McLean, G. *Chem. Mater.* **2005**, *17*, 387-394.

(5) Xia, Y.; Whitesides, G. M. *Angew. Chem. Int. Ed.* **1998**, *37*, 550-575.

(6) Rolland, J. P.; Hagberg, E. C.; Denison, G. M.; Carter, K. R.; DeSimone, J. M. *Angew. Chem. Int. Ed.* **2004**, *43*, 5796-5799.

(7) Rossier, J.; Reymond, F.; Michel, P. E. *Electrophoresis* **2002**, *23*, 858-867.

(8) Rolland, J. P.; Dam, R. M. V.; Schorzman, D. A.; Quake, S. R.; DeSimone, J. M. *J. Am. Chem. Soc.* **2004**, *126*, 2322-2323.

(9) Si, Y.; Lin, J.-C.; Kunz, H. R.; Fenton, J. M. *J. Electrochem. Soc.* **2004**, *151*, A463-A469.

Chapter 5

EFFECTS OF CROSS-LINK DENSITY ON THE PROPERTIES OF FLUOROPOLYMER PROTON EXCHANGE MEMBRANES

5.1 Introduction

Fuel cells are devices that convert the chemical energy stored in a fuel directly into electricity. As a highly efficient and environmentally benign power source, fuel cells are attracting a lot of interest, both academically and industrially.[1-3] Of the various fuel cell systems considered, polymer electrolyte membrane (PEM) fuel cells seem to be the most suitable power source for passenger vehicles and portable devices due to their simplicity in design, low operation temperature and good CO_2 tolerance. In the heart of PEM fuel cells, a solid polymeric membrane serves as a proton conductor as well as a fuel barrier and a mechanical separator between the anode and the cathode. Significant efforts have been devoted to develop high performance and reliable membranes.

Proton exchange membranes suitable for fuel cell applications should have the following properties: (1) high protonic conductivity and low electric conductivity; (2) low fuel crossover; (3) good chemical and mechanical stability.[4] High proton conductivity can be achieved by incorporating a high concentration of ion conducting sites into the membrane, namely, high ion exchange capacity (IEC). However, this also leads to compromised mechanical stability and perm-selectivity for linear PEM materials.[5] Chemically cross-linkable ionomeric systems offer the potential of achieving both high proton conductivity and good mechanical properties without the associated challenges for linear polymers. Furthermore, chemical cross-linking can reduce the swelling effects[5-10] and improve the mechanical and hydrolytic stability[7-9] of the membrane. It is also reported that cross-linked membranes demonstrate lower fuel cross-over[9-11] and better performance[7,9] than the corresponding linear PEMs.

Compared to the extensive studies on linear PEM materials, research on cross-linked PEMs is limited. Several cross-linked ion exchange membrane systems are reported in the literature. The important systems include:

(1) Copolymerization of styrene and divinylbenzene and subsequent sulfonation of the cross-linked membranes.[12] Since cross-linked systems are not processable, thickness of the membranes is fixed by the copolymerization conditions.

(2) γ – irradiation of polytetrafluoroethylene (PTFE),[6] poly(tetrafluoroethylene-*co*-hexafluoropropylene) (FEP),[7,9] poly(vinyl fluoride) (PVDF)[13] or Nafion[14] thin films with subsequent grafting of styrene/divinylbenzene or alkyl vinyl ether onto the produced radical sites, and followed by sulfonation of the grafted chains. Membranes prepared in this way are not homogeneous with sulfonation occurring only in the grafted layers, and the membrane thickness is fixed by the thickness of the center PTFE/FEP/PVDF/Nafion layer.

(3) Cross-linking of block copolymers containing a polystyrene block.[8,11] Sulfonation of the polystyrene blocks can be carried out pre- or post- cross-linking. Cross-linking of the pre-sulfonated membranes usually takes place between the sulfonic acid groups on different molecules, resulting in a decrease in conductivity; while post-sulfonation is slow and not uniform across the membrane.[8]

(4) Crosslinking through intra/inter chain bridging links to the sulfonic acid functionalities.[15,16] Similar to the cross-linking of pre-sulfonated block copolymers, reaction between sulfonic acid groups results in a decrease in acid content and therefore lower proton conductivity of the membrane.

(5) Cross-linking of poly(vinyl alcohol) (PVA) based materials through the reaction of hydroxyl groups with external cross-linkers.[10,17-20] The acid functionalized components (e.g. polystyrene sulfonic acid -*co*- maleic acid, poly (2-acrylamido-2-methyl-1-propanesulfonic acid), or poly(acrylic acid)) in these systems are blended with PVA and have the potential to leach out. Moreover, the thermal stability of these membranes is lower than most PEM systems.

In Chapter 3 and Chapter 4, we reported a novel cross-linked PEM material prepared from 100% curable liquid precursors without the use of solvents or the generation of volatiles. Highly fluorinated liquid precursors based on styrenically functionalized reactive perfluoropolyethers (sPFPEs) were used in conjunction with a fluorinated derivative of sulfonated styrenic (SS) monomers. These liquid precursors are like oil at room temperature and can be cured into any shape and size without further processing. PEMs were prepared by copolymerization of these fluorinated species into fully cured membranes and subsequent hydrolysis (Figure 5.1). By employing chemically cross-linked systems, PEMs with very high proton conductivity were achieved while maintaining good mechanical integrity. Patterned, 3-dimensional membranes were prepared from these liquid precursors using imprint lithographic technique and the increased surface area of patterned PEMs resulted in increased power output over standard flat membranes within the same geometric size. sPFPE precursors with different molecular weights can be used to make membranes of different cross-link density. In this chapter, the influence of cross-link density on the properties of the PEMs is studied.

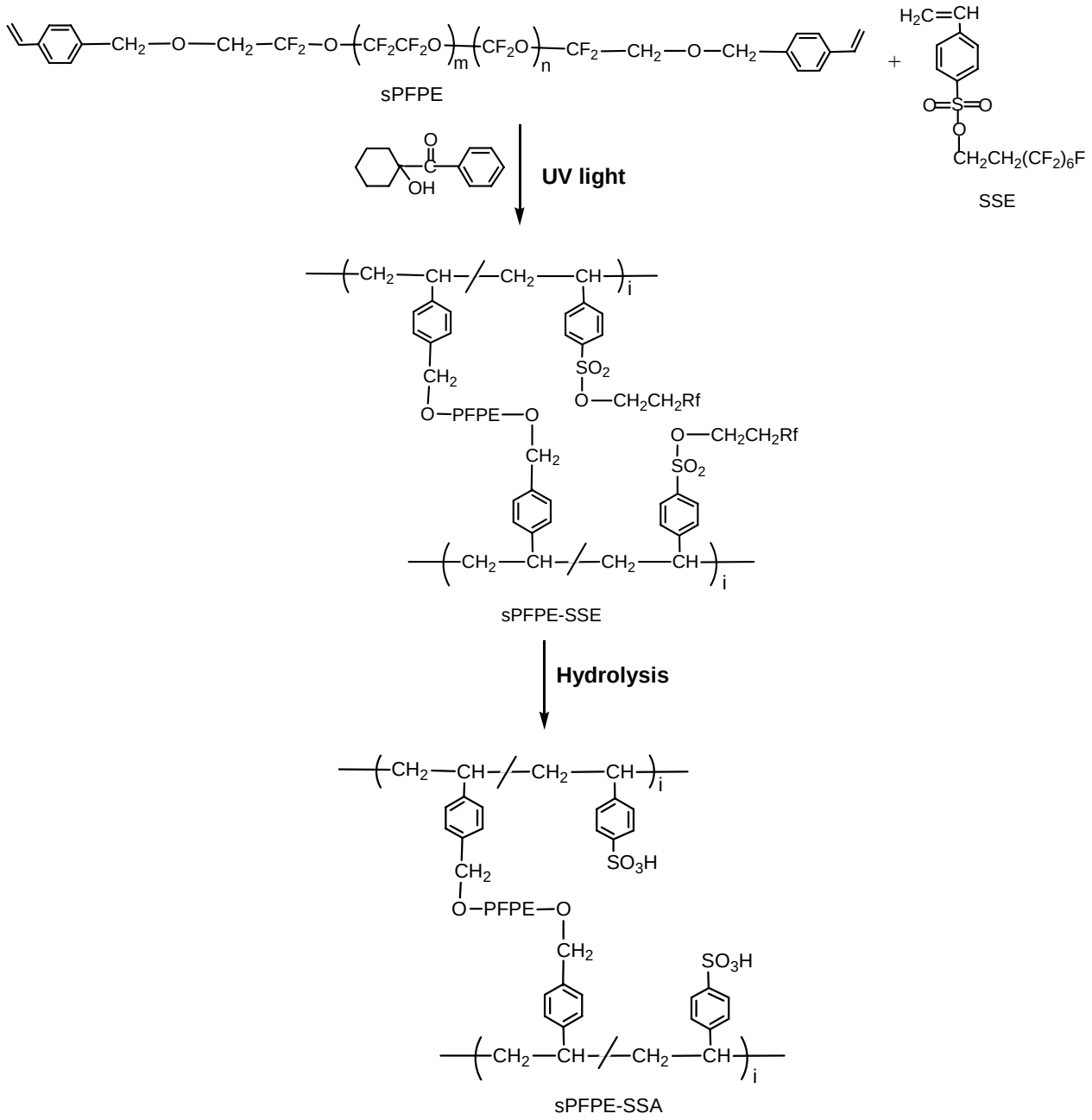

Figure 5.1 Synthesis and chemical structure of sPFPE-SSA membranes

5.2 Experimental

5.2.1 Materials and Synthesis

Poly(tetrafluoroethylene oxide-*co*-difluoromethylene oxide) (PFPE) α-, ω- diol was purchased from Solvay Solexis. 1, 1, 1, 3, 3-pentafluorobutane was obtained from Solvay Fluoride. All other chemicals were purchased from Aldrich and used as received. The synthesis of styrene modified poly(tetrafluoroethylene oxide-*co*-difluoromethylene oxide) (sPFPE) and the synthesis of the fluorinated sulfonated styrenic ester (SSE) monomers have been reported in Chapter 2. Two different sPFPEs with number average molecular weight of 4000 g/mol and 1000 g/mol, respectively, were used to control the crosslink density of the cured membrane.

5.2.2 Membrane preparation

To make a cross-linked membrane, sPFPE with 1wt% photo-initiator (1-hydroxycyclohexyl phenyl ketone) and SSE were mixed in the desired ratios with 30-70 wt% SSE. The mixture was heated above 40 ^{o}C to form a homogeneous yellow liquid. The liquid precursor was poured onto a preheated substrate fitted with a standard steel spacer and chemically crosslinked by irradiation with UV light (λ=365 nm) for 40 min under nitrogen purge. The resulting solid membrane is in the ester form, transparent and slightly yellow.

To convert the sulfonate ester groups (SSE) into sulfonic acid (SSA), the membrane was soaked in a 5:6 (v/v) mixture of 30% NaOH aqueous solution and methanol for 12 h and then refluxed in the same mixture for an additional 10 h. After rinsing with distilled water, the membrane was stirred for a total of 20 h in fresh 20 wt% HCl solution, which was refreshed four times. Residual HCl was removed by washing with distilled water.

5.2.3 Characterization

Ion exchange capacity (IEC) of the membranes was determined by titration of the sulfonic acid groups. In a titration measurement, a piece of membrane (typically 0.2~0.3g) in acid form was stirred with saturated NaCl solution overnight; the resulting solution was then titrated with standardized 0.01 mol/L NaOH solution using phenolphthalein as the indicator. The titrated membrane was in the salt form and dried over phosphorus pentaoxide (P_2O_5) for a week at room temperature, at which point it was accurately weighed. The equivalent weight (EW) and IEC of the membranes were calculated as follows:

$$EW\ (H^+,\ g\ mol^{-1}) = [Dry\ weight\ /(V_{NaOH}*[NaOH])] - 22$$

$$IEC\ (meq\ g^{-1}) = 1000/EW$$

After hydrolysis, the membranes were kept in water for at least 24 h at room temperature. The wet membranes were blotted dry and quickly weighed. The membranes were then dried over P_2O_5 for at least a week at room temperature and the dried membranes were weighed again. The water uptake of the membranes expressed as a weight percentage is calculated as follows:

$$Water\ uptake\ (wt\%) = (W_{wet} - W_{dry})/\ W_{dry}\ *100$$

Water sorption of the PEMs was also expressed as the number of water molecules per acid group (λ).

Proton conductivity was measured with AC Impedance over the frequency range of 1 Hz – 1 MHz. Impedance spectra were recorded using Solartron 1287 Impedance and Solartron 1255 HF frequency response analyzer. The conductivity cell was designed to ensure that the membrane resistance dominated the response of the system.[21] The membrane resistance was taken at the frequency that had zero phase angle. The proton conductivity (σ) was calculated using $\sigma = L/(RS)$, where L, R, S denoted the distance of the two electrodes, the measured resistance, and the cross-section area of the membrane perpendicular to the proton transport direction, respectively.

To evaluate the fuel cell performance of the PFPE-SSA membranes, LT 140E-W low temperature ELAT® gas diffusion electrodes (E-TEK, NJ) with a Pt catalyst loading of 5 g/m^2 painted with 5 wt% Nafion dispersion were used to achieve the most reproducible results. Membrane electrode assembly was fabricated by sandwiching the PEM and a piece of painted electrode on each side into the fuel cell testing hardware. The MEAs were tested at 50 ^oC and 75% relative humidity under atmospheric pressure using hydrogen and oxygen as the fuel and the oxidant. A flow rate of 0.1 L/min was used for all the experiments.

5.3 Results and discussion

In order to study the effect of cross-link density on the properties of PEM materials, two sPFPE liquid precursors were used, with number average molecular weight of 4000 g/mol and 1000 g/mol, respectively. Since the two sPFPE precursors have the same chemical structure, differing only in molecular weight, their reactivity should be the same. For both the sPFPE precursors and the SSE monomers, the reacting groups are styrene functionality connected to a fluorocarbon chain. Therefore, the reactivity ratio of the two precursor

materials is about one, and the composition of their copolymer should be very similar to the precursor feed ratio. Based on the precursor feed ratio, the IEC of the product PEM can be calculated. By comparing the measured IEC value with the calculated one, it was confirmed that both precursors were incorporated into the network structure of the membrane after curing and the composition of the membrane agreed with the precursor feed ratio. Therefore, the cross-link density of the sPFPE-SS system can be controlled systematically by changing the molecular weight of the sPFPE precursor. For most of the cross-linked PEM systems reported so far, the cross-link density can not be accurately controlled. Moreover, the cross-link density of the sPFPE-SSA PEMs can be controlled independent of the IEC of the membranes since the IEC value is determined only by the relative ratio of the two precursors.

By using different sPFPE precursors, two series of PEMs were fabricated with IEC ranging from 0.5 to 1.8 meq/g. The cross-link density of the PEMs made of sPFPE with a molecular weight of 1000 g/mol (sPFPE1000) is about 4 times that of membranes made of sPFPE with a molecular weight of 4000 g/mol (sPFPE4000).

5.3.1 Mechanical properties

In PEM fuel cells, the polymeric membrane serves as a proton conductor as well as a fuel barrier and a mechanical separator between the anode and the cathode. Therefore it is very important for the membrane to have good mechanical strength. The mechanical properties of the cross-linked membranes were measured by using an Instron and the effect of cross-link density was studied. With a glass transition temperature of -120 ^{o}C, the cross-linked sPFPE homopolymer is an elastomer at room temperature. As discussed in Chapter 2 and Chapter 3, the cured sPFPE-SS membranes displayed higher transition temperatures,

especially in the acid (H) form. As a result, the cured membranes started to lose their elastomeric features and displayed a higher modulus. The acid form membranes displayed properties of pure solid materials, and their moduli were shown in Figure 5.2. For both series of PEMs, increasing in SS content resulted in higher modulus due to the intrinsic properties of the SS. Compared to PEMs made from sPFPE4000 precursor, PEMs made from sPFPE1000 displayed higher modulus due to increase in cross-link density. But the increase in cross-link density did not result in linear increase in mechanical strength. For example, for PEMs with an IEC value of 0.83 g/mol, the membrane made from sPFPE4000 displayed a modulus of 55 MPa, while the one made from sPFPE1000 had a modulus of 108 MPa. Four times increase in cross-link density resulted in a doubling in the mechanical strength of the membranes.

The modulus of a polymer network can be approximated as a simple sum,[22]

$$G \approx G_x + G_e \approx \rho RT\,(1/M_x + 1/M_e)$$

Where ρ is the network density, R is the gas constant, T is absolute temperature, M_x is the molar mass of a network strand between cross-links and M_e is the entanglement molar mass. For PEMs made from sPFPE1000 precursor, the network strands are short ($M_x < M_e$) and there are no entanglements between network strands, therefore the modulus is controlled by cross-links for these network materials with short strands ($G \approx G_x$). For PEMs made from sPFPE4000 precursor, the network strands are longer and start to entangle, therefore both cross-links and entanglements contribute to the mechanical strength of the PEMs. This explains why the modulus of the PEMs was not linearly correlated with the cross-link density.

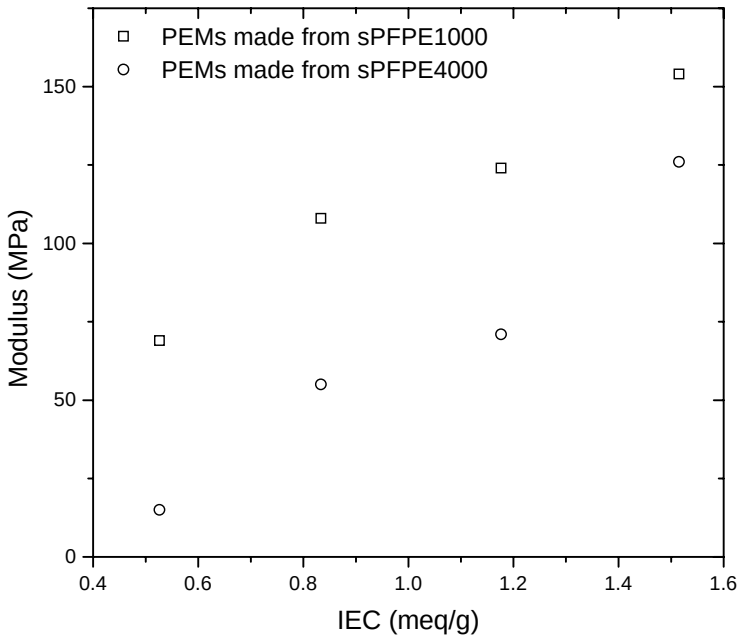

Figure 5.2 Effect of cross-link density on the moduli of sPFPE-SSA PEMs

5.3.2 Water uptake and swelling

Water uptake is important in determining the performance of PEM materials. Certain amount of water is necessary to facilitate proton transport in almost all current polymeric PEM materials. However, too much water can also result in excessive swelling of the membrane, loss of mechanical strength by acting as a plasticizer, and delamination between the membrane and the catalyst layer during fuel cell operation. Figure 5.3 shows the water uptake of the two series of sPFPE-SSA membranes due to water absorption from liquid water at room temperature. For PEMs made from sPFPE4000 precursor, the water uptake increased from 14 wt% to 113 wt% as IEC increased from 0.53 to 1.82 meq/g, while for PEMs made from sPFPE1000 precursor, the water sorption increased from 12 wt% to 67 wt% as IEC increased from 0.62 to 1.74 g/mol. Increase in cross-link density resulted in lower water

uptake, and this effect is more significant for PEMs with higher acid concentrations. Further analysis of this data indicated that not only membranes with higher cross-link density absorbed less water, but each acid group in these membranes interacted with less water molecules as demonstrated by the number of water molecules per acid group (λ). As shown in Figure 5.3 (b), for membranes made from the sPFPE4000 precursor, λ was in the range of 15~37 as IEC increased from 0.53 to 1.82 meq/g; while this number was only 11~21 for membranes made from the sPFPE1000 precursor within a similar IEC range.

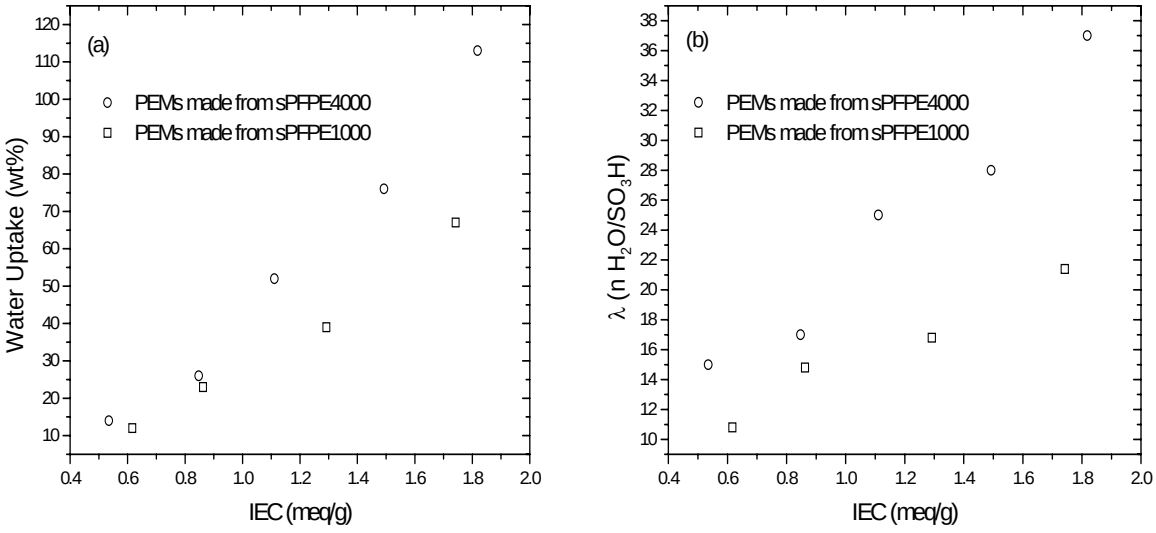

Figure 5.3 Effect of crosslink density on water uptake from liquid water

Compared to linear PEM materials, chemically cross-linked systems typically show a significantly smaller degree of swelling upon uptake of water. The influence of cross-link density on swelling was studied for the sPFPE-SSA systems. As shown in Figure 5.4, for PEMs made from sPFPE4000, the dimensional change was 9-42% as IEC increased from 0.53 to 1.82 meq/g under the testing conditions; while for membranes made from sPFPE1000, the dimensional change was in the range of 6-28% as IEC increased from 0.62

to 1.74 meq/g. Comparison of membranes of similar ion concentration displayed that a four-fold increase in cross-link density resulted in about 30% decrease in swelling. Increase in cross-link density can increase the structure density of the material and may result in decreased molecular mobility due to the tight network structure. Therefore, cross-linking can help to maintain the mechanical strength of the membranes and good interfacial properties between the membrane and the catalyst layer.

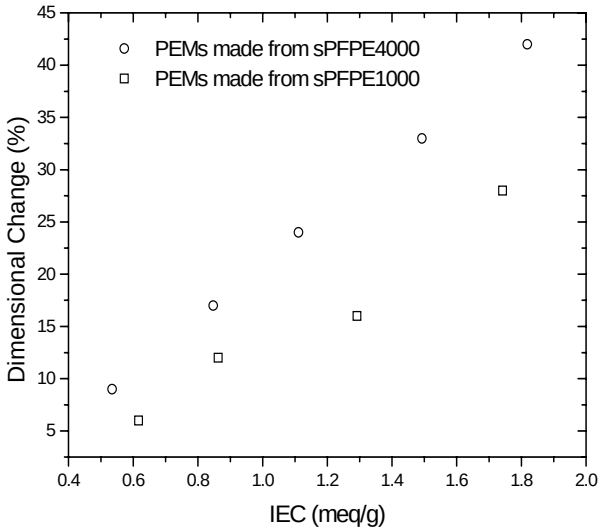

Figure 5.4 Effect of crosslink density on dimensional change

5.3.3 Proton conductivity

Proton conductivity is one of the most important properties for PEM materials to be effective. Figure 5.5 compares the proton conductivity of the two series of sPFPE-SSA PEMs at room temperature under fully hydrated conditions. As mentioned earlier, IEC and cross-link density can be controlled independently for this system. As IEC increased, there were more ion conducting sites in the membrane and higher conductivity was obtained for both

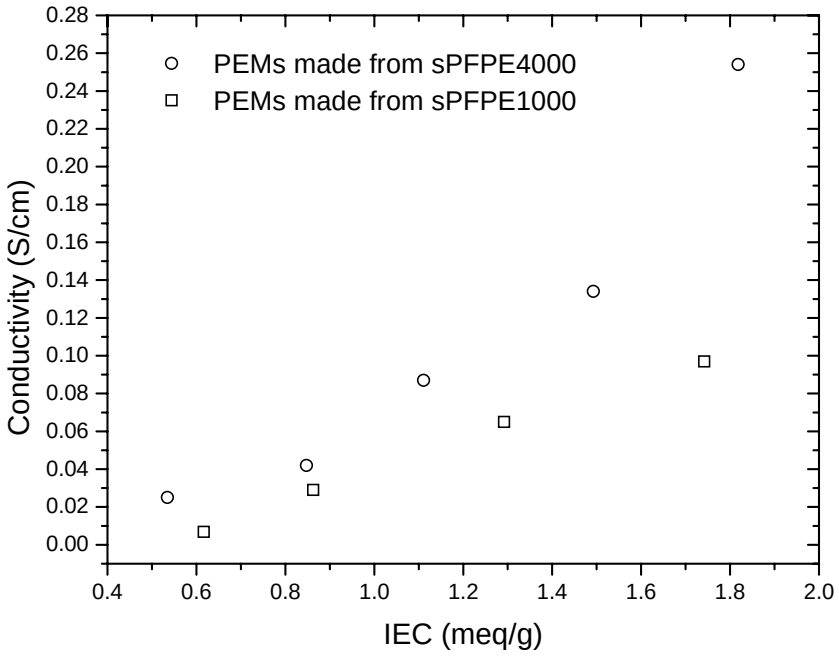

Figure 5.5 Effect of crosslink density on proton conductivity at room temperature and fully hydrated condition.

series of PEMs. For PEMs made from sPFPE4000 precursors, the proton conductivity increased from 0.025 to 0.254 S/cm as IEC increased from 0.53 to 1.82 meq/g; while for membranes made from sPFPE1000 precursors, the proton conductivity increased from 0.007 to 0.097 S/cm as IEC increased from 0.62 to 1.74 meq/g. Moreover, Figure 5.5 clearly demonstrates that proton conductivity strongly depend on the cross-link density of the membrane. The proton conductivity of PEMs made from sPFPE1000 was much lower than PEMs made from sPFPE4000. The magnitude of the specific conductivity is determined by the product of charge carrier density and charge carrier mobility. Therefore, the proton conductivity of PEMs strongly depends on IEC of the membrane and the mobility of protons. As the cross-link density increases, the tight network structure results in decreased molecular

mobility of protons. Moreover, highly cross-linked membrane has smaller water content, which also leads to decreased proton mobility. More important, the morphology of the cross-linked PEMs is strongly related to the use of different precursors. Compared to sPFPE4000, the use of sPFPE1000 precursor may result in PEMs with less favorable phase separation for proton conduction or smaller hydrophobic/hydrophilic domains. As a result, higher cross-link density result in lower proton conductivity.

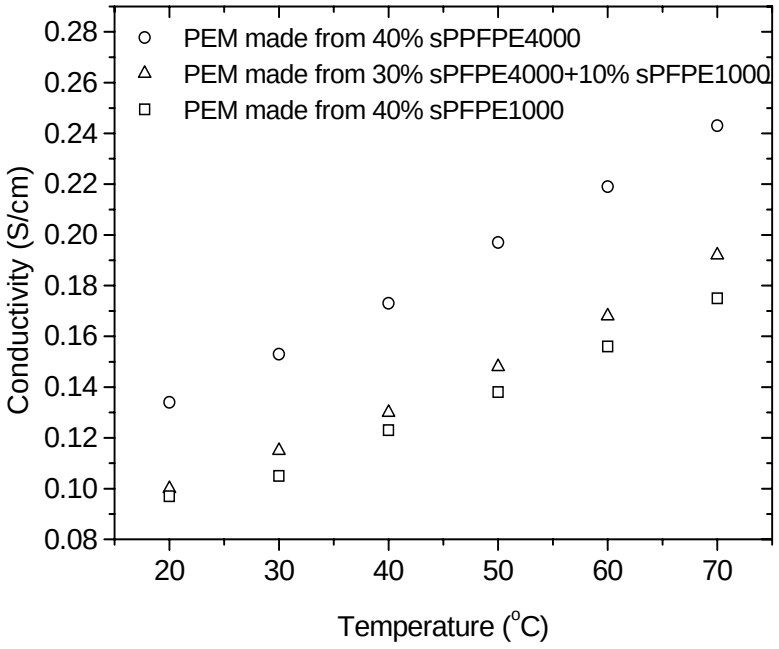

Figure 5.6 Effect of crosslink density on proton conductivity at different temperatures under fully hydrated conditions.

In order to study this effect in more detail, three membranes with the same ion concentration were prepared by using different sPFPE precursors while keeping the same sPFPE/SS ratio and their proton conductivity was compared at different temperatures. In order to obtain an IEC value of 1.5 meq/g after hydrolysis, a precursor feed ratio of

sPFPE/SSE = 40:60 by weight was used for all three membranes. For the 40% sPFPE, sPFPE4000, sPFPE1000 or a mixture of 30% sPFPE4000 and 10% sPFPE1000 was used, respectively. In Figure 5.6, their proton conductivity was compared at temperatures between 20 to 70 ^{o}C under fully hydrated conditions. All three membranes displayed better conductivity at higher temperatures and exhibited Arrehenius behavior. It was calculated that the activation energy for proton conduction was 10.0 kJ/mol, 10.8 kJ/mol, and 10.9 kJ/mol for PEMs made from sPFPE 4000, 3:1 mixture of sPFPE4000 and sPFPE 1000, and sPFPE 1000 precursors, respectively. It was also noted that the proton conductivity of the PEMs did not linearly correlate with the change in crosslink density. Compared to PEMs made from sPFPE1000, the network strands in the PEMs made from the sPFPE mixture was about 3 times longer on average, and the proton conductivity increased by less than 10%. On the other hand, the network strands in the PEMs made from sPFPE4000 were 4 times longer, and the conductivity increased by about 40%. This data is in agreement with the difference in activation energy for these membranes. Due to the very different properties of sPFPE and SSA units, they tend to form phase-separated micro-domains within the membrane. When the cross-link density was increased, the average network strands became shorter, and this may result in less phase separation and/or smaller domain size for membranes with the same IEC value. The molecular mobility of protons is closely related to the different micro-phase structures of the membrane. It is concluded that cross-link density has a strong effect on the phase-separation and micro-phase structure of the PEMs and plays a crucial role in determining the proton conductivity in addition to the concentration of ionic sites in the membrane.

5.3.4 Fuel cell performance

Membrane electrode assemblies (MEAs) were prepared from the three membranes with different cross-link densities. In order to achieve the most reproducible results, Nafion® impregnated LT 140E-W low temperature ELAT® gas diffusion electrodes (E-TEK, NJ) with a Pt catalyst loading of 5 g/m^2 were used for MEA fabrication. The MEA performance was measured at 50 ^{o}C and 75% relative humidity (R.H.) using hydrogen and oxygen as the fuel and the oxidant and the results were shown in Figure 5.7. The effect of cross-link density on proton conductivity almost directly transferred to MEA performance. Membrane with lower cross-link density displayed better fuel cell performance due to its higher proton conductivity and lower resistance. Similar to proton conductivity, the influence on MEA performance was not linearly related to the membrane cross-link density due to difference in the molecular mobility of protons, size of the segregated micro-phases, and the morphology of the membranes.

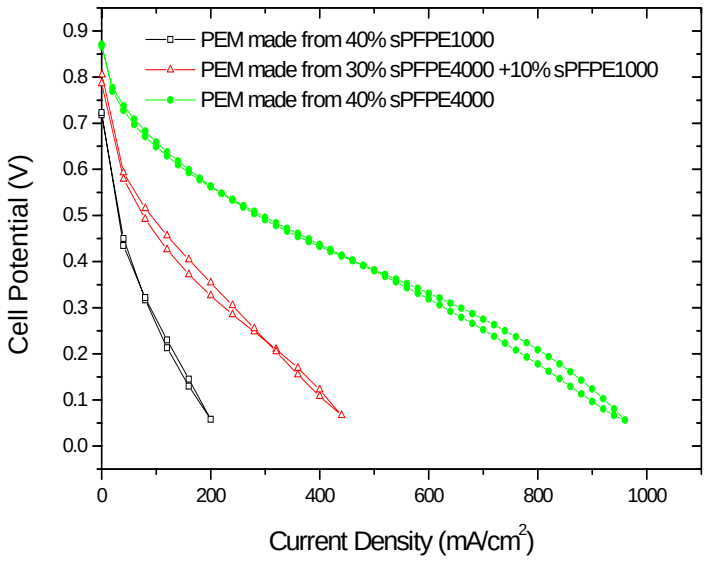

Figure 5.7 Effect of crosslink density on MEA performance at 50^{o}C and 75% R. H.

5.4 Conclusion

This chapter describes the influence of cross-link density on the performance of sPFPE-SSA based membranes. The cross-link density was systematically controlled independently of IEC by using sPFPE liquid precursors with different molar mass. Increase in cross-link density resulted in membranes with stronger mechanical properties. Change in the cross-link density and therefore length of network strands had strong effect on the formation of the micro-phase separated domains and morphology of the membrane. It may also affect the molecular mobility in the tight network structure. Therefore, higher cross-link density resulted in less water uptake and less swelling of the membrane. The proton conductivity depended on the concentration of the ion conducting sites as well as the ionic domain size and micro-structure of the membrane. Within the range of cross-link density studied, the proton conductivity decreased with increase in cross-link density in a nonlinear fashion. Similar to proton conductivity, cross-linking of the membranes also had strong influence on the MEA performance of the membranes.

5.5 References:

(1) Appleby, A. J.; Foulkes, R. L. *Fuel Cell Handbook*; Van Nostrand Reinhold: New York, **1989**.

(2) Whittingham, M. S.; Savinell, R. F.; Zawodzinski, T. A. *Chem. Rev.* **2004**, *104*, 4243-4244.

(3) Minh, N. Q. In *Electronic Materials Chemistry*; Pogge, H. B., Ed.; Marcel Dekker, Inc: New York, **1996**.

(4) Hickner, M. A.; Ghassemi, H.; Kim, Y. S.; Einsla, B. R.; McGrath, J. E. *Chem. Rev.* **2004**, *104*, 4587-4612.

(5) Kerres, J.; Cui, W.; Disson, R.; Neubrand, W. *J. Membr. Sci.* **1998**, *139*, 211-225.

(6) Chen, J.; Asano, M.; Yamaki, T.; Yoshida, M. *J. Membr. Sci.* **2005**, *256*, 38-45.

(7) Schmidt, T. J.; Simbeck, K.; Scherer, G. G. *J. Electrochem. Soc.* **2005**, *152*, A93-A97.

(8) Chen, S.-L.; Benziger, J. B.; Bocarsly, A. B.; Zhang, T. *Ind. Eng. Chem. Res.* **2005**, *44*, 7701-7705.

(9) Buchi, F. N.; Gupta, B.; Hass, O.; Scherer, G. G. *Electrochem. Acta.* **1995**, *40*, 345-353.

(10) Kang, M.-S.; Kim, J. H.; Won, J.; Moon, S.-H.; Kang, Y. S. *J. Membr. Sci.* **2005**, *247*, 127-135.

(11) Won, J.; Park, H. H.; Kim, Y. J.; Choi, S. W.; Ha, H. Y.; Oh, I.-H.; Kim, H. S.; Kang, Y. S.; Ihn, K. J. *Macromolecules* **2003**, *36*, 3228-3234.

(12) Kusomoto, K.; Sata, T.; Mizutani, Y. US 2,962,454, **1960**.

(13) Vie, P.; Paronen, M.; Stromgard, M.; Rauhala, E.; Sundholm, F. *J. Membr. Sci.* **2002**, *204*, 295-301.

(14) Bae, B.; Ha, H. Y.; Kim, D. *J. Membr. Sci.* **2006**, *276*, 51-58.

(15) Kerres, J.; Cui, W.; Junginger, M. *J. Membr. Sci.* **1998**, *139*, 227-241.

(16) Mikhailenko, S. D.; Wang, K.; Kaliaguine, S.; Xing, P.; Robertson, G. P.; Guiver, M. D. *J. Membr. Sci.* **2004**, *233*, 93-99.

(17) Qiao, J.; Hamaya, T.; Okada, T. *Chem. Mater.* **2005**, *17*, 2413-2421.

(18) Qiao, J.; Hamaya, T.; Okada, T. *Polymer* **2005**, *46*, 10809-10816.

(19) Rhim, J.-W.; Park, H. B.; Lee, C.-S.; Jun, J.-H.; Kim, D. S.; Lee, Y. M. *J. Membr. Sci.* **2004**, *238*, 143-151.

(20) Kim, D. S.; Park, H. B.; Rhim, J. W.; Lee, Y. M. *Solid State Ionics* **2005**, *176*, 117-126.

(21) Zawodzinski, T. A.; Neeman, M.; Sillerud, L.; Gottesfeld, S. *J. Phys. Chem.* **1991**, *95*, 6040-6044.

(22) Rubinstein, M.; Colby, R. H. *Polymer Physics*; Oxford: New York, **2003**.

Chapter 6

RECOMMENDATION FOR FUTURE DIRECTIONS

6.1 Thinner membranes

The performance of fuel cells is directly related to the thickness of the polymer electrolyte membranes (PEMs). Thinner membranes will result in better fuel cell performance because of their lower resistance. At the time of writing, membranes with a thickness of 25 μm is the industry standard for hydrogen fuel cells. For direct methanol fuel cells, thicker membranes are needed in order to decrease methanol crossover. In this thesis, membranes based on styrenically modified perfluorpolyether (sPFPE) and a sulfonated styreneic (SS) monomer were prepared and characterized both in the ester form (sPFPE-SSE) and in the acid form (sPFPE-SSA). The thickness of sPFPE-SSA membranes was typically 190 μm for comparison with Nafion® 117. Some initial efforts on making thinner membranes displayed promising results. A sPFPE-SSA PEM with an IEC value of 1.5 meq/g and a thickness of 140 μm was prepared and compared with a thicker membrane of the same composition. MEAs based on these membranes were tested at 50 ^{o}C and 75% relative humidity (RH) using hydrogen and oxygen as the fuel and the oxidant. Nafion® impregnated LT 140E-W low temperature ELAT® gas diffusion electrodes (E-TEK, NJ) with a Pt catalyst loading of 5 g/m^2 was used as the electrodes in membrane electrode assembly (MEA) fabrication. Figure 6.1 shows the polarization curves and power output results for these MEAs. Since the concentration of ion conducting sites is the same for these two sPFPE-SSA membranes, their specific proton conductivity should be the same. The resistance of MEAs based on these membranes is proportional to the membrane thickness. Therefore, thinner membranes with smaller resistance would correlate with better MEA performance. As shown in Figure 6.1, the MEA based on the 140 μm membrane displayed better performance than that of the 190 μm PEM and 15% increase in power generation was achieved. More

investigation is needed to make thinner sPFPE-SSA based membranes with high proton conductivity, good perm-selectivity and minimum fuel crossover to meet the industrial requirements.

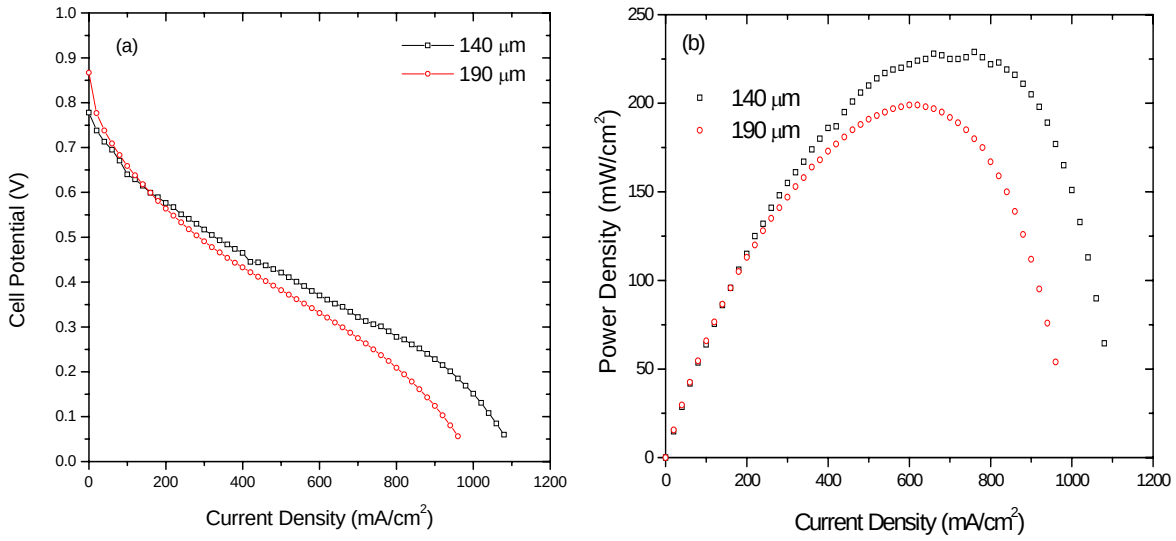

Figure 6.1 Effect of membrane thickness on fuel cell performance. (MEA performance was tested at 50 ^{o}C and 75% RH with H_2 and O_2 as the fuel and the oxidant at a flow rate of 0.1 l/min).

6.2 More robust membranes

6.2.1 Improve chemical stability

For commercial application, PEMs with a lifetime of a few thousand hours are needed. The current version of the sPFPE-SSA based system can not meet this requirement. To achieve PEMs with good long term stability under fuel cell operations, both the chemical and the mechanical properties of the current sPFPE-SSA system need to be improved. In Chapter 3, some efforts were invested to improve the chemical stability of the sPFPE-SSA based PEMs by fluorination of the membrane with elemental fluorine gas. Initial results

indicated improved stability of the fluorinated membranes. More experiments are needed in this area to tune the fluorination conditions, confirm the chemical structure of the fluorinated samples, measure their properties, and test the MEA performance and long term stability of the fluorinated PEMs. Alternatively, perfluorinated or more stable precursor materials can be used to improve the chemical robustness of the PEMs. For example, precursors with σ, β, β-trifluorostyrene functional groups can be prepared and used to replace those with styrene functionalities. The elimination of aliphatic hydrocarbon moieties will help to improve the chemical resistance of the resulting PEM materials. Since the membrane degradation under fuel cell operation conditions is believed to be a free radical initiated process, inclusion of a radical scavenger into the PEM system can prevent or slow down the degradation process and improve the lifetime of the membrane. However, such a radical scavenger should be included in a clever way so that it does not affect the polymerization of the precursors into a cross-linked membrane, which is also a free radical initiated process.

6.2.2 Improve mechanical properties

The mechanical properties of the PEMs play an important role in membrane durability. It has been reported that mechanical reinforcement has a strong effect on membrane life. GORE-SELECT® membranes with ePTFE reinforcement offered much longer lifetime compared with non-reinforced Nafion® films.[1] For non-reinforced membranes, crack propagation seems to be the leading cause for catastrophic membrane failure and employing ePTFE as reinforcement can effectively slow down this mechanism. Similarly, mechanical reinforcement can be applied to the sPFPE-SSA based PEM systems in order to improve the mechanical properties and long term stability of the membranes. As

an initial effort, porous Tetratex® membranes (a poly(tetrafluoroethylene) material) were used as a matrix and impregnated with the sPFPE and SSE liquid precursors. To make such a composite membrane, liquid precursors were painted onto the Tetratex® membrane and then cured by UV-light. By doing so, the pores were filled with the cured copolymers in the ester form. The Tetratex® membrane itself is white, and the impregnated membrane is semi-transparent. Figure 6.2 shows the scanning electron micrograph (SEM) pictures of the porous Tetratex® and the composite membrane. To convert the sulfonate ester groups to sulfonic acid, the membranes were hydrolyzed by base and acid treatment. Due to the different properties of the matrix material and Nafion® dispersion, it is very hard to impregnate Nafion® dispersion into the porous Tetratex® matrix. However, the sPFPE-SS liquid precursors are highly fluorinated and compatible with the matrix material. It is very easy to impregnate the matrix with the liquid precursors. After curing, there is no de-lamination problem between the matrix and the impregnated material.

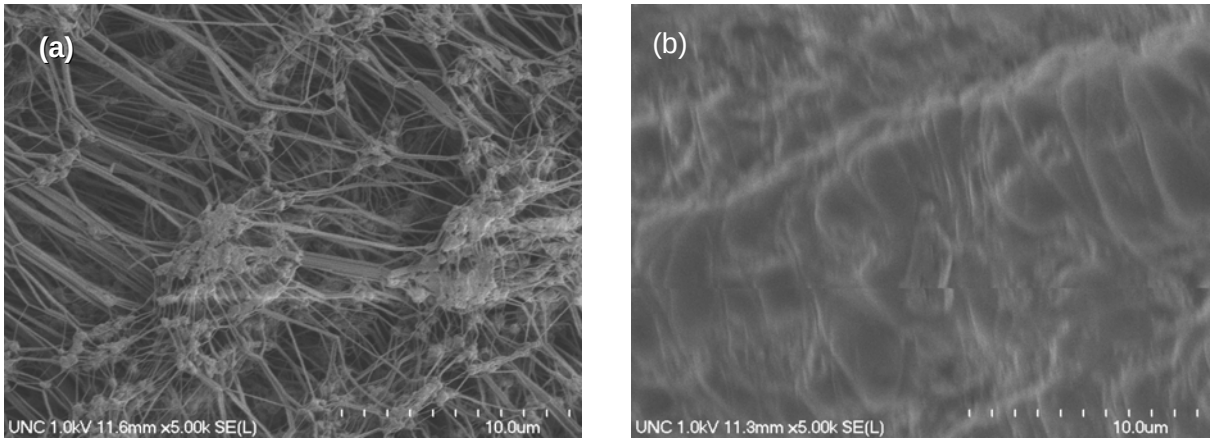

Figure 6.2 SEM pictures of (a) a porousTetratex® film; (b) a composite membrane before hydrolysis

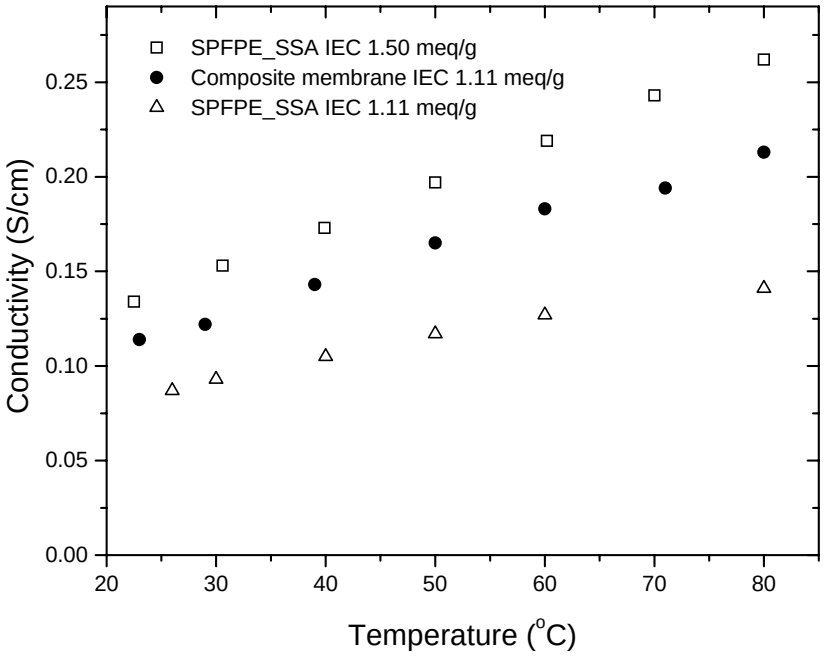

Figure 6.3 Conductivity of the composite membrane under fully hydrated conditions

A mixture of the liquid precursors, 40wt% sPFPE and 60wt% SSE, was painted onto a Tetratex® 1314 membrane and cured by UV light. PEM made of this liquid precursor without using Tetratex® would have an IEC of 1.50 meq/g. Due to the presence of the matrix material, the composite membrane had an IEC value of 1.11 meq/g after hydrolysis and its thickness is 125 μm. The conductivity of this membrane under fully hydrated conditions is shown in Figure 6.3 and compared with pure sPFPE-SSA membranes. The conductivity of the composite membrane was lower than the sPFPE-SSA PEM with IEC 1.50 meq/g. This is reasonable since the impregnated membrane had lower IEC and therefore lower concentration of ion conducting sites. However, its conductivity was higher than a sPFPE-SSA PEM with an IEC of 1.11 meq/g. Even though the average acid concentration

was the same for both the membranes, there were macroscopic regions of higher acid concentration in the composite membrane. It is easier for protons to migrate through these regions and this helps to improve the proton conductivity of the composite membrane.

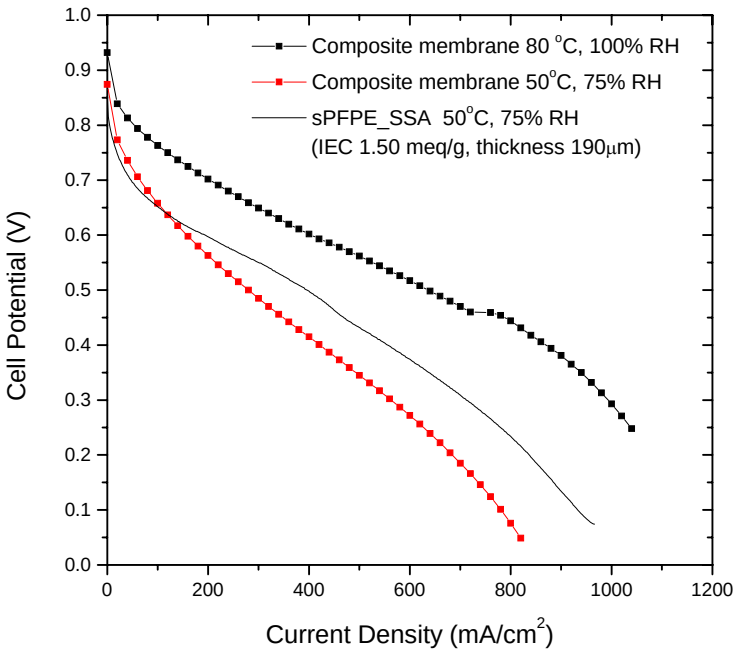

Figure 6.4 MEA performance of the composite membrane

An MEA based on the composite membranes was fabricated by using Nafion impregnated LT 140E-W low temperature ELAT® gas diffusion electrodes (E-TEK, NJ) with a Pt catalyst loading of 5 g/m^2. The MEA performance was tested by using hydrogen and oxygen as the fuel and the oxidant at a flow rate of 0.1 l/min and the results were shown in Figure 6.4. At 50 ^{o}C and 75% RH, the performance of this membrane was not as good as sPFPE-SSA membrane with IEC of 1.50 meq/g and a thickness of 190 μm. This can be explained by their conductivity difference. However, the flexibility and mechanical stability

of the composite membrane is better than pure sPFPE-SSA membranes. An IEC 1.50 meq/g sPFPE-SSA PEM can not be operated at 80 ^{o}C and 100% RH, but the composite membrane can be used under this condition without obvious failure. The MEA performance of the composite membrane at 80 ^{o}C and 100% RH is also shown in Figure 6.4. More systematic study in this direction should be performed in the future.

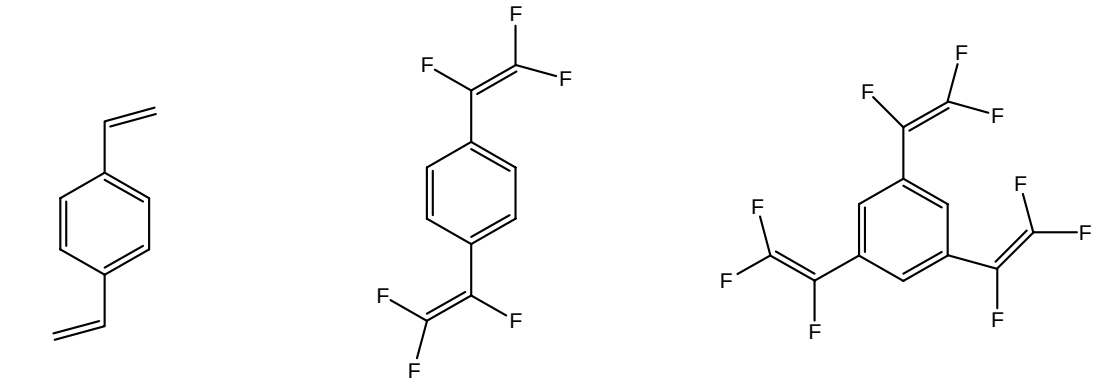

Figure 6.5 Examples of cross-linkers that have been tested

Another approach to improve the mechanical properties of the sPFPE-SSA PEM system is to increase the membrane cross-link density by adding external cross-linkers. The added cross-linkers should be miscible with the fluorinated sPFPE and SSE precursors and

have similar reactivity with these precursors. Figure 6.5 shows the chemical structures of some cross-linkers that have been tested. Of these cross-linkers, a mixture of difluorovinyl benzene and trifluorovinyl benzene (FVB) gave the best results. A sPFPE-SSA-FVB membrane with 5wt% external cross-linker was prepared and the membrane had an IEC of 1.45 meq/g. This PEM absorbed 92wt% water for liquid water at room temperature and displayed a dimensional change of 38% due to water uptake. Figure 6.6 shows the proton conductivity of this membrane under fully hydrated conditions and compares with sPFPE-SSA PEMs with similar ion concentrations. Compared to sPFPE4000-SSA PEM with IEC 1.50 meq/g, the conductivity of this membrane was lower due to the lower ion concentration and possible morphology changes corresponding to the addition of FVB. However, its conductivity was higher that that of sPFPE1000-SSA PEM with IEC 1.50 meq/g.

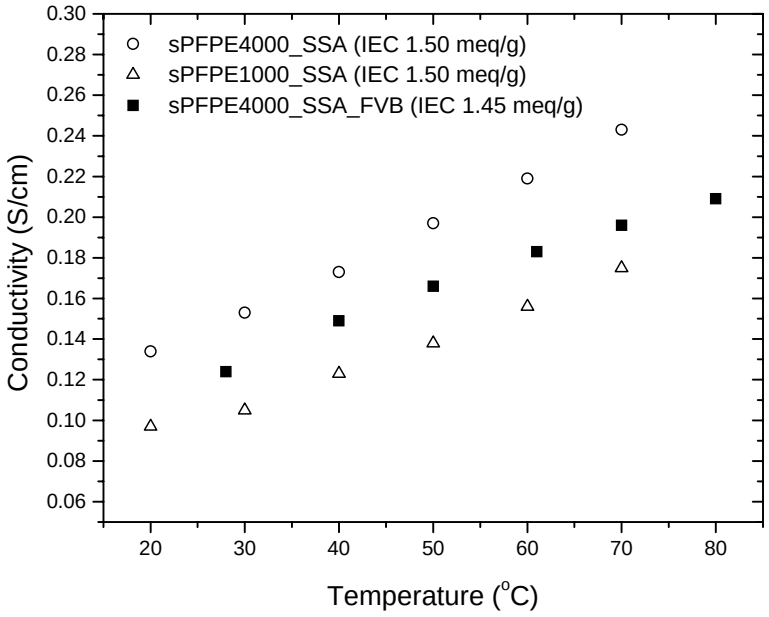

Figure 6.6 Proton conductivity of sPFPE-SSA-FVB PEM under fully hydrated conditions

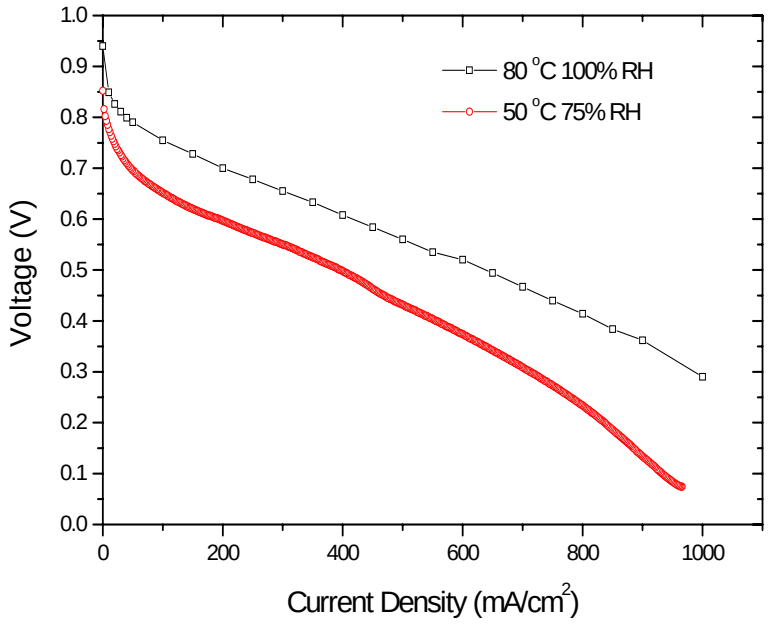

Figure 6.7 MEA performance of sPFPE4000-SSA-FVB membrane with IEC of 1.45 meq/g and thickness of 190 μm

Without addition of FVB, the sPFPE4000-SSA PEM could not be used for fuel cells which operated at 80 °C and 100% R. H. The membrane would mechanically break into pieces under this condition. With FVB incorporated, the mechanical strength of the sPFPE4000-SSA-FVB membrane was improved and the membrane could stand the testing conditions. Figure 6.7 shows the polarization curves of a MEA based on this membrane using Nafion® impregnated LT 140E-W low temperature ELAT® gas diffusion electrodes (E-TEK, NJ) with a Pt catalyst loading of 5 g/m^2. Divinyl benzene can not form single phase mixture with the sPFPE and SSE liquid precursors and can not be used to improve the mechanical properties of the system. Divinyl perfluorinated hexane (DVPH) can form homogeneous mixtures with the liquid precursors, but its reactivity is lower than the styrene functional groups of the precursor materials. After curing a mixture including 60wt%

sPFPE4000, 35wt% SSE and 5wt% DVPH and subsequent hydrolysis, a PEM with IEC 1.67 meq/g was obtained and no improvement in mechanical properties was observed. It is believed that DVPH was not able to be included into the network due to its low reactivity. A small molecule analog of sPFPE was synthesized and used as a cross-linker for the sPFPE-SSA system. This molecule was miscible with the precursor materials and helped to improve the membrane mechanical properties as indicated by water boiling test. More cross-linkers should be tested in the future and the study of mechanical properties should be coupled with proton conductivity, MEA performance and the membrane morphology.

Other approaches to improve the membrane durability include impregnating a porous block copolymer matrix with the liquid precursors, making homopolymer/block copolymer blends with the precursor materials, and fabricating organic-inorganic composite membranes, etc. For the block copolymer approachs, a bi-continuous morphology is preferred for maintaining high proton conductivity of the materials.

6.3 High surface area, patterned PEMs

In Chapter 4, patterned membranes with high fidelity micron scale features were prepared by imprint lithography techniques. It has been demonstrated that patterned membranes can provide much larger active surface area and a fuel cell based on such membranes can generate more power compared to those based on flat membranes with the same geometric size. However, only a doubling of the surface area has been achieved. More efforts should be invested in this area to achieve a 10 times increase in surface area, even for thinner membranes. Further increases in fuel cell power density by increasing the interfacial area between the proton conducting membrane and the catalyst layer should be coupled with

studies of making smaller catalyst particles so that they can be loaded into the high aspect ratio, sub-micron scale patterned features and form good contact with the membrane. Alternatively, liquid precursors can be injected into patterned, pre-assembled electrodes with catalyst loaded, and then cured into solid membranes. The difficulty of this approach is to pattern the electrodes and hydrolyze the membrane within the injection-molded MEA.

Furthermore, complicated transport phenomena are involved for effective operation of fuel cells. For example, the fuel and the oxidant are supplied to the fuel cell as gases and water is generated as by-product of this electro-chemical process. While certain amount of water is necessary to partially hydrate the proton exchange membrane, extra water has to be removed from the system for effective gas supply to the fuel cell. Excess water can result in flooding of the electrodes and mass transport limitation of the running fuel cells. The feature shape, size and aspect ratio of the patterned membranes will couple with these complicated transport issues and affect the performance of the fuel cells. Therefore, systematic studies in this area should be planned for future directions and some guidance from simulation studies would be helpful.

6.4 Catalyst ink formulation

The quality of catalyst inks and the interfacial properties between the PEM and the catalysts are critical for achieving good fuel cell performance. Formulation of catalyst inks is a very important and delicate project. Slight changes in the ink composition and preparation steps can dramatically change the ink quality. Conventional catalyst inks are formulated using Nafion® dispersion to obtain three phase contact between the proton conducting sites, the catalyst and the fuel. Nafion® based ink works well for Nafion® membranes, but are not

necessarily good for other PEM systems due to different chemical natures, structures, and interfacial properties. Moreover, the membranes swell and shrink under fuel cell operation cycles and this can result in de-lamination between the membrane and catalyst layers. The high ion concentration liquid precursors can be used to replace Nafion® dispersion in ink formulation, which would possibly help to maintain good contact between the membrane and the catalyst layer upon curing. Furthermore, the carbon support of catalyst particles can be chemically modified to polymerize with the precursor materials and covalently attach to the network structure.

6.5 Morphology studies

In order to understand the structure-property relationship for the sPFPE-SSA based PEM systems, scattering and microscopy techniques should be employed for morphology studies. Microscopic studies can provide direct visualization of size, shape and geometrical distribution of separated domains, but usually give "local pictures" of the sample and need expertise in sample preparation. The scattering techniques, on the other hand, are indirect methods and usually need to assume a particular model in data analysis, but display a "global picture" of the sample. Combination of these two techniques would compensate each other and give a good understanding of the membrane morphology.

Some initial small angle x-ray scattering (SAXS) studies were performed for the sPFPE-SSA PEMs. Figure 6.8 shows the SAXS results of the membranes neutralized with tetrabutylammonium hydroxide (TBA+) under dry conditions. In the dry state, these materials appear to show a general trend of increasing ionic domain dimensions with increasing SSA content. This is reasonable since the volume fraction of ionic domains

increase with increasing SSA content. The domain dimension of the sPFPE-SSA based materials is observed to be in the range of 12-16 nm, which is much larger than that of Nafion®. The ionic cluster size is 3.5 nm for Nafion® in the TBA+ form under dry conditions. This suggests that the sPFPE-SSA membranes have a much larger range of heterogeneities as compared to Nafion®. Since the sPFPE-SS membranes are cross-linked in the protected ester form and then hydrolyzed to the acid form, the crosslinks may inhibit ordered cluster development on the size scale of that observed with Nafion®. Furthermore, sPFPE-SS membranes are prepared from macro-monomers and the segment length of sPFPE and SS is longer than that of Nafion®, which would also contribute to larger domain size.

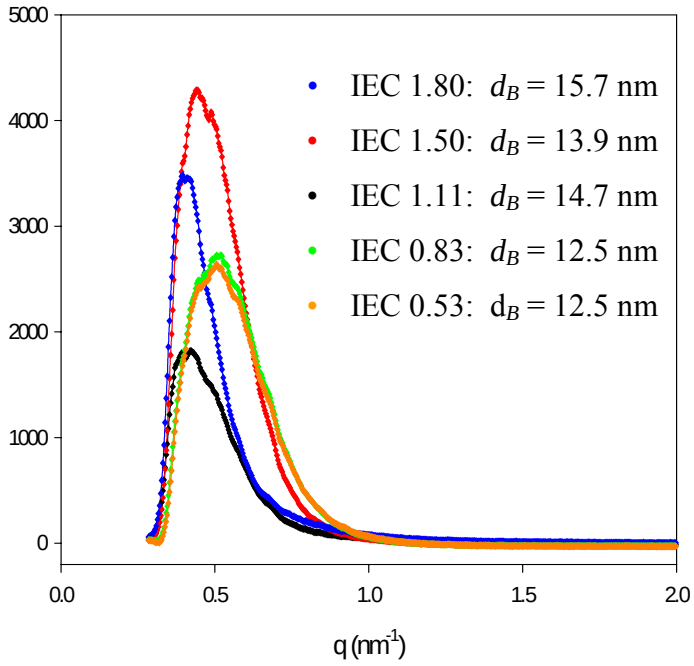

Figure 6.8 SAXS of sPFPE-SSA samples neutralized by TBA+ in the dry sate

In the hydrated state, the sPFPE-SSA ionomers in the acid form displayed a Bragg spacing of 15.7 nm independent of SSA content as shown in Figure 6.9. The intensity

variations are simply due to uncorrected sample thicknesses and different transmission factors. This domain spacing of 15.7 nm is the same as that of the IEC 1.80 meq/g sample in the dry state, indicating that the ionic domains are overlapping for the sample with such high ion concentration, even in the dry state. For other samples, this size is bigger than their domain sizes in the dry state, indicating that uptake of water swells the ionic domains. As shown in Figure 6.9, the very low scattering angles are pushing the limits of the SAXS system used for these measurements. High-resolution synchrotron SAXS that gives access to lower scattering angles should be used for more accurate measurements.

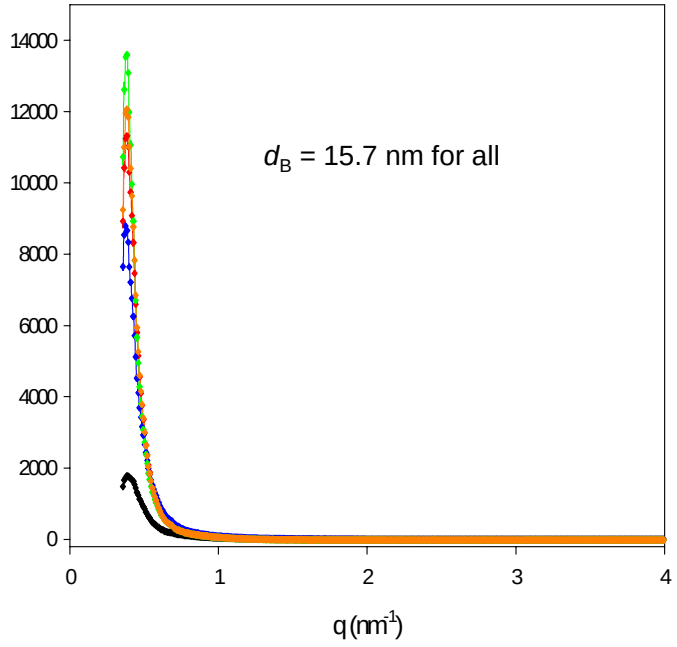

Figure 6.9 SAXS of sPFPE-SSA samples in the acid form under hydrated conditions

6.6 Direct methanol fuel cells

Up to now, the sPFPE-SSA PEMs have been used in hydrogen fuel cells and their performance in direct methanol fuel cells has not been tested. In order for a PEM to have

good performance in direct methanol fuel cells, the membrane needs to have low methanol crossover as well as good proton conductivity. One way to achieve both is to fabricate tri-layer membranes with a centered methanol barrier layer. Moreover, by spin-coating and curing sPFPE-SSE precursors with different IECs layer by layer, PEMs with a controllable gradient in ion content and virtually continuous changing properties can be obtained with good adherence between the layers. The high IEC layers can help to maintain good proton conductivity while the low IEC center layer can serve as a methanol barrier. These ideas should be planned for future directions.

6.7 References

(1) Liu, W.; Ruth, K.; Rusch, G. *J. New. Mater. Electrochem. Syst.* **2001**, *4*, 227-231.